Chalcogenide glasses development for the elaboration of innovative waveguides and fibers

Yiming Wu

UNIVERSITE MATIERE BRETAGNE MOLECULES LOIRE ET MATERIAUX

UNIVERSITÉ DE RENNES 1

THESE DE DOCTORAT DE

L'UNIVERSITE DE RENNES 1

COMUE UNIVERSITE BRETAGNE LOIRE

ECOLE DOCTORALE N° 596
Matière Molécules et Matériaux
Spécialité : Sciences de matériaux

Par

Yiming WU

Chalcogenide glasses development for the elaboration of innovative waveguides and fibers

Thèse présentée et soutenue à Campus de Bealulieu à Rennes, le 20 Décembre 2018
Unité de recherche : ISCR, UMR CNRS 6226, Institut des Sciences Chimiques de Rennes
Thèse N° :

Rapporteurs avant soutenance :

Anne-Marie JURDYC, Directeure de recherche, Institut Lumière Matière, Université Claude Bernard Lyon 1
Pascal MASSELIN, Maitre de conferences, Université du Li ttoral Côte d'Opale

Composition du Jury :

Anne-Marie JURDYC	Directeure de recherche CNRS, Institut Lumière Matière, Université Claude Bernard Lyon 1, rapporteur
Pascal MASSELIN	Maitre de conferences, Université du Littoral Côte d'Opale, rapporteur
Xianghua ZHANG	Directeur de recherche CNRS, Université de Rennes 1, President
Johann TROLES	Professeur, Université de Rennes 1, Directeur de thèse
Shuangchen RUAN	Professeur, Shenzhen Technology University, Co-directeur de thèse

Acknowledgement

The research work presented in the thesis is accomplished in collaboration between Laboratoire de Verres et Céramiques of Université de Rennes 1 and Shenzhen University.

First of all, I would like to express my gratitude to my PhD supervisor in France, Prof. Johann Troles. Your enthusiasm and wisdom really impressed me, and I so admire your passion for scientific research. I have learnt so much from you and made a lot progress during the time we worked together and not to mention that you helped me through some difficult time during the PhD which I am always grateful for. It is a great honor to have been working with you in the past 3 years, “Glass Guru”.

Also, I want to thank my supervisor in China, Prof. Shuangchen Ruan, for offering me this opportunity and all the support you provided. It was a memorable experience for me and I am really gratitude for it.

Besides, I want to say thank you to Prof. Xianghua Zhang and Hongli Ma who have helped us so much during the time we were in Rennes. Your caring and support made it easier for us to assimilate into the life in France. And not to exaggerate, I think our relationships surpass friendship and are more like families.

I also want to thank people who workrd with me in the lab. I want to thank Cahterine for the guidance and help in the TeGe-AgI experiments and thank you for your patience and enduring my immaturity. And I want to thank Celine for giving me the basic training and introduction around the lab and Marcello for working together on the graded-index fiber.And all the other people in the lab who helped me with the experiments.

As for the personal life, I want to thank all my Chinese friends who have helped me during my PhD, Yimin Wu, Guangxing Liang, Yanghai Xu, Shuo Chen, Muzhi Cai, Zhuanghao Zheng, Renguang Ye, Qing Jiao.It is a great pleasure to know you guys here and to be kept accompanied by you guys. And also, I really appreciate the time I spent with the friends in the lab: Laure, Anna, Bhuvanesh and et al.

It has been an amazing 3 years for me, and I want to thank all the people who helped me in the lab and daily life and the support from my parents.

Table of Content

French Abstract

Résumé en français de la thèse

Les travaux de recherche présentés et discutés dans cette thèse sont issus d'un échange avec l'Université de Shenzhen en Chine et l'Université de Rennes 1.
L'objectif de cette thèse est la réalisation et l'étude d'objets optiques en verre de chalcogénures pour le développement de nouvelles sources infrarouges dans le moyen infrarouge (2-12 µm).

Le présent document est divisé en trois chapitres distincts. Le premier chapitre, introductif, présente les propriétés générales des verres et fibres en verres de chalcogénures ainsi que leurs intérêts, notamment dans le développement de sources supercontinuum générant des longueurs d'onde de 2 à 12 µm (source large bande issue de phénomènes optiques non linéaires). Ce domaine de longueur d'onde est très apprécié dans le domaine de la spectroscopie, car c'est dans ce domaine que l'on retrouve la majorité des signatures infrarouges des toutes les substances chimiques et biologiques. Le deuxième chapitre exploite, la photosensibilité des verres de chalcogénures pour la réalisation de guides d'onde photo-inscrits. Dans ce chapitre, 3 différentes compositions ont été étudiées mais ont présenté un comportement différent voire contradictoire. Le dernier chapitre explore la réalisation de fibres optiques nouvelles à base de verre de chalcogénures. Les premières fibres étudiées sont les fibres réalisées avec des compositions à base de tellure, afin d'augmenter la fenêtre de transmission des fibres vers les grandes longueurs d'onde. La deuxième partie du chapitre présente une méthode originale qui pourrait permettre de réaliser des fibres en verres de chalcogénures à gradient d'indice. Puis la dernière partie est consacrée au développement de fibres hybrides en verres de silice et verres de chalcogénures.

Chapitre 1: Les verres et fibres de chalcogénures, propriétés et applications

Les verres chalcogénures sont des verres à base de soufre, de sélénium et de tellure (colonne VIA du tableau périodique). Une multitude d'autres éléments peut entrer dans la composition des verres, ces éléments sont plutôt situés dans les colonnes IIIA, IVA et VA du tableau périodique des éléments (As, Sb, Bi, Ge, etc.). La particularité de ces matériaux est donc étroitement liée à toutes les applications situées

dans ce domaine spectral.

Tableau 1: Caractéristiques physiques et optiques des quelques exemples de verre de chalcogénures

Caractéristique	As_2S_3	$As_{38}Se_{62}$	$Te_{20}As_{30}Se_{50}$	$Ge_{10}As_{22}Se_{68}$
Fenêtre de transparence (µm)	0,5 à 12	0.8 à 16	2 à 18	0.8-16
T_g (°C)	192	165	132	175
T_x (°C)	-	250	-	473
$\Delta T=T_g-T_x$ (°C)	-	85	-	298
ρ (g/cm^3)	3,15	4,53	4,88	4,45
α ($10^{-6}.K^{-1}$)	21,6	25,4	23,0	17,3
n (1,55µm)	2,44	2,81	2,96 (2µm)	2,63
n_2 (10^{-18} $m^2.W^{-1}$)	2,5 à 5,94	11 à 24	-	11,6
$n_2/n_{2\ SiO2}$	114 à 270	500 à 1090	-	530

Dans la communauté scientifique, les verres de chalcogénures sont classés dans la famille des "soft glasses". En effet, en comparaison avec la silice qui présente une température de transition vitreuse (T_g) autour de 1200-1300 °C ou bien en comparaison avec le verre à vitre et une T_g de 600-700°C, les verres de chalcogénures présentent des températures de transition vitreuses allant de la température ambiante à 300-400°C (tableau 1). Au-delà de la transition vitreuse le verre recristallise (état thermodynamique plus stable) à une la température de cristallisation Tx. Pour les applications pratiques, les deux températures T_g et Tx sont fondamentales. En effet pour toute mise forme du verre (moulage, fibrage…) il faudra élever la température au-delà de Tg, pour profiter d'une viscosité suffisamment basse mais endeçà de la Tx pour éviter la cristallisation du matériau.

Les verres utilisés en optique sont très sensibles à la présence d'impuretés et nécessitent une synthèse particulièrement méticuleuse. La synthèse de verres de chalcogénures demande à être réalisée en atmosphère exempte d'oxygène, d'eau et

d'impuretés telles que des poussières par exemple. La présence d'impuretés peut gêner la vitrification et surtout altérer la transmission des échantillons, par des phénomènes de diffusion ou d'absorption dans le proche ou moyen infrarouge. Les verres de chalcogénures sont alors synthétisés sous vide, dans des tubes de silice et en utilisant des produits de départ de grande pureté.

Le montage permettant la préparation d'un tube scellé est composé d'une pompe à vide (10^{-5} mBar), d'un piège refroidi à l'azote, d'un montage en Pyrex et d'un tube réactionnel en silice qui accueille les différents produits de départ. L'utilisation d'un piège refroidi par de l'azote liquide présente plusieurs intérêts, le premier est de protéger la pompe contre les vapeurs issues des différents éléments et d'éviter de polluer l'atmosphère ambiante par ces mêmes vapeurs. Le deuxième intérêt est de protéger les différents éléments d'une pollution provenant cette fois des vapeurs issues de l'huile de la pompe à vide. L'ampoule réactionnelle est obtenue par scellage à l'aide d'un chalumeau (butane - oxygène). Au cours de la synthèse, on est parfois amené à faire intervenir des éléments chimiques additionnels pour pousser plus loin la purification. C'est notamment indispensable lorsqu'il s'agit de verre destiné à la fabrication de fibre optique. Ainsi, de l'aluminium ou du magnésium, éléments très réducteurs permettent de fixer les traces résiduelles d'oxygène encore présentes. Les particules solides d'oxyde d'aluminium et/ou de magnésium sont alors éliminées par distillation. On peut également utiliser des chlorures de chalcogène comme le $TeCl_4$, pour éliminer les traces d'hydrogène. L'acide chlorhydrique HCl est formé à l'état gazeux et est éliminé par pompage sous vide du montage de synthèse.

En exploitant les propriétés viscoplastiques des verres, il est alors possible de réaliser des fibres optiques permettant alors le déport de signaux lumineux. L'exemple le plus connu est bien évidement la fibre de silice utilisée notamment pour le transport optique d'informations.

Deux méthodes de fabrication de fibres de chalcogénures sont répertoriées et utilisées. La première est basée sur la méthode classique d'étirage de préforme (figure 1a). Dans ce cas la fibre est obtenue en étirant soit: un barreau simple de verre ou bien simultanément un barreau de cœur inséré dans un tube de verre de gaine. Pour ce faire

l'extrémité d'une préforme (barreau simple ou barreau dans tube) est chauffée au-delà de la température de transition vitreuse. Sous l'effet de la chaleur et de la gravité une goutte de verre se forme et tombe en entrainant avec elle la future fibre que l'on fixe au tambour d'enroulement. Afin d'avoir un apport de matière constant, la préforme est progressivement descendue au niveau du four. Le diamètre de la fibre est alors contrôlé par la vitesse de la descente de la préforme et la vitesse d'enroulement du tambour. Les fibres dites mono-indices (une seule composition) sont fabriquées par cette méthode. La deuxième est la méthode dite du double creuset dans laquelle les deux verres, de gaine et de cœur sont coulés simultanément en haut d'une tour de fibrage (Figure 1b). Dans cette méthode, seul le four est diffèrent (Figure 1b), l'ensemble de la tour de fibrage reste identique. La méthode consiste à étirer à travers une filière une fibre constituée lors de la coulée d'un verre de gaine autour d'un cœur (Figure 1b). A la sortie de la filière, la fibre est également fixée sur un tambour d'enroulement. Avec cette méthode, le ratio entre le diamètre de la gaine et du cœur peut être contrôlé par une pression de gaz appliquée au-dessus des deux verres en fusion. Les fibres commerciales de chalcogénures à double indice sont élaborées par cette méthode du double creuset.

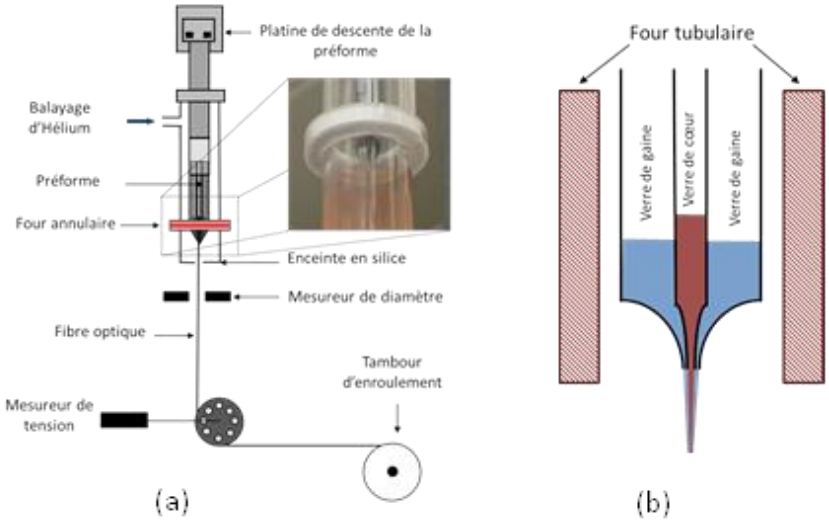

Figure 1: Tour de fibrage (a) et four à double creusets (b)

La Figure 2 présente les courbes d'atténuation des fibres de chalcogénures comparées à celle d'une fibre de silice. L'atténuation (α) d'une fibre est donnée en dB/m ou dB/km. Une courbe d'atténuation est obtenue par la méthode du cut back qui

consiste à mesurer l'intensité lumineuse en fonction de la longueur d'onde à la sortie de la fibre pour deux longueurs différentes. On mesure alors une intensité $I_1(\lambda)$ à une longueur L1 et une l'intensité $I_2(\lambda)$ à une longueur L_2. L'atténuation est alors calculée pour une longueur de fibre coupée de $L_1 - L_2$.

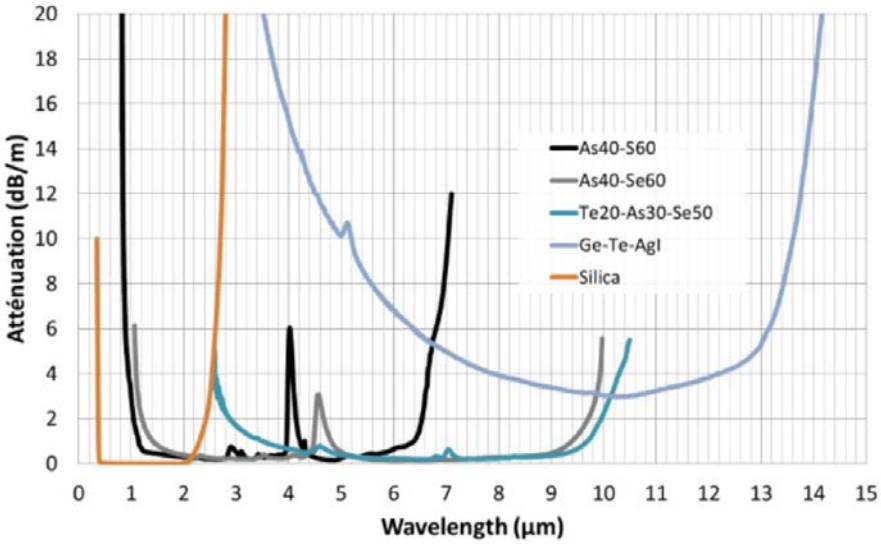

Figure 2: Courbes d'Atténuation de fibres de chalcogénures comparées à celle de la silice télécom

De nos jours, les fibres optiques en silice (SiO_2) sont très largement utilisées pour le transport d'informations. Ces fibres télécoms sont des fibres à saut d'indice dont le cœur est dopé à l'oxyde de germanium qui permet d'augmenter l'indice du cœur par rapport à celui de la gaine en pure oxyde de silicium. La transmission d'une fibre en silice est comprise entre 0,4 et 2,5 µm avec un minimum d'atténuation à 1,55 µm ce qui correspond au domaine de longueurs d'ondes utilisées en télécommunication (Figure 2). Les fibres en verre de chalcogénures sont quant à elles transparentes dans le proche et moyen infrarouge. En effet, leur courbe d'atténuation montre une transmission qui, dépendant de la composition, s'étend jusqu'à 10 µm (Figure 2). Par exemple, une fibre en $As_{40}S_{60}$ transmet de 0,8 µm à 6,5 µm, une fibre en $As_{40}Se_{60}$ transmet de 1,3 à 10 µm alors qu'une fibre en tellure sera transparente de 5 à16 µm. Plusieurs phénomènes contribuent à la diminution de la transmission d'une fibre optique et peuvent être dissociés en deux catégories : les pertes intrinsèques qui sont inhérentes au matériau constituant la fibre et les pertes

extrinsèques provenant de la présence de défauts et/ou d'impuretés. Les bornes inférieures et supérieures de la transmission d'une fibre optique sont liées aux transitions électroniques aux courtes longueurs d'onde et aux absorptions multiphonons du réseau du solide pour les grandes longueurs d'onde. L'écart d'énergie des transitions électroniques (aussi appelé band-gap) et les absorptions multi phonon dépendent très fortement de la nature chimique des verres et sont à l'origine des différences de transmission de chaque famille de fibre. On notera par exemple, que l'énergie du band gap des verres de chalcogénures est plus faible que celui de la silice ce qui a pour conséquence de décaler le début de transmission des fibres en chalcogénures vers l'infrarouge. Par contre, les masses élevées des atomes constituant les fibres de chalcogénures décalent fortement les vibrations du réseau vers l'infrarouge ce qui leur donne leurs propriétés de transparence au-delà de 3 µm. On peut remarquer également qu'en plus des pertes intrinsèques liées au band-gap et aux vibrations multiphonons des pertes dues à la présence d'impuretés peuvent altérer le spectre de transmission (Figure 2). A titre d'exemple, on peut citer la présence de bandes d'absorption liées à la présence de liaisons chimiques O-H (à 2,9 µm), S-H (à 3,1 et 4,0 µm) et Se-H (à 4,6 µm).

Depuis le début des années 90, un nouveau design de fibre optique a révolutionné le monde des fibres. Il s'agit des fibres optiques microstructurées (FOMs). La réalisation de ce type de fibre en verre de chalcogénures est plus récente et date des années 2000. Pour ces fibres optiques on distingue deux mécanismes de propagation: soit la lumière se propage par réflexion totale interne modifiée, soit par bande interdite photonique. Dans les deux cas, le guidage est conditionné par la géométrie de la microstructure et par la différence de composition chimique entre le cœur et la gaine comme dans le cas des fibres à saut d'indice. Les fibres microstructurées se composent d'un arrangement d'inclusions de bas indices (généralement des trous d'air). Cet arrangement est invariant le long de l'axe de la fibre. L'absence d'inclusion dans le centre de la fibre définit le cœur de celle-ci. Les inclusions autour du cœur abaissent l'indice de réfraction moyen qui est alors compris entre celui de l'air et celui du verre. Ainsi, bien qu'il n'existe pas d'interface

clairement définie entre le cœur et la gaine, la lumière est guidée selon le même principe que pour les fibres à saut d'indice : elle se propage dans une zone d'indice élevé (le cœur) entouré d'un milieu d'indice moyen plus faible. On parle alors de guidage par réflexion totale interne modifiée. La microstructure est caractérisée par deux paramètres principaux d et Λ, d correspond au diamètre des trous et Λ à la distance entre deux trous. Ces deux paramètres permettent de définir le rapport d/Λ traduisant la fraction d'air présente dans la fibre. Les avantages de ce type de fibre sont multiples, les propriétés de propagation peuvent être contrôlées par la géométrie (régime de propagation, dispersion …)

L'application principale des guides d'ondes et fibres de chalcogénures est la spectroscopie dans le moyen infrarouge. Il est alors important de noter qu'il existe très peu ou pas de sources larges brillantes et laser dans la fenêtre 2-12µm. Et finalement encore aujourd'hui la source large bande infrarouge la plus utilisée reste l'émission d'un corps noir. Les verres de chalcogénures de par leurs priorités dans le moyen infrarouge sont des matériaux prometteurs pour la réalisation de nouvelles sources. Deux approches actives sont possibles, l'utilisation de dopage par des terres rares et la génération en optique non linéaire de sources supercontinuum. Les travaux effectués dans cette thèse concernent l'étude d'objets optiques exploitant cette deuxième approche c'est-à-dire l'utilisation de phénomènes optiques non linaires pour la génération d'une source supercontinum.

Un état de l'art des résultats de supercontinua obtenus dans les fibres de chalcogénures est présenté dans le tableau 2. On notera que l'étude bibliographique effectuée, sur la génération de supercontinuum dans les fibres de chalcogénures a été publié en 2018 dans le cadre de la présente thèse [1].

Table 2 : Exemple de supercontinua obtenus dans les fibres et guide d'onde en verres de chalcogénures [1]

Composition de la fibre	Largeur spectrale du supercontinua	Longueur d'onde de pompe (durée impulsion)	Puissance moyenne obtenue
*Ge-Sb-Se	1.4 – 13.3 µm	4-7 µm (100fs)	0.7 mW
*As_2-S_3	1.9 – 4.8 µm	2-2.4 (> 100 ps)	565 mW
*As_2-S_3 & As_2-S_3	1.6-11 µm	Cascade de 1.5 à 6.5 µm (200-300fs)	140 mW
**As2S3	2.1-3.2µm	2.5µm(100fs)	-
**As2S3	1-2.6µm	1.55µm(400fs)	-
**$AsSe_2$-As_2S_5	1.2-5.37µm	3.3µm(200fs)	214mW(input)
**$As_{38}Se_{62}$	1.9-7.1µm	cascade from 1.55 to 4.5 µm (3 ns)	6.5 mW
**$Ge_{10}As_{22}Se_{68}$	1-11.5µm	4µm (252 fs)	35,4 mW
**$Ge_{10}As_{22}Se_{68}$	1-8µm	4µm (252 fs	57.3 mW
***As-Se	2-15 µm	9.8 (170 fs)	-
***Ge-As-Se	2-10 µm	4.18 (330fs)	-

*-*Fibre à saut d'indice ; ** fibre microstructurée, *** guide d'onde*

Les sources ainsi obtenues sont très prometteuses et provoquent un fort engouement de la communauté scientifique. Ces sources sont des sources fibrées, brillantes, cohérentes spatialement et dépassent les performances en densité spectrale de sources large bande générées dans les synchrotrons. Dans ce contexte, les supercontinuums ainsi générés dans les verres et fibres de chalcogénures ouvrent la voie vers de nouvelles techniques de microscopie infrarouge. D'ailleurs, en 2017, des images dans le moyen infrarouge de cellules ont été réalisées avec un supercontinum généré dans une fibre microstructurées en verres de chalcogénures.

Chapitre 2: Photo inscription de guides d'onde dans les verres de chalcogénures

De la même façon que pour les fibres optiques, les études et le développement de guides d'onde sont motivés par de futures applications dans le domaine de la spectroscopie et des capteurs dans le moyen infrarouge. Là encore, le but est d'exploiter la transparence des verres de chalcogénures au-delà de 10 µm. Une des solutions pour l'élaboration de guides d'onde avec les verres de chalcogénures est la réalisation de guides d'onde par photo-inscription. La photosensibilité des verres de

chalcogénures et la possibilité d'induire des changements d'indice de réfraction sous l'action de la lumière ont été largement démontrées. La variation d'indice peut alors avoir diverses origines, photo-contraction, changements structuraux, relaxation thermique, formation de nano pores et suivant les cas, la variation d'indice peut être soit négative soit positive. Le plus souvent, les méthodes de photo-inscription de guide utilisent les variations positives de l'indice. En effet, l'augmentation locale de l'indice peut alors être utilisée pour le guidage par l'indice de la lumière.

Dans le cadre de cette thèse, 3 verres de chalcogénures ont été étudiés, le premier est un verre commercial de Ga-La-S ($70Ga_2S_3{:}24La_2S_3{:}6La_2O_3$, ou encore GLS) et le deux autres verres ont été fabriqués au laboratoire : les verres $Ge_{20}As_{20}S_{60}$, et $Ge_{15}As_{15}S_{70}$. Des études antérieures, sous l'action d'impulsions femto secondes à 800 nm, avaient montré des variations positives de l'indice de réfraction de l'ordre de 10^{-3}. Les premiers résultats indiquaient alors que l'origine de l'augmentation de l'indice semblait provenir d'une photo-contraction obtenue par une relaxation locale du verre. Il a souvent été noté que lorsque l'énergie engagée dans la photo-inscription devient trop importante, la variation d'indice est presque toujours négative et très souvent causée par la présence de nanopores dans les zones exposées.

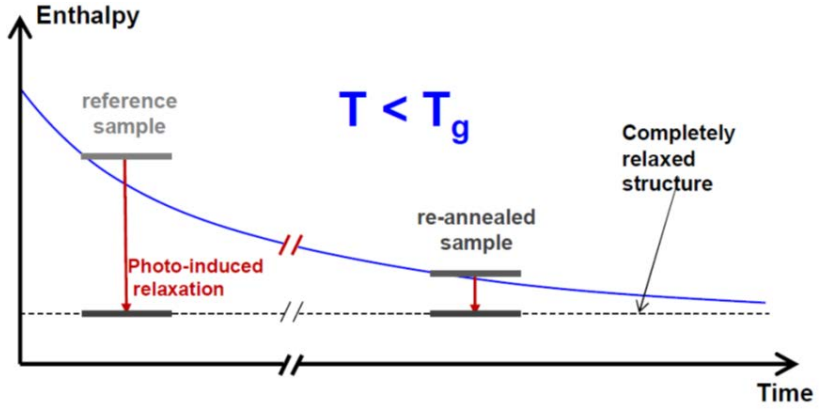

Figure 3: Principe de la relaxation thermique d'un verre photo –relaxé

Dans la cadre de cette thèse, afin de mieux comprendre les phénomènes engagés lors de la photo-inscription, de nombreux essais en fonction de l'histoire thermique des verres ont été entrepris. L'idée première lorsque la variation d'indice est provoqué par une relaxation locale est que la lumière agit comme un recuit local. La conséquence est alors une diminution locale de volume de verre, une densification et

donc une augmentation de l'indice de réfraction (Figure 3). Dans ce modèle, on comprend alors que l'état initial du verre est fondamental (Figure 3).

La photo-inscription des 3 verres: GLS, $Ge_{20}As_{20}S_{60}$, and $Ge_{15}As_{15}S_{70}$ a alors été étudiée en fonction de différents cycles thermiques. Les verres sont traités thermiquement à une température maximum, entre 0.7 et 0.8 fois leur température de transition vitreuse (figure 4a), puis leur comportement vis à vis de la photo inscription est mesuré en statique et en dynamique (avec translation de l'échantillon). Les résultats principaux obtenus sont présentés dans la figure 4.

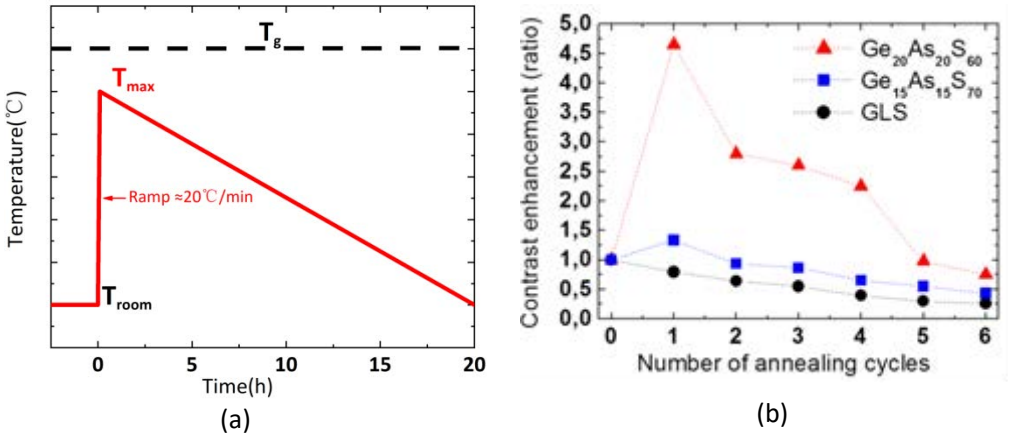

Figure 4: (a) Profil d'un cycle thermique ou recuit (b) variation d'indice mesurée après chaque cycle thermique (ou recuit)

On remarque alors que les 3 verres de chalcogénures ne présentent pas le même comportement vis-à-vis de la photo-inscription en fonction du nombre de cycles thermiques (figure 4b). Le GLS présente un comportement totalement en accord avec un modèle de pure relaxation structural. En effet, pour celui-ci, le contraste d'indice obtenu après chaque cycle diminue fortement. Cela s'explique simplement par le fait que la photo-relaxation à moins d'effet sur un verre qui devient de plus en relaxé (suite à l'enchainement de plusieurs cycles de recuit). Par contre, le verre $Ge_{15}As_{15}S_{70}$, et c'est encore plus marqué pour le verre $Ge_{20}As_{20}S_{60}$, montrent que la photo-inscription est plus efficace après le ou les traitements thermiques. Par exemple, le contraste d'indice obtenu dans le $Ge_{20}As_{20}S_{60}$ (dans les mêmes conditions laser de photo-inscription) est 4 fois plus important après un premier recuit. Ce comportement du verre $Ge_{20}As_{20}S_{60}$ a été confirmé lors de l'inscription de guide d'onde. En effet, il a

été montré que le même confinement de lumière (et donc de contraste d'indice) peut être obtenu en multipliant par 4 la vitesse de deplacement pendant la photo-inscription (Figure 5).

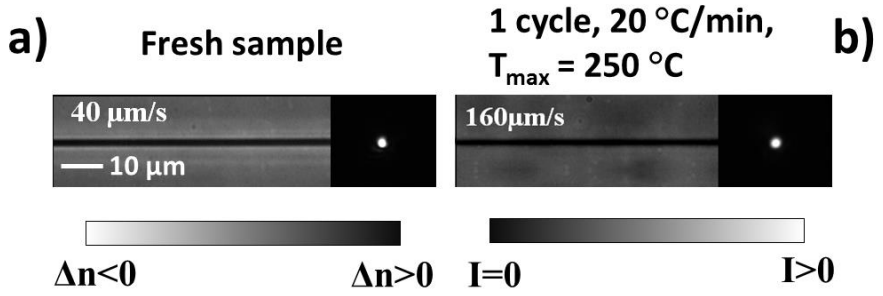

Figure 5 : Contraste d'indice et guidage obtenu (@ 800 nm) dans des guides d'onde photo-inscrits dans un verre de $Ge_{20}As_{20}S_{60}$ (a) dans verre sans recuit (b) dans un verre après un cycle de recuit.

Malheureusement, et ce malgré les efforts entrepris, l'ensemble des caractérisations effectuées pendant cette étude, n'a pas permis de trouver une explication et une origine claire à ce comportement atypique du verre $Ge_{20}As_{20}S_{60}$ (et dans une moindre mesure du verre $Ge_{15}As_{15}S_{70}$). Cependant, ces résultats ont été communiqués à la communauté scientifique à travers la publication d'un article paru en 2018 [2].

Chapitre 3: Elaboration de fibres innovantes en verre de chalcogénures pour la génération de supercontinuum

Dans ce dernier chapitre, trois approches différentes, trois types de fibres innovantes vont être développées. L'objectif principal est toujours de proposer des fibres permettant la génération de nouvelles sources dans le moyen IR. Les premières fibres sont des fibres à base de tellurures qui seront développées pour déplacer vers les grandes longueurs d'onde la coupure multiphonon. La deuxième étude présentée dans ce chapitre est la fabrication inédite de fibres à gradient d'indice en verre de chalcogénures. Puis la dernière partie est consacrée au développement de fibres hybrides en verre de silice et verres de séléniures.

A/ Fibres de tellurure $(GeTe_4)100-x(AgI)x$

Dans cette étude, les verres de composition $(GeTe_4)100-x(AgI)x$ avec x = 5, 10, 15, 20, 25 et 30 ont été synthétisés par la méthode de fusion-trempe dans des tubes sous vide dans le but de réaliser des fibres optiques monoindices dans un premier temps, puis des fibres à saut d'indice dans un second temps, transmettant le plus loin possible dans l'infrarouge. Afin d'obtenir les meilleures transmissions possibles dans les fibres optiques fabriquées, un soin particulier de purification des verres a été entrepris. En effet, l'ensemble des synthèses à nécessité l'utilisation de aluminium pour fixer les résidus d'oxygène et l'utilisation de procédés de distillation des verres. La figure 6 présente la courbe d'atténuation obtenue sur le verre $(GeTe_4)_{90}(AgI)_{10}$, composition du cœur de la future fibre double indice.

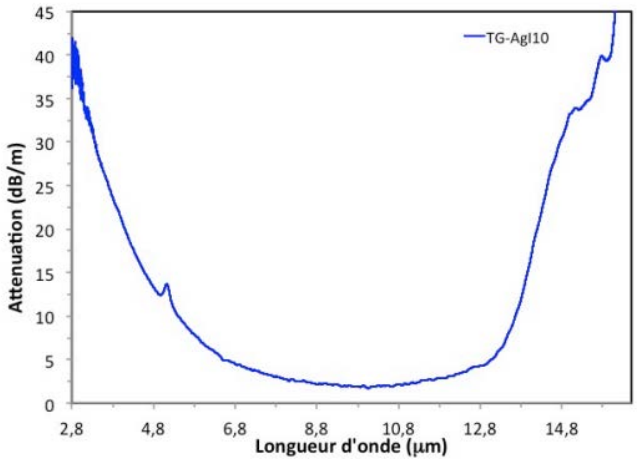

Figure 6: Atténuation de la fibre monoindice de composition $(GeTe_4)_{90}(AgI)_{10}$

Pour la réalisation d'une fibre à saut d'indice coeur gaine, deux compositions ont été sélectionnées : le verre $(GeTe_4)_{90}(AgI)_{10}$ avec un indice de 3.1143 sera utilisé pour le cœur de la fibre et le verre $(GeTe_4)_{90}(AgI)_{10}$, compte tenu de la forte tendance à la cristallisation des verres de la famille $(GeTe_4)_{85}(AgI)_{15}$, avec un indice plus faible de 3.1132 sera utilisé pour réaliser la gaine de la fibre. Dans cette étude, une méthode originale de fabrication de barreau dans tube a été utilisée. En effet, le tube de verre a été réalisé à l'aide d'une méthode de moulage. Cette méthode est couramment utilisée au laboratoire pour la réalisation de préforme microstructurée. La méthode consiste à couler le verre de chalcogénures sur un moule en silice. Ici, dans le cas des verres de tellures, le moule est constitué d'une ampoule extérieure de silice et d'un capillaire de

silice au centre. Apres avoir vérifié que les verres de tellure étaient compatibles à un traitement à l'acide fluorhydrique (étape indispensable à l'utilisation de la méthode de moulage), un tube du verre $(GeTe_4)_{85}(AgI)_{15}$ a été fabriqué avec diamètre extérieur d'environ 10 mm avec un trou d'environ 0,5 mm. Enfin, une fibre avec un diamètre extérieur d'environ 300 µm et un cœur de 16 µm a été étirée à partir du tube de $(GeTe_4)_{85}(AgI)_{15}$ réalisé par moulage, dans lequel a été inséré une fibre de 0,49 mm de composition $(GeTe_4)_{90}(AgI)_{10}$.

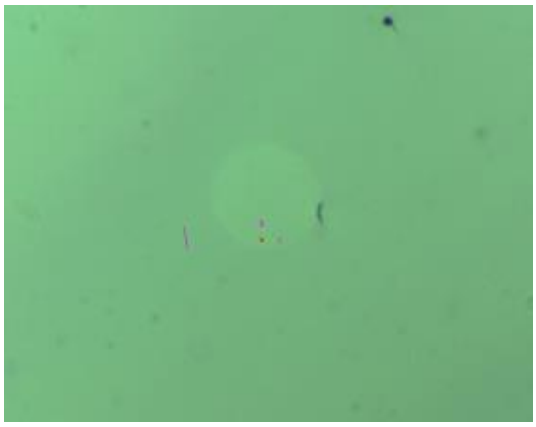

Figure 7: photo de la fibre à saut d'indice au microscope optique

Une mesure de champ proche a été effectuée afin de vérifier que la lumière se propage dans la fibre. La source utilisée est un laser CO_2 à 10,6 µm. Le faisceau laser, après avoir été focalisé par une lentille en germanium, est injecté dans la fibre et le signal est collecté en sortie de fibre sur le détecteur d'une caméra IR. On obtient ainsi une image de la sortie de la fibre. Ensuite, afin de vérifier que le cœur de la fibre transmet la lumière, du carbone est déposé sur la fibre dans le but de vider les modes se propageant dans la gaine. Cependant, aucun faisceau lumineux n'a été détecté en sortie du cœur de la fibre. Ceci peut s'expliquer par la faible différence entre les indices de réfraction du cœur et de la gaine. De plus, le processus de fibrage produit des vapeurs d'iode ce qui induit une modification de la composition de la fibre et ainsi diminue la différence d'indice entre le cœur et la gaine, empêchant le guidage de la lumière dans le cœur. Pour les prochains fibrages, il faudra donc choisir deux compositions de verre avec des indices de réfraction plus contrastés pour éviter ce problème. Il est également possible que la fibre de cœur soit cristallisée. Enfin, l'intérieur et l'extérieur du tube n'ont pas été polis. Afin de remédier à ces deux

dernières hypothèses, un travail de polissage plus approfondi devra être réalisé.

B/ Fibres à gradient d'indice en verres de chalcogénures

Lors de la réalisation de source par génération de super continuum, la gestion de la dispersion de la fibre est fondamentale. Les fibres doubles indice n'offrent que très peu de latitude sur le profil de dispersion. Une réponse possible est la fabrication de fibres à gradient d'indice. On notera qu'aucune fibre de chalcogénures à gradient d'indice n'a jamais pu être fabriquée. L'approche proposée ici est inspirée de la fabrication des fibres microstructurées. L'idée est de réaliser une fibre avec un cœur en gradient d'indice en utilisant des centaines voire des milliers de plots d'indice décroissant, du centre vers la gaine de la fibre (Figure 8). Dans cet objectif, une préforme constituée de plus de 800 barreaux de verres a été étirée sous forme de cane. Cette cane a été ensuite insérée dans un tube de la composition des plots de bas indice et à nouveau fibrée. Dans notre cas, les plots de haut indice seront le verre d'$As_{38}Se_{62}$ (n@1.55µm = 2.81) et les plots de bas indice ainsi que le tube de gaine seront en $Ge_{10}As_{22}Se68$ (n@1.55µm = 2.62).

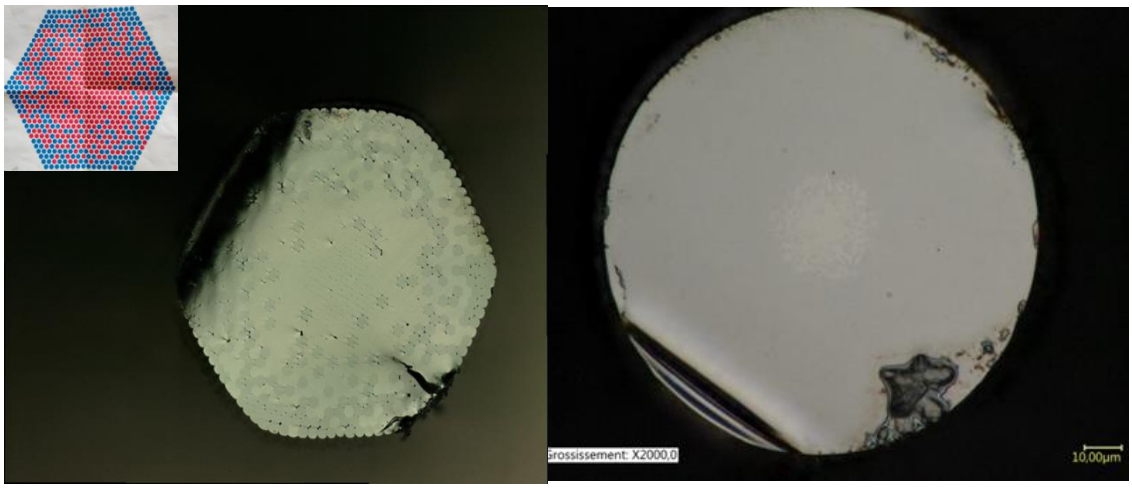

Figure 8: Fabrication d'une fibre chalcogénures à gradient d'indice, (a) architecture des plots de bas indice (en bleu) et haut indice (en rouge), (b) section de la cane obtenue (3mm de diamètre), (c) section de la fibre obtenu

Les fortes pertes optiques dues à une cristallisation excessive du verre de haut indice, n'a pas permis de mettre évidence la propagation d'ondes lumineuses dans le cœur à gradient d'indice. Cependant, au cours de cette étude de nombreuses

difficultés techniques ont été surmontées et il a été montré qu'il était possible de réaliser une telle fibre avec des verres de chalcogénures. Dans un prochain essai, le verre d'$As_{38}Se_{62}$ sera remplacé par un autre verre plus stable.

C/ Fibres hybrides silice-chalcogénures

Depuis une vingtaine d'années, la communauté scientifique montre un fort engouement pour les fibres en verre de silice, hybrides et/ou multi-matériaux. La réalisation de fibres hybrides silice-chalcogénures poursuit 2 buts, le premier comme dans l'ensemble de la thèse, est de réaliser des fibres optiques exploitant la non linéarité et la transmission moyen infrarouge des verres de chalcogénures pour la génération de supercontinuum. Mais également, dans cette étude, la réalisation de cages à photon a été mise en œuvre en exploitant les indices de réfraction élevés des verres à base de soufre, sélénium et /ou tellure

Les températures utilisées pour fibrer la silice sont comprises entre 1700 et 2000 °C et sont incompatibles avec les températures de mise en forme des verres de chalcogénures. Le procédé qui sera utilisé pour réaliser les fibres hybrides silice-chalcogénures se fera donc en deux étapes: fibrage d'une fibre microstructurée avec inclusions d'air (collaboration avec l'université de Lille), puis infiltration des inclusions d'air par les verres de chalcogénures. Le principe est alors assez simple: la première extrémité de la fibre à trous en verre de silice est placée dans un bain liquide de verre de chalcogénures. La deuxième extrémité est connectée à une pompe à vide afin "d'aspirer" le verre de chalcogénures dans les inclusions de la fibre en silice. Cette première étude a été réalisé avec un verre de chalcogénures présentant une Tg assez faible (pour faciliter le remplissage des trous) et très stable vis-à-vis de la cristallisation, le verre $Te_{20}As_{30}Se_{50}$.

Les premiers essais ont montré qu'il était possible de remplir les trous d'une fibre en silice sur 8 cm de long. On notera que cette longueur de remplissage est suffisante pour l'observation d'effets non linéaires et pour l'obtention de cages à photon. Cependant, la totalité des inclusions ne sont pas remplies, dans le meilleur des cas 70 % de remplissage a pu être obtenu (Figure 9). Cette première étude a été

effectuée afin de montrer qu'il était possible de réaliser des fibres hybrides par ce procédé. De nombreuses optimisations sont possibles: augmentation de la qualité du vide appliqué, application d'une pression sur le bain fondu, mais aussi optimisation de la qualité de la section de la fibre de silice plongée dans le bain fondu.

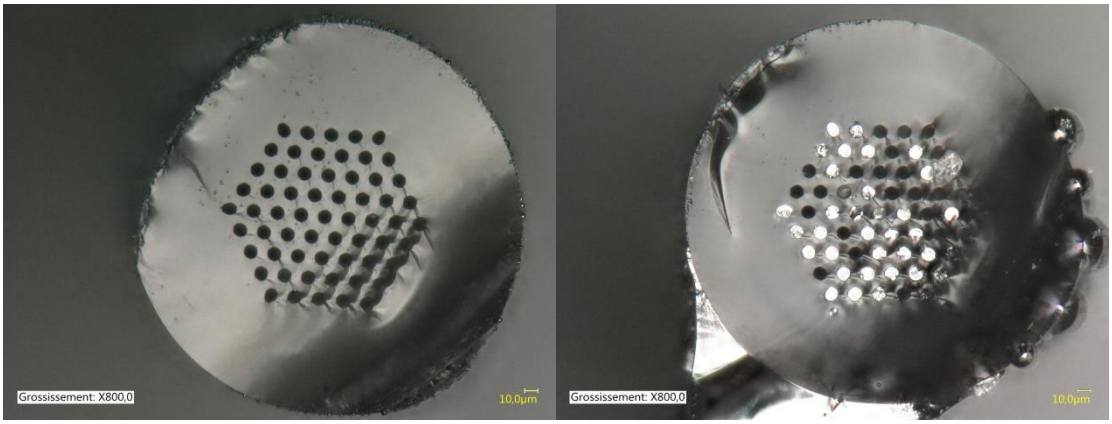

Figure 9: section de fibre en silice microstructurées avant et après remplissage des trous par le verre de chalcogénures

Comme très souvent, l'ensemble des résultats obtenus dans le cadre de cette thèse répondent à peu de questions posées et offrent encore plus d'interrogations. Mais n'est-ce pas là, l'expression du plus grand malheur et grand plaisir de la recherche scientifique !

Articles publiés au cours de la thèse

[1]. Y. M. Wu, M. Meneghetti, J. Troles, and J. L. Adam, "Chalcogenide Microstructured Optical Fibers for Mid-Infrared Supercontinuum Generation: Interest, Fabrication, and Applications," Applied Sciences-Basel **8** (2018).

[2]. M. Somayaji, C. D'Amico, Y. Wu, J. Troles, and R. Stoian, "Influence of Thermal Annealing on Ultrafast Laser-induced Local Densification in Bulk Sulfur-based Chalcogenide Glasses," Physica Status Solidi A: Applications and Materials Science (2018).

General Introduction

Chalcogenide glasses are a non-oxide class of glasses that are mainly composed by one or more chalcogenide elements in group VI of the periodic table, such as sulfur, selenium, and tellurium, in combination with other metalloid elements like arsenic, antimony, germanium, etc. These elements provide the existence of a broad range of possible glass forming systems with large composition space and good resistance to crystallization yields glasses with optical properties such as nonlinearity, photosensitivity and infrared transparency, which can all be optimized for photonic applications.

Normally, Chalcogenide glasses are covalently bonded with heavy elements, which gives them some extraordinary properties for applications in the infrared region, nonlinear and waveguide optics. Duet to their inter-atomic bonds are weak relative to those in oxides, the bandgap of Chalcogenide glass is redshifted to the visible or near-infrared region of the spectrum. The vibrational energies of the bonds are low because the constituent atoms are particularly heavy, which means that Chalcogenide glasses are transparent into the mid-infrared and, as a consequence, their low phonon energies make them interesting hosts for rare-earth dopants. Therefore, Chalcogenide glasses has been well applied in a various of research fields, especially based on the optical and nonlinear properties they possess. Of all the applications of Chalcogenide glasses, supercontinuum generation in the Mid-infrared range is of particular interest, as most of the molecular fingerprint lies in this region and both waveguides and fibers made of Chalcogenide glasses have been utilized in it. Mid-infrared supercontinuum generation can be achieved in different types of materials such as fluoride glass and tellurite glass, due to the intrinsic limitations, it is difficult to extend the wavelengths coverage of the supercontinuum over 5μm. Besides, the dispersion profile of the glass and fiber is essential for efficient generation of Mid-infrared supercontinuum. Thus, different format of Chalcogenide glass such as waveguides and fibers with broader

transmittance range, more flexibility of dispersion modification and innovative structure are needed for Mid-infrared supercontinuum generation.

In the first chapter, basic properties of Chalcogenide glasses are introduced as well as the optical and thermal properties which exhibit the potential of Chalcogenide glasses and fibers for the application in the Mid-infrared region. The different structure and fabrication methods of chalcogenide glass fibers will be listed. And also the advantages and disadvantages of the Mid-infrared supercontinuum generation in fluoride fibers, tellurite fibers, step-index Chalcogenide fibers and micro-structured Chalcogenide fibers will be compared.

Chapter two is dedicated to investigating the enhancement of the refractive index contrast of the Chalcogenide waveguides to thermal treatment. Three compositions of chalcogenide waveguides will be undergoing a thermal annealing treatment to test the change of the enhancement of the refractive index contrast under laser irradiation in two different conditions (static condition and dynamic condition). Different behaviors of the waveguides will be verified and the inner mechanism will be analyzed and discussed.

In chapter three, the fabrication of Te-Ge-AgI step-index fiber will be presented first. By measuring the thermal and optical properties of different glass composition, the compositions for the core and cladding of the step-index fiber will be selected. A two-steps purification for achieving a better quality of the fiber will be introduced. With the aid of a modified casting method, the designed step-index structure is achieved and the fiber drawn from the preform will be measured and tested. Then, we will introduce a grade-index Chalcogenide fiber for a higher flexibility of dispersion engineering. Two glass compositions with similar thermal properties are selected and drawn into rods. By stacking the rods as previously designed and collapsing them, a cane will be obtained. After inserting the cane into the cladding tube achieved by rotation method, the fiber preform will be assembled. And the final graded-index fiber drawn from the fiber preform will be measured and light propagation in it will be tested. In the last part of chapter III, a hybrid fiber structure will be illustrated. The fiber is made by inclusion of Te-As-Se glass in to the air holes of silica photonics

crystal fiber. The hybrid structure is realized by immersing one end of the silica photonics crystal fibers in melted the Te-As-Se glass and the other end to vacuum pump. The factors that affect the obtained results will be investigated and discussed.

Chapter I Chalcogenide glasses and fibers and Mid-infrared Supercontinuum generation

1.1 General properties of Chalcogenide glass

Chalcogenide glasses (ChGs) are a group of inorganic glassy materials which are normally formed with one or several different kinds of the chalcogenide elements from group 6a of the periodic table, such as Sulphur, Selenium and Tellurium, but excluding oxygen. And usually they are covalently bonded to network formers such as Arsenic, Germanium, Antimony, Gallium, and Silica. Chalcogenide glasses are also an important class of amorphous semiconductors for which they have a variety of applications in phase-change memories, solar cells, sensors and photonics devices.

1.1.1 Compositions and structure

As described in [1], the components elements of chalcogenide glasses have relatively similar electronegativity and consequently they form well defined directional covalent bonds following the 8-N octet rule [2]. Then, the glass structure of chalcogenide can be described as a network of covalent bonds. There has been numerous investigations dedicated to the ranges of glass formation and structures of chalcogenide glasses [3-8], and a variety of glass compositions have been synthesized and tested, for example As-S, As-Se,As-Se-S,Ge-S,Ge-As-S,Ge-As-Se,Ga-La-S and etc. And of all the glass compositions, more enthusiasm has been focused on glasses composed of Arsenic and Germanium.

As a matter of fact, chalcogenide glasses have been the main content of many investigations aimed at establishing correlations between macroscopic physical properties and the microscopic connectivity of the amorphous network, of which they are mainly from Phillips [9], Thorpe et al [10], Tanaka [11] and Boolchand et al [12].One of the One of the main appeals of the model brought up by Philips and thorp was its ability to characterize a given glass using a single structural parameter $<r>$ called the average coordination or mean coordination. The mean coordination is a measure of the network connectivity and corresponds to the average number of covalent bonds per atom according to:

$$< r >= r_i a_i \quad (1.1)$$

where a_i is the molar fraction and r_i is the covalent coordination of atom i. For a normal binary chalcogenide glass, the network is a two-dimensional structure bonded by weak van der Waal between the layers, as in As_2Se_3. When four-fold-coordinated atoms like Germanium is inserted into the structure, it will transform the two-dimensional network into three dimensional networks by creating now bonding among the layers and further improve the rigidity, glass transition temperature (T_g), strength and hardness. In Ref [10], it was found that there existed a phase transition when MCN is 2.4, at which an under-constrained 'floppy' network would become an over-constrained "rigid" phase. Also, a second phase transition where MCN was equal to 2.67 was found in Ref [11], proving a topological change from a two-dimensional to a three-dimensional 'stressed rigid' phase [9-11, 13] .

1.1.2 Thermal properties

Thermal analysis is one of the most ubiquitous set of measurement techniques in glass science, and can deliver information about glass structure and properties over a wide range of length scales and application areas. Due to the fundamental differences in chemistry between chalcogenide glasses and their oxide counterparts, the thermal behavior and response of these glass families is markedly different in many important ways.

Differential scanning calorimetry

Differential scanning calorimetry (DSC) is a thermal analysis technique that measures the heat flow into or out of a sample as a function of temperature, and it is normally used to detect thermodynamic transitions processes such as glass transition, crystallization or melting. Typical procedure is to put the glass sample powder in order to increase the surface area for heat transfer, then it is heated in an inert sample pan and the heat flux is compared to that of an adjacent, empty, reference pan. Phase transitions are detected through the differential in heat flow supplied to the sample and reference pans; for example, the first-order phase transition of crystallization is an

exothermic event, meaning that less heat flow is required from the calorimeter heaters to the sample pan in order to maintain the sample and reference pans at equivalent temperatures. Thus the difference in the heat flow supplied to the reference and sample shows a maximum during the phase change from amorphous to crystalline network structure. Figure 1.1 shows a representative DSC trace for a multi-component chalcogenide glass, indicating the positions of the glass transition (T_g), crystallization onset (T_x), crystallization peak (T_p), and melting peak (T_m).

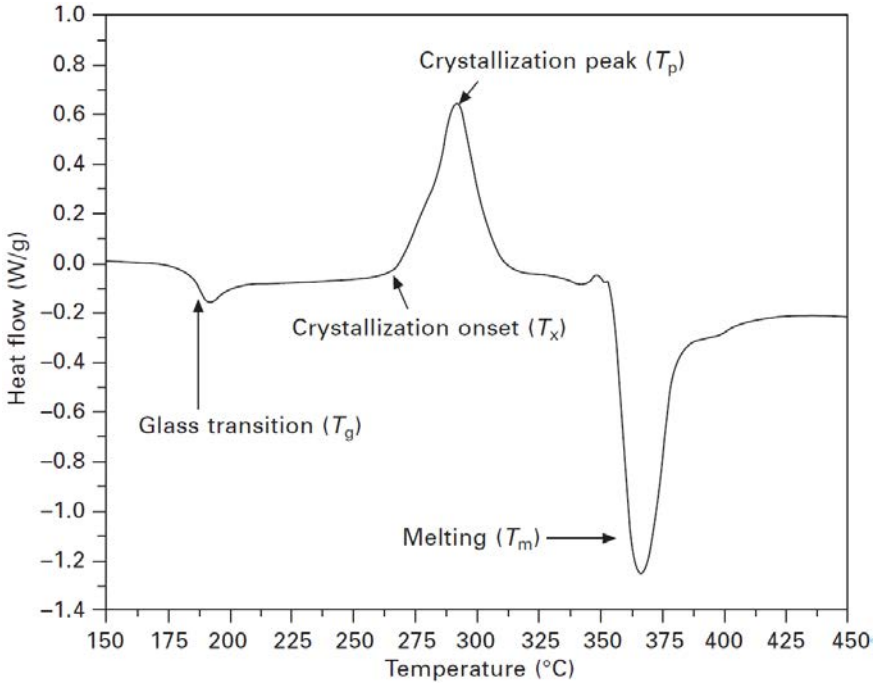

Figure 1.1 Example of a DSC trace for a multicomponent chalcogenide glass showing the characteristic temperatures of interest [1].

Glass transition temperature

The glass transition process is one of the most important thermal characteristic of an amorphous material in determining its utility in different fields, since it imply the temperature at which the material stops behaving as a rigid solid and begins to show the mechanical response of a deeply super cooled liquid. The temperature of this change in mechanical response and its relationship to the onset of melting is critical in hot-forming applications in glasses in general, and chalcogenide glasses in particular, which tend to have much smaller working temperature ranges than oxide glasses. In

addition to its utility in optical applications, the glass transition is also profoundly interesting from a fundamental science perspective. Though the existence of a glass transition is one of the defining characteristics of glass as an amorphous solid, the precise atomic-scale nature of the transition is still not completely understood.

Crystallization stability

Crystallization stability represents the temperature difference between the glass transition and the onset of crystallization (i.e., $\triangle T = T_x - T_g$), which determines the suitability of a given chalcogenide glass composition for various hot-forming applications. Stability towards crystallization in hot-forming processes represents a balance between the need to deform the glass, which must be above its glass transition temperature in order to flow, and the need to retain a crystal-free network in order to maintain the optical properties and shaping amenability of the amorphous material. It has been suggested that a minimum $\triangle T$ of 120 ℃ is needed to provide a sufficient temperature difference for applications such as fiber drawing, and multi-component systems which show a lower tendency for crystallization. As an example, Table 1.1 shows the evolution of the crystallization stability window as a function of composition in a four-component series of glasses as the chalcogen element is gradually changed from sulfur to selenium.

Table 1.1 Glass transition and crystallization temperatures, with corresponding stability windows, for two families of chalcogenide glasses [1]

Composition	T_g(℃)	T_x(℃)	$\triangle T$(℃)
$Ge_{28}Sb_{12}Se_{60}$	341	526	185
$Ge_{28}Sb_{12}S_{45}Se_{15}$	322	510	188
$Ge_{28}Sb_{12}S_{30}Se_{30}$	319	493	174
$Ge_{28}Sb_{12}S_{15}Se_{45}$	322	497	175
$Ge_{28}As_{12}Se_{60}$	404	424	120
$Ge_{28}As_{12}S_{45}Se_{15}$	386	515	129
$Ge_{28}As_{12}S_{30}Se_{30}$	377	511	134
$Ge_{28}As_{12}S_{15}Se_{45}$	375	508	133
$Ge_{28}As_{12}Se_{60}$	341	504	163

1.2 Optical properties of Chalcogenide glasses

Optical transmission

The optical transmission range of chalcogenide glasses is an essential property. It is determined by three factors: the electronic absorption at short wavelengths, multi-phonon absorption at long wavelengths, and Rayleigh scattering in between. There also exists another loss mechanism namely the weak absorption tail (WAT) which is unique to chalcogenide glasses. And other losses are normally caused by the impurities of the glass during synthesis. Although the theoretical estimation of the attenuation of chalcogenide glasses can be as low as 0.1-0.01dB/km, the actual attenuation obtained is still much higher. The practical attenuation can be described as the sum of the absorption and scattering losses, defined as:

$$\text{Absorption loss} = A_0 \exp\left(\frac{A}{\lambda}\right) + B_0 \exp\left(-\frac{B}{\lambda}\right) + \sum c_i C_i + D_0 \exp(D/\lambda) \quad (1.2)$$

$$\text{Scattering loss} = \frac{\mathrm{E}}{\lambda^4} + \frac{\mathrm{F}}{\lambda^4} + \frac{\mathrm{G}}{\lambda^2} + \mathrm{H} \quad (1.3)$$

where the first two absorption terms represent the intrinsic electronic and multi-phonon absorptions, respectively. The third term describes extrinsic absorption due to impurities and the fourth represents the WAT. Also, the scattering losses in optical materials depend on the size of the scatter-center relative to the wavelength of the light. Rayleigh, Rayleigh-Gans, and wavelength-independent scattering are caused by scattering centers much smaller than, approximately the same size as, and much larger than the optical wavelength, respectively. Rayleigh scattering can be material intrinsic, arising from density and composition fluctuations frozen into the glass upon cooling from the melt or extrinsic, as impurities and defects. The first and second terms in equation1.3 represent intrinsic and extrinsic Rayleigh scattering, respectively. The third and fourth terms represent Rayleigh-Gans and wavelength-independent scattering, respectively, also arising from extrinsic defects [14].

The infrared cutoff is determined by the multi-phonon absorption edge and is governed by vibrational resonances of the atomic network which depend on atomic mass and bond strength. For glasses with larger atoms and weaker bonds, as is the

intended case for chalcogenide glasses, this vibrational resonance occurs at lower frequencies, pushing the fundamental absorption infrared cutoff to longer wavelengths.

Refractive index

Chalcogenide glasses in general have larger refractive indices than other glasses, due to the considerable degree of polarizability of the chalcogenide elements. Refractive index for chalcogenide glasses can range from 2.2 for germanium arsenic sulfides to 3.4 for glasses with large tellurium concentrations. Indices of refraction for several chalcogenide glasses are summarized in Table 1.2.

Table 1.2 Optical index, n_0, and nonlinearities for chalcogenide glasses measured at 1.55 mm [15-17]

Glass	n_0	λ_{gap}(μm)	$n_2/n_2(SiO_2)$	Reference
$Ge_{25}SE_{75}$	2.7	0.60	120	[16]
$Ge_{25}Se_{65}Te_{10}$	2.5	0.72	220	[16]
$Ge_{28}Se_{60}Sb_{12}$	2.61	0.69	360	[16]
$As_{40}Se_{60}$	2.78	0.70	500	[16]
$As_{40}Se_{60}$	2.81	0.70	930	[15]
$As_{39}Se_{61}$	2.81	0.70	660	[15]
$As_{40}Se_{55}Cu_5$	2.93	0.79	850	[15]
$As_{25}Se_{55}Te_{20}$	2.52	0.79	470	[15]
$As_{40}S_{60}$	2.45	0.52	220	[15]
$As_{40}S_{50}Se_{10}$	2.49	0.55	380	[15]
$As_{40}S_{40}Se_{20}$	2.55	0.59	300	[15]
$As_{40}S_{30}Se_{30}$	2.62	0.62	430	[15]
$As_{40}S_{20}Se_{40}$	2.70	0.64	460	[15]
$As_{40}S_{10}Se_{50}$	2.76	0.67	560	[15]
$Ge_{15.38}As_{30.77}S_{53.85}$	-	0.49	130	[17]
$Ge_{15.38}As_{30.77}S_{32.31}Se_{21.54}$	-	0.56	250	[17]
$Ge_{15.38}As_{30.77}S_{10.77}Se_{43.08}$	-	0.61	390	[17]
$Ge_{20}As_{40}Se_{40}$	-	0.68	620	[17]

$Ge_{12.5}As_{25}Se_{62.5}$	-	0.63	450	[17]
$Ge_{11.1}As_{22.2}Se_{66.67}$	-	0.63	530	[17]

It can be concluded from the data that there exists some general evolutions of refractive index. As the polarizability of the chalcogenide elements increases with atomic weight, the refractive index increases, which can be found in replacing selenium in As_2Se3 with larger, and more polarizable tellurium increases the refractive index, while the lighter, less polarizable sulfur decreases the refractive index. Addition of germanium or silicon lowers the refractive index, while lead, tin and antimony increase it [18].

1.3 Chalcogenide glass fibers

Chalcogenide glass fiber is an important application of chalcogenide glasses. As can be seen in Figure 1.2, among glass fibers, chalcogenide glass is the only one with a transparent domain paving the Mid-IR region. The transmission varies with the constituting chalcogenide elements, like sulfur, selenium and tellurium [19]. Thus, As-S fiber can transmit from 1 to 6.5 μm [20], As-Se fiber from 1.5 to 10 μm [20], and Te-based fibers, due to heavy atom weight, can transmit further than 14μm. In terms of optical non-linearity, chalcogenide glasses possess non-linear refractive index that is 2 to 3 orders of magnitude higher than that of silica [19]. In addition, if we consider the non-linear parameter of a waveguide or fiber, defined as $\gamma=2\pi n_2/\lambda A_{eff}$, where n_2 is the refractive index, λ is the wavelength, A_{eff} is the effective mode area, the non-linear behaviors are even enhanced in small-core single-mode fibers, due to higher light density.

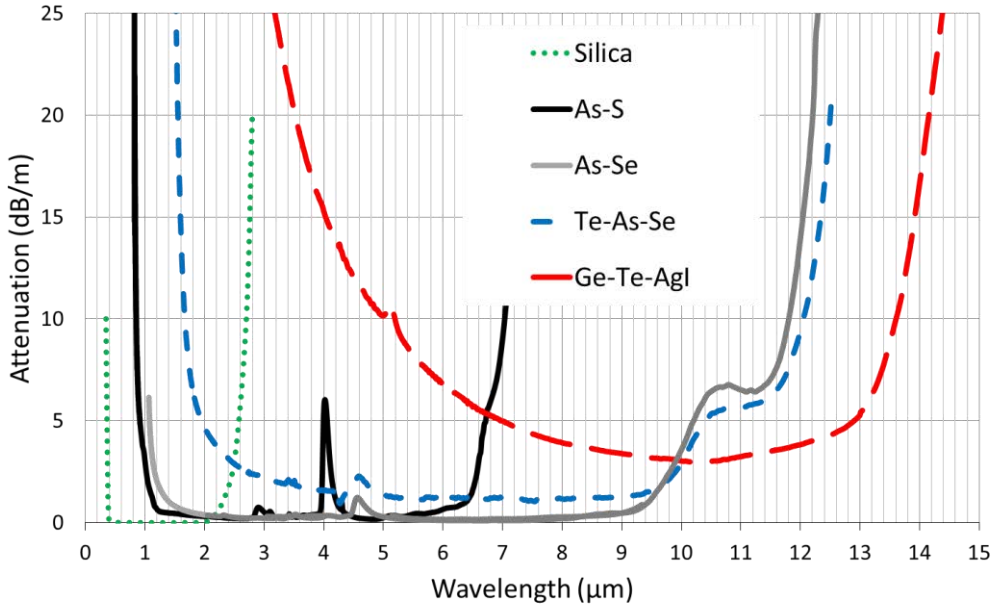

Figure 1.2 Mid-infrared attenuation of chalcogenide optical fibers in comparison to silica attenuation

In micro-structured optical fibers (MOF), the mode of the light propagating in the fiber is determined by the diameter of the air holes (d) and the distance between air holes (Λ), as depicted in Figure 1.3. Thus, single-mode guiding regardless of the wavelength can be achieved in MOF, as long as the d/Λ ratio is less than 0.42 [21, 22]. Also, by reducing the diameter of the core in MOF, the nonlinearity can be increased and the zero-dispersion wavelength (ZDW) can be controlled over a wide range of wavelengths [23]. Indeed, in order to obtain an efficient supercontinuum source, the fiber has to be pumped close to the ZDW. One of the main advantages of MOFs is to obtain strong flexibility in dispersion modification. The intrinsic ZDWs of chalcogenide glasses are normally located beyond 5µm, where it is difficult to find available powerful laser pump sources, not to mention fiber lasers. Then, it would be beneficial to shift the ZDW to a shorter wavelength: 1.55µm for the telecom wavelength, 2µm, or at least less than 4µm.

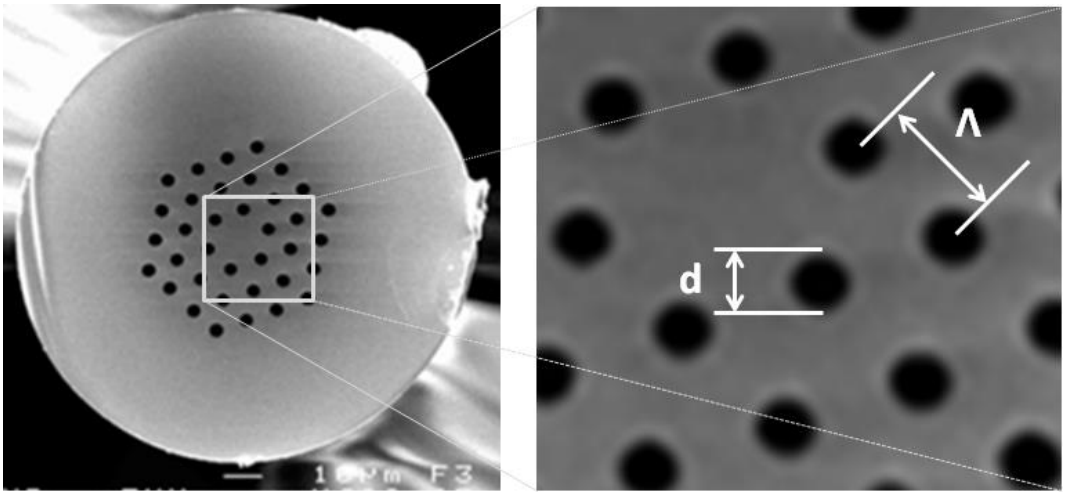

Figure 1.3 Cross section of a chalcogenide micro-structured optical fiber. d: hole size, Λ: distance between the holes

1.3.1 Fabrication of Chalcogenide glass fibers

In order to have better photonics applications, chalcogenide glass has to be synthesized under vacuum conditions and purified to avoid optical absorption caused by the presence of chemical bonds such as O-H, Se-H, and As-o or impurities such as CO_2 and H_2O. To date, several purification methods have been reported, such as the purification of raw material before synthesis [24] or using microwave treatment before synthesis [25]. Also, distillation of the glass after synthesis in presence of chemical getters proved to be efficient in reducing optical losses in fibers [26]. This last process consists in the addition of halides (such as $TeCl_4$) and metals (such as Mg or Al) to the charge before synthesis. During the melting of the charge, metals will react with oxygen-based pollutants while halides will react with hydrogen and carbon impurities. The byproducts of this reaction are either refractory or volatile, allowing for their removal by distillation of the glass.

Standard chalcogenide fibers exhibit a step-index profile that can be achieved by implementing two different fabrication methods: the “rod-in-tube” method and the double-crucible method， as is shown in Figure 1.4 [27-29]. The first technique allows a better control of the fiber-core size, and consequently of the core-clad ratio [30-32]. The second one permits a better control of the core-clad interface [33, 34], and

commercial step-index chalcogenide fibers have been fabricated by using this technique. Micro-structured optical fibers have been obtained with a variety of different glasses, including chalcogenide glasses [35, 36]. In 2000, the first chalcogenide MOF, with Ga-La-S composition, was successfully fabricated by using the "stack-and-draw" technique originally utilized for making silica MOF, yet guidance of light was not observed [35]. Later on, light propagation in chalcogenide MOFs based on sulfur and selenide was realized [37, 38]. Then, in 2006, single mode propagation in a chalcogenide MOF with Ge-Ga-Sb-S composition was reported [36]. Propagation losses of the fiber were quite high, between 15 and 20 dB/m at 1.55µm; this was attributed to the poor quality of chalcogenide glass preforms prepared by the "stack-and-draw" method [39]. Indeed, it has been shown that important defects at the interfaces between the chalcogenide capillaries constituting the stack induce strong optical losses [39].

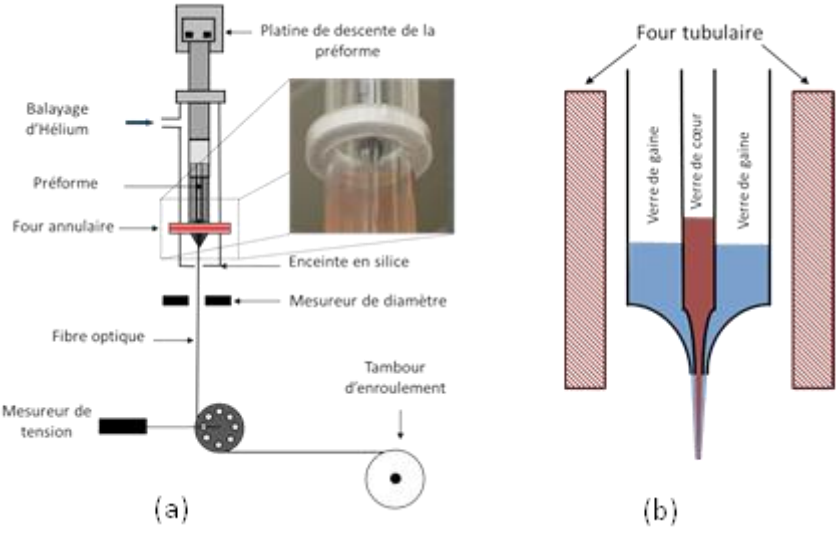

Figure 1.4 (a) Fiber Tower and (b) Double Crucible Furnace

Consequently, other fabrication methods had to be developed for chalcogenide glasses. For example, the geometry of chalcogenide MOF can be realized by "drilling method" or "casting method". The "drilling method" exploits mechanical drilling in chalcogenide glass preforms to create various geometrical structures. In order to avoid structure destruction, the position of the holes and the friction between glass and drills has to be precisely controlled. Besides, for the protection of the inner side of the holes,

it is necessary to optimize the rotation speed and the force applied by the drills [40]. For the "casting method", a mold made of silica capillaries thread in hexagonal silica guides is designed with the desired distribution of holes. Then the chalcogenide glass, which has been heated to quasi-liquid state, is poured into the mold. After, the mold & glass ensemble is quenched in air and annealed. The silica tube and capillaries, which are still inside the MOFs preform at this stage, are removed with diamond tool and soaking in 40% concentrated hydrofluoric acid [41]. Both methods have been tested for making monolithic preforms suitable for obtaining micro-structured optical fibers [38-40].

1.4 Supercontinuum generation in the Mid-Infrared region

Spectral broadening and the generation of new frequency components are intrinsic features of nonlinear optics, and have been studied intensively since the early 1960s. When optical pulses propagate through nonlinear substrates, its temporal and spectral evolution is affected not only by a variety of nonlinear effects such as Self-phase modulation (SPM), Cross-phase modulation (XPM), Four-wave mixing (FWM) and Stimulate Raman scattering (SRS), but also by the dispersive properties of the material. All of these nonlinear processes are capable of generating new frequencies within the pulse spectrum and when the pulse is intense enough, the pulse spectrum becomes so bread that it can be extended over a wide range. This particular process is known as the supercontinuum (SC) generation. Supercontinuum generation was first reported by Alfano and Shapiro in bulk glass [42, 43], and in the case of optical fibers it was first observed in 1976 by injecting Q-switched pulses into a 20m-long fiber [44]. And ever since then, it has been the subject of numerous investigations in a wide variety of nonlinear media, like solids, organic and inorganic liquids, gases, and various types of waveguide and fibers.

Compared to other light sources, SC sources poses a number of advantages as spatial coherence, broad bandwidth, and high brightness, which is the reason that

considerable attention has been paid to them due to their significant potential in various applications, such as spectroscopy [45], hyperspectral microscopy [46], and spectral tissue imaging [47]. In particular, the mid-infrared spectral region is considered to be an important field because fundamental vibrational absorption bands of most molecules lie in this region, leaving distinctive spectral fingerprints which are critical for applications, such as biomedical science [48], sensing [49], and defense and security [50].

For the generation of Mid-infrared (Mid-IR) SC generations, different types of soft-glass fibers made of fluoride [51-55], tellurite [56-58], and chalcogenide glasses [59-61] have been utilized, and numerous achievements have been accomplished. Fluoride and tellurite are both transparent in the wavelength range below 5.5 μm and thus, cannot be used for wavelengths longer than 5.5 μm. In contrast, Chalcogenide glasses have comparatively wider transparency window (over 20 μm) [62] and higher optical nonlinearity (up to a thousand times greater than that of silica glasses) [63], making them good candidates for Mid-infrared SC generation.

1.4.1 Mid-infrared SC generations in fluoride fibers

Fluoride fibers, especially heavy metal ZBLAN (ZrF_4-BaF_2-LaF_3-AlF_3-NaF) fibers are particularly attractive due to their technological maturity and low transmission losses in the Mid-infrared region, which make it one of the appropriate candidates for Mid-infrared SC generation. Meanwhile, ZBLAN fiber's zero dispersion wavelength (ZDW) is normally located between 1.6 to 1.9μm，pumping at longer wavelength in the anomalous dispersion region can easily achieve broad SC generation.

In 2006, Chenan Xia et el reported a Mid-infrared SC generation in ZBLAN fluoride fibers produced by laser diode pumping [53]. The SC extended to 4.5μm with an average power in the SC of 23mW with power conversion efficiency over 50%. The SC was induced through modulation instability in 1m of single mode fiber, and the long-wavelength edge was limited by the ZBLAN fiber loss. The SC edge was

estimated to be potentially extended beyond 5μm with modified fluoride glass compositions. Also, the SC average power could be scaled up by increasing the pulse repetition rate while maintaining approximately the same peak power and pulse width.

Then, a Mid-infrared SC generation with broader output spectrum was reported by Guanshi Qin et al in 2009. By pumping a 2cm-long fluoride fibers with a femtosecond laser centered at 1450nm with a pulse width of 180 fs and repetition rate of 1 kHz, ultra-broad SC generation expanding from ultraviolet to 6.28μm (see Figure 1.5) was generated. The spectral broadening in the fluoride fiber was caused by self-phase modulation, Raman scattering and four-wave mixing. Based on the experimental and simulated results, the fiber utilized was a promising candidate for generating the mid-infrared SC generation up to 8μm.

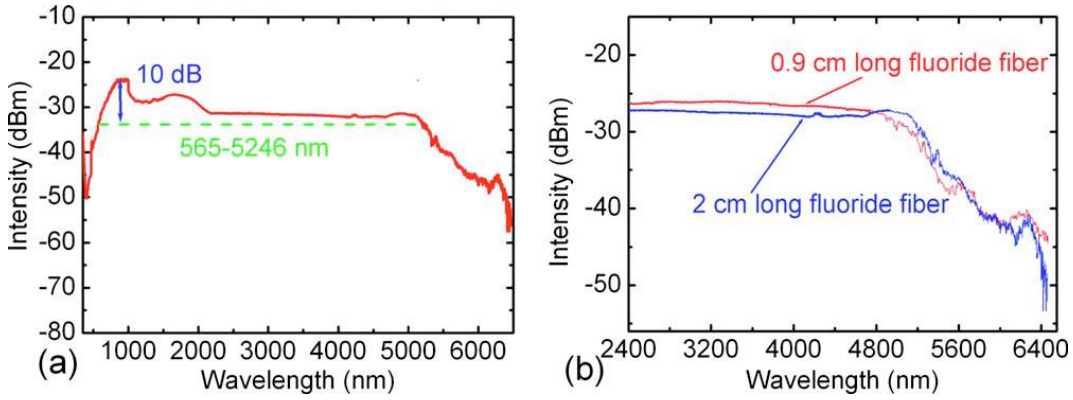

Figure 1.5 (a) The measured SC spectra from the 2-cm-long fluoride fiber when the average pump power of 1450 nm femtosecond laser was fixed at 20mW(the corresponding peak power is about 50 MW) (b) A comparison of the long-wavelength edge of SC spectra in 0.9 or 2 cm long fluoride fiber [51]

Meanwhile, different method of mid-infrared SC generation in fluoride fibers was also presented. Jacek Swiderski et al used a 2μm gain-switched self-mode-locked thulium-doped fiber laser to pump a single-mode ZBLAN fiber with a zero dispersion wavelength (ZDW) shifted to ~1.9μm in ref [54]. SC radiation ranging from 1.9 to 3.8μm with an average output power of 0.74W with 0.27W at wavelengths longer than 2.4μm was obtained.

In addition, power scaling of SC generation in fluoride fibers was also conducted. In 2015, Hongxing Shi et al presented a Mid-infrared SC generation in a single mode

ZBLAN fiber pumped by nanosecond pulses from a diode-seeded Tm-doped laser amplifier. The spectrum coverage of the SC generation was from 1900nm to 3600nm. And the output power measured from the ZBLAN fiber reached 22W at the maximum pump power, with an estimated power at wavelength ＞2.4μm about 9.5W. The overall optical conversion efficiency was calculated to be 26.8%. The schematic of the experimental setup and the output spectrum against the pump power is illustrated in Figure 1.6[52].

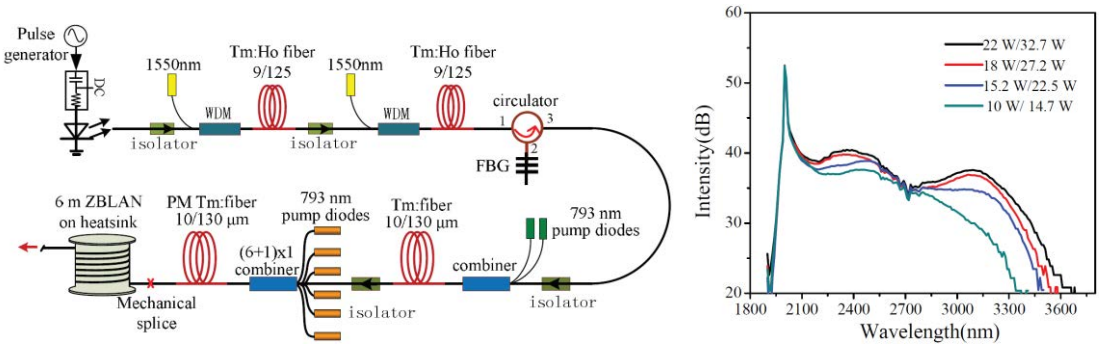

Figure 1.6 (left) schematic of the experimental setup (right) evolution of the output spectrum versus the pump power[52]

Nowadays, the maturity of fluoride supercontinuum, leads to several available commercials product from different companies, le verre fluoré, Leukos, novae, NKT and Thorlabs.

1.4.2 Mid-infrared SC generations in tellurite fibers

Besides the fluoride glass fibers, tellurite fibers (especially photonic crystal fibers) are also frequently applied in SC generation in the Mid-infrared region and also sometimes in the visible range. The interest of tellurite fiber is their nonlinear optical properties. Indeed the tellurite fibers present the same optical transmission windows than fluoride fibers but with a nonlinear refractive index 50 times higher.

As example, by using a 8-mm-long highly nonlinear tellurite micro-structured photonic crystal fiber, P. Domachuk et al [58] realized a broad bandwidth, mid-IR SC generation covering the range from 789 to 4870nm in 2008. The pump light was a femtosecond laser at 1550nm with a pulse width of 100fs and pulse energy of 1.9μJ.

The average output power of the obtained SC generation reached 90mW and the short length of tellurite fiber proved to offer a convenient pump wavelength, smoother SC spectra, lower dispersion, and reduced material absorption at longer wavelengths making the use of this PCF particularly interesting.

Besides using ultrafast pulsed laser to generate SC, quasi continuous wave laser was also applied. In 2012, Meisong Liao et al [57] reported a SC generation in highly nonlinear tellurite micro-structured fibers pumped by a continuous wave /quasi continuous wave laser. In the experiment, two fibers with different longitudinal diameter distribution was tested and it was discovered that for the fibers with a constant core diameter, when pumped in the anomalous dispersion region, the SC is symmetric in a fiber that has a zero dispersion wavelength close to the pump wavelength and for the fibers with a longitudinally varying diameter, the calculated phase-matching conditions show that they have a broad wavelength range of dispersive waves, and therefore the measured SC spectrum can be broader than one octave.

Unlike using tellurite PCF fibers with varying diameter, J. Picot-Clemente et al [56] exploited a tapered tellurite suspended core fiber for the Mid-infrared SC generation. A broadband SC generation covering 0.6-3.3μm range was achieved in a10cm-long tapered tellurite suspended core fiber pumped by nJ-level 200-fs pulses from an optical parametric oscillator. The moderate tapering procedure based on a commercial glass processing platform allowed the development of short tapers of suspended core fiber to benefit from additional increased nonlinearity and dispersion engineering which optimized the SC generation bandwidth through underlying solitons-DWs interactions and related group-velocity matching. The fiber cross section images, profiles of core diameter and outer fiber diameter and Additional optical losses induced by similar fiber tapering is shown in Figure 1.7. The obtained SC spectrum is listed in Figure 1.8.

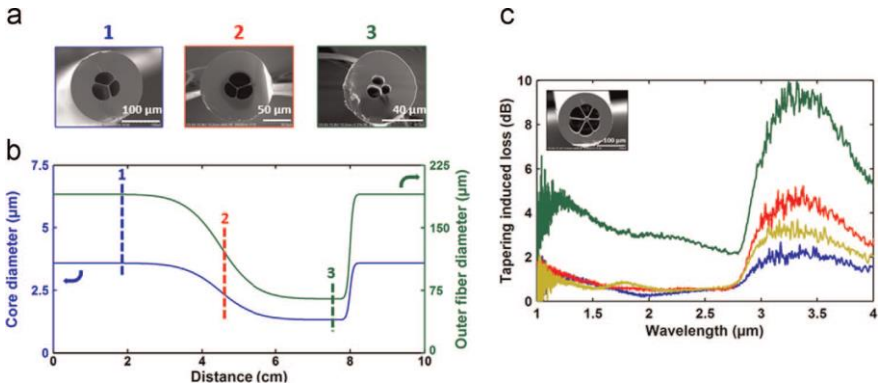

Figure 1.7 (a) Fiber cross section images at different positions along the taper. (b) Profiles of core and outer fiber diameter along our short taper based on measurements from cross-section images. (c)Additional optical losses induced by similar fiber tapering[56]

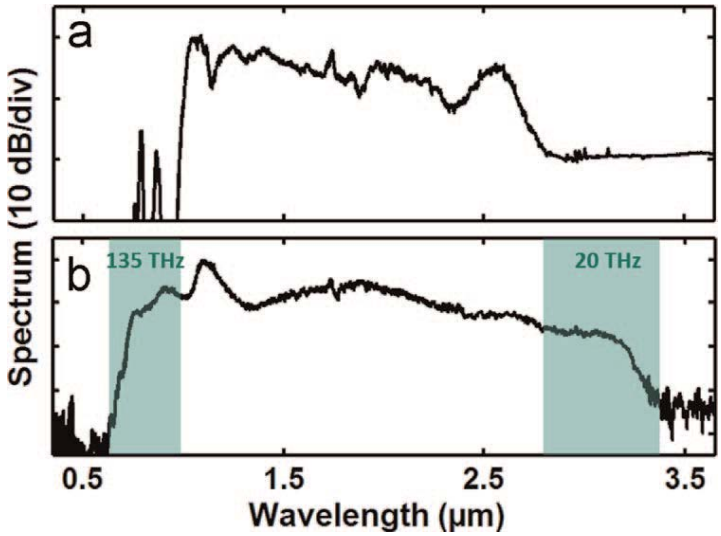

Figure 1.8 SC generation in (a) 10-cm-long uniform suspended core fiber and (b) 10-cm-long tapered suspended core fiber by injecting 200-fspulses at1730nm with 12-kWpeakpower.SCenhancement is obtained on both frequency edges[56]

1.4.3 Mid-infrared SC generations in step-index chalcogenide fibers

The study of SC generation in Chalcogenide step-index fibers started in 2005. Wei et al [60] obtained a SC generation in a 1.5m-long As_2S_3 single-mode step-index fiber pumped in the normal dispersion regime. A passively 1.5µm mode-locked Er-doped fiber laser with a pulse duration of 100 fs at a repetition rate of 20 MHz was

used as the pump source. Using the maximum fiber-input power of 16.4mW, the output spectrum was broadened with a −15 dB bandwidth of 310 nm. Although the spectral width of the SC generation was not wide, the observed spectral broadening was very attractive, and it confirmed the potential for Chalcogenide fibers to be used for Mid-Infrared SC generation. Highly nonlinear Chalcogenide fibers are therefore promising media for compact broadband MIR sources designed for different potential applications.

The research work was followed by a serious of SC generations in Chalcogenide step-index fibers pumped by light sources with short wavelengths [64-66], but the broadband Mid-infrared SC generation was not achieved in Chalcogenide step-index fibers pumped in the normal dispersion regime with a short pump wavelength. It is mainly due to that during the process of spectral extension in the normal dispersion regime, the nonlinear effects as self-phase modulation (SPM), optical wave break (OWB), and stimulated Raman Scattering (SRS) which are critical for the spectral extension are limited by the pump peak power and dispersion slopes.

Normally, broadband and efficient SC generation should be generated by pumping in the anomalous dispersion region which is close to the zero dispersion wavelength of the fiber. However, due to the intrinsic material dispersion, the zero dispersion wavelength of Chalcogenide step-index fibers are usually located at long wavelengths (>5μm). Therefore, it is difficult to match the ZDWs of Chalcogenide fibers with the operation wavelengths of commercial fiber lasers. Moreover, the use of Chalcogenide step-index fibers in SC generation was limited by the lack of high peak power pump sources in the Mid-infrared until the discovery of optical parametric amplifiers (OPAs) and oscillators (OPOs) for the pump sources to excite fibers in the anomalous dispersion regime [67, 68].

In 2014, an ultrabroad Mid-infrared SC, spanning from 1.4 to 13.3μm, was generated by injecting 100fs laser pulses centered at 6.3μm with a repetition rate of 1 kHz into an 85-mm-long step-index fiber made of As_2Se_3 core and $Ge_{10}As_{23.4}Se_{66.6}$ cladding. The peak power of the pump source was estimated to be 2.29MW, and the pump wavelength was located at the anomalous dispersion region, which was just

above the fiber ZDW of 5.83μm [69]. The setup of the experiment is shown in Figure 1.9 and the collected SC output spectrum is illustrated in Figure 1.10. This was the first time that an SC generation with a spectral width over 10μm had been achieved in Chalcogenide fibers. The transparent atmospheric windows of 3–5μm and 8–13μm, and the significant part of the fingerprint region of molecular vibrational resonances were covered. Since then, the generation of broadband SC sources in Chalcogenide step-index fibers has made rapid development, driven by the large number of potential applications in Mid-infrared technology.

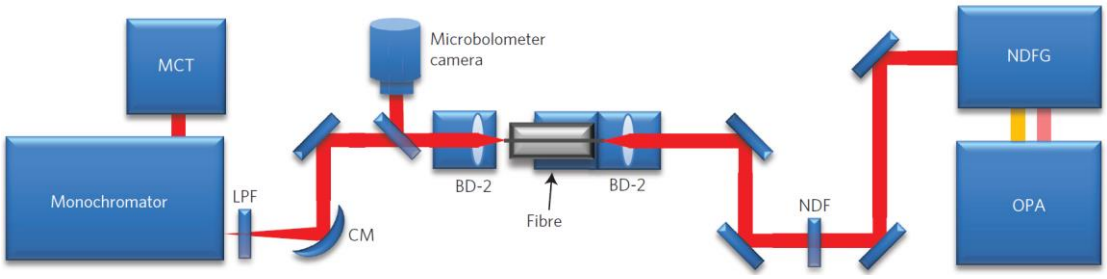

Figure 1.9 Setup for SC generation in the Chalcogenide fiber. BD-2,black-diamond-2 aspheric lenses; CM, concave mirror; LPF, long-pass filter; MCT, mercury cadmium telluride; NDF, neutral density filter; NDFG, noncollinear difference frequency generation; OPA, optical parameter amplifier[69]

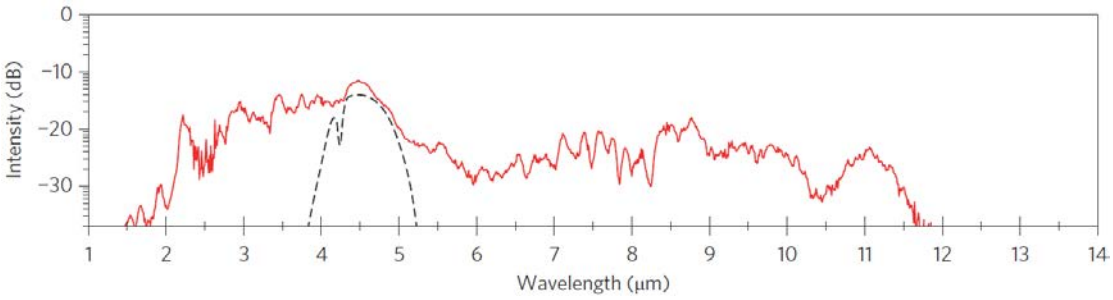

Figure 1.10 Measured SC output spectrum in the Chalcogenide fiber pumped at 4.5μm[69]

Subsequently, more attention was focused on the enhancement of the spectrum broadening of SC generation. Different Chalcogenide fiber of short length, small core diameters, high nonlinearity and suited pump sources were utilized in generating Mid-infrared SC to obtain a better result [61, 70-74]. Meanwhile, more novel glass

systems of Chalcogenide fibers were designed to achieve Mid-infrared SC. Ou et al. [75] reported the fabrication of a fiber with the core and cladding made of $Ge_{15}Sb_{25}Se_{60}$ and $Ge_{15}Sb_{20}Se_{65}$ glasses, respectively. A SC generation spanning from 1.8 to 14μm was achieved in a 20-cm-long fiber with a core diameter of 23μm by pumping at 6.0μm in the anomalous dispersion region. The optical nonlinearity of the core glass was greater than that of As_2Se_3 because of the replacement of As by Sb [72, 76, 77]

Tellurium (Te)-based glasses have low phonon energies and high linear refractive indices, which results in wide optical windows and high nonlinear refractive indices [78-80]. Therefore, relatively broader SC generation can be expected from Te-based fibers. However, the metallic characteristic of Te can lead to a higher tendency for crystallite, which may prevent the production of low-loss optical fibers due to scattering and surface defects. Previous work has demonstrated the potential of Ge–Ga–Te [80],Ge–Te–I [78], and Ge–Te–AgI [81, 82] glass systems without Se for FIR applications. Iodine can trap free electrons from tellurium, helping to form more stable glass. Moreover, the high atomic weight of iodine, which is a neighbor of Te in the periodic table, allows the low phonon characteristics of the glass matrix to be maintained and the Far-infrared transparency to be retained, while providing improved rheological properties.

A list of the results of SC generation in Chalcogenide step-index fibers is shown in Table 1.3. It can be seen that the spectral bandwidths of SCs generated in Chalcogenide step-index fibers are limited when pumped with shorter laser pulses. In contrast, when fibers are pumped with pulses longer than 6.0μm, the long wavelength edges of generated SCs can be extended to over 12μm. In addition, broader SC spectrums can be obtained in Chalcogenide fibers with higher refractive indexes. It is worth noting that the maximum average power of a generated SC is generally low, limited to the order of mili-watts, or even micro-watts, due to the low repetition rate of the pump source [69].

Table 1.3 Partial results of supercontinuum generation in Chalcogenide step-index fibers.

Composition	Fiber length	Pump wavelength/Pulse width/Repetition	SC Bandwidth	Output power	Reference
As_2S_3	2m	2.45μm/40ps/10MHz	1.9-4.8μm	565mW	[65]
AS_2Se_3	8.5cm	6.3μm/100fs/1kHz	1.4-13.3μm	150μW	[69]
$Ge_{12}As_{24}Se_{64}$	11cm	4.0μm/330fs/21MHz	1.8-10μm	1.26mW	[72]
$Ge_{11.5}As_{24}Se_{64.5}$	13.5cm	4.1μm/320fs/10.5MHz	1.8-9.8μm	3mW	[70]
As_2S_3	23cm	3.83μm/450fs/42MHz	3.0-4.8μm	550mW	[83]
As_2Se_3	3cm	9.8μm/170fs/1kHz	2.0-15.1μm	-	[84]
$Ge_{15}Sb_{15}Se_{70}$	11cm	4.485μm/3f00s/21MHz	2.2-12μm	17mW	[85]
As_2S_3	3m	2.19μm/1ns/100kHz	2.0-4.0μm	143mW	[86]
As_2Se_3	12cm	6.5μm/150fs/1kHz	2.0-12.7μm	300μW	[87]
$(Ge_{10}Te_{43})_{90}(AgI)_{10}$	14cm	7μm/150fs/1kHz	2.0-16μm	-	[88]

1.4.4 Mid-infrared SC generations in micro-structured chalcogenide fibers

Compared with step-index structure Chalcogenide fibers, micro-structured chalcogenide fibers possess the flexibility in dispersion to match the wavelength of the pump sources. By changing the core diameter and the pitch, the dispersion can be modified over a wide range.

The first generation of supercontinuum was demonstrated in 2006 for chalcogenide MOFs [89]. One-meter of a selenide based chalcogenide MOF was pumped by a Ti:sapphire laser, with an output wavelength at 2.5μm and pulse duration and pulse energy of 100fs and 100pJ, respectively. The experiment results displayed in Figure 1.11 show that effective wavelength broadening can be achieved through pumping around the ZDW or the anomalous region [90] of the fiber.

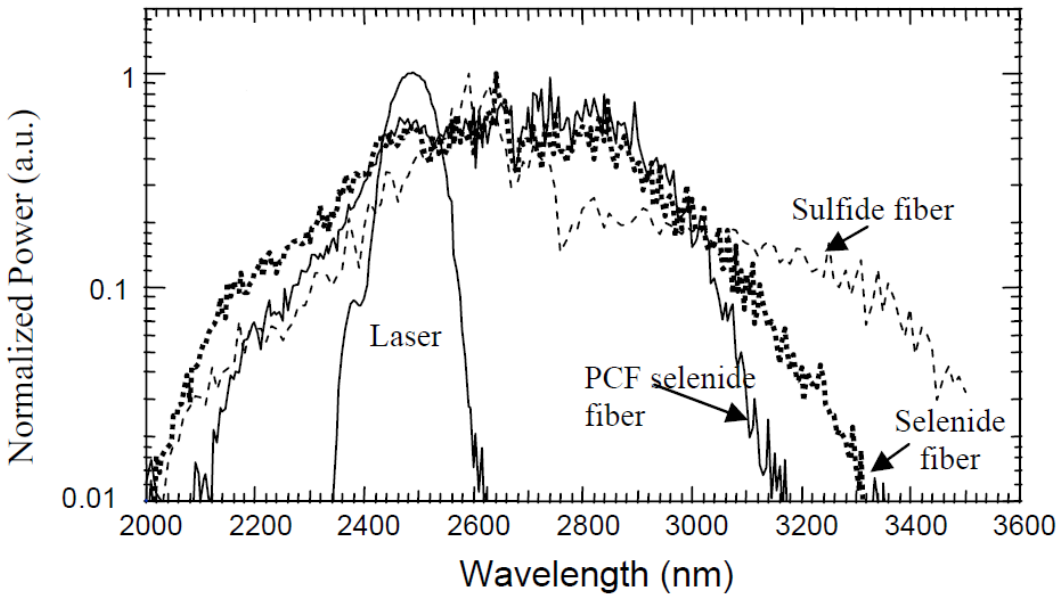

Figure 1.11 Output spectrum of supercontinuum generated in chalcogenide micro-structured fibers made by the stack and draw technique[89]

Later in 2010, M. El-Amraoui et al reported the fabrication of the first As_2S_3 chalcogenide MOFs with a suspended core. Instead of "stack-and-draw" method, mechanical drilling was used to prepare the fiber preform. By pumping a section of 45-m-long MOF with a 8 ps mode-locked laser around 1.55μm, a continuum covering more than 200 nm from 1450 nm to over 1700 nm was obtained [91].

Several other pumping schemes have also been investigated to generate Mid-IR supercontinuum. In 2016, Petersen et al. used a two-cascading configuration, based on a 1.55-μm laser- diode-pumped thulium-doped silica fiber and a Zr-Ba-La-Al-Na fluoride (ZBLAN) fiber, to pump a chalcogenide MOF, which generates Mid-IR supercontinuum up to 4.4μm [92]. By comparing the output spectra of ZBLAN fibers with different chromatic dispersions, it was concluded that solitons located in the long-wavelength part of the pump are essential for effective generation of supercontinuum. This was corroborated by a series of simulations. The spectrum of the supercontinuum was extended to 7 μm with a total output power of 6.5mW. Then, in 2017, Petersen et al. demonstrated a Mid-IR SC generation from tapered large-mode-area chalcogenide MOF [93]. The tunable Mid-IR pump light utilized in the experiment was achieved by combining a tunable seed laser and a 1.04-μm mode-locked Yb:KYW (ytterbium-doped potassium yttrium tungstate crystal)

solid-state laser into periodically-poled MgO:$LiNbO_3$ crystal to obtain quasi-phase-matched parametric anti-Stokes generation from 3.7 to 4.5µm. In order to increase the spectral broadening and reduce the confinement losses, tapered fibers with a diameter of 15.1µm and shorter lengths before and after the taper with length before taper (L_{bt}) of 7.5cm and length after taper (L_{at}) of 4.5cm, was utilized in the experiment. At the end, an output spectrum from 1 to 11.5µm with an average output power of 35.4mW was obtained, as shown in Figure 1.12.

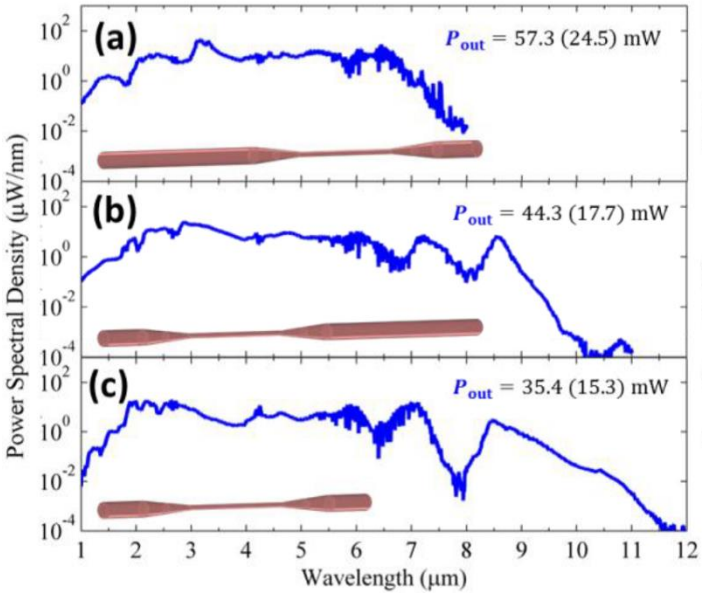

Figure 1.12 Supercontinuum spectra obtained from a tapered chalcogenide MOF, for three different configurations of lengths of non-tapered zones at the input and output of the fiber (in brown color) (a) L_{bt} = 25 cm, L_{at} = 7.5 cm; (b) L_{bt} = 7.5 cm, L_{at} = 25 cm; (c) L_{bt} = 7.5 cm, L_{at} = 4 cm. (With L_{bt} : length before taper, L_{at} :length after taper and P_{out}: average integrated out power)[93]

Besides, hybrid chalcogenide MOFs were fabricated by Cheng et al, to generate Mid-IR supercontinuum [94]. The hybrid MOF has been made with four $AsSe_2$ capillaries and inserted into an As_2S_5 glass tube (Figure 1.13a). The high refractive index difference (around 0.61) between the core and the cladding would improve light confinement in the fiber, which was the original intent of the fiber designing. As for the pump light, a tunable optical parametric oscillator (OPO) emitting 200-fs pulses at a repetition of 80 MHz was employed. For the purpose of extending the output spectra,

different pump wavelengths: 3062 nm, 3241 nm and 3389 nm located at positions far from ZDW in the normal dispersion range, close to the ZDW in the normal dispersion range and close to ZDW in the anomalous dispersion range, respectively, were used to pump the 2cm-long hybrid MOF. Compared to the other wavelengths used, the broader spectrum, from 1250 nm to 5370 nm was obtained by pumping at 3.389 µm (Figure 1.13b).

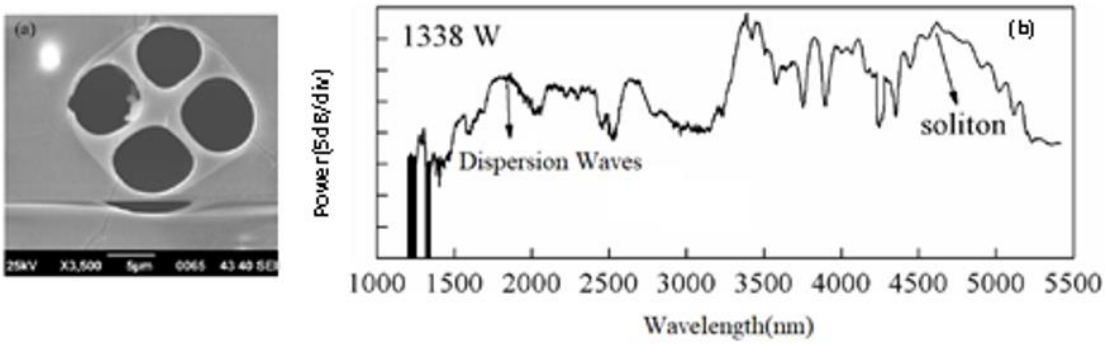

Figure 1.13 (a) Cross section of the $AsSe_2$–As_2S_5 hybrid MOF. (b) Output spectrum of the mid-infrared supercontinuum obtained by pumping at 3389 nm[94]

A summary of supercontinuum generated in chalcogenide MOF with different glass compositions, geometries and pumping regimes, discussed in this article are presented in Table1.4. The broader supercontinuum spectrum obtained in a chalcogenide MOF presents a spectral coverage from 1 to 11.5µm with an average output power of 35mW. The higher output power obtained in a chalcogenide MOF reaches more than 57mW in the 1-8 µm wavelength range.

Table 1.4 Mid-IR supercontinuum generation obtained in chalcogenide MOFs

Fiber composition	Spectral Coverage	Pump Wavelength (Pulse duration)	Output average Power	References
As_2S_3	2.1-3.2µm	2.5µm(100fs)	-	[89]
As_2S_3	1-2.6µm	1.55µm(400fs)	-	[95]
$AsSe_2$-As_2S_5	1.2-5.37µm	3.3µm(200fs)	214mW(input)	[94]
$As_{38}Se_{62}$	1.9-7.1µm	Cascading from 1.55 to 4.5 µm (3ns)	6.5mW	[92]
$Ge_{10}As_{22}Se_{68}$	1-11.5µm	4µm (252fs)	35.4mW	[93]

$Ge_{10}As_{22}Se_{68}$	1-8µm	4µm (252fs)	57.3mW	[93]

1.4.5 Applications of Mid-IR Supercontinuum Generation

Thanks to the broad Mid-infrared range coverage, high coherence, and good beam quality, Mid-infrared supercontinuum sources are potential candidates for a variety of applications in domains such as spectroscopy, sensing, biology, metrology, and spectral imaging [96, 97].

As an example of this, the IR signature of propanol and acetone has been detected by fibers evanescent wave spectroscopy (FEWS) using a chalcogenide MOF [97]. In this experiment, it was demonstrated that an exposed-core chalcogenide MOF, as shown in Figure 1.14, can be more sensitive to the environment than classical single-index fibers, such as those used in ref [24].

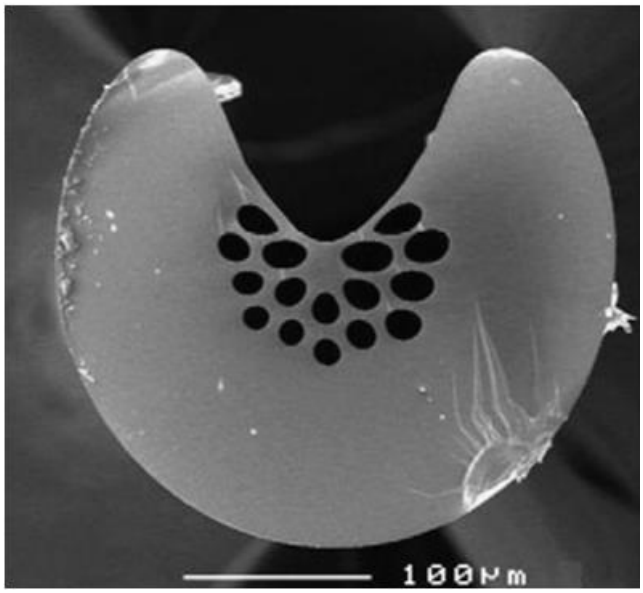

Figure 1.14 Scanning electron microscope image of an exposed-core chalcogenide micro-structured optical fiber[24]

Mid-IR spectral imaging, combined with data mining algorithms, has been utilized as an aid for diagnosing some types of cancers [98-101]. The acquisition speed and penetration depth of traditional Mid-IR spectral imaging is subject to low brightness and lack of flexibility for the delivery and detection of light [47]. Therefore, intense laser source with high signal-to-noise ratio become an ideal choice for rapid

acquisition through the Mid-IR range. Quantum cascade lasers (QCL) were once used in Mid-IR spectral imaging systems to reduce the acquisition time, but the limited frequency coverage of QCLs cannot satisfy the diagnostic requirements and maintain, in the same time, the simplicity of the system at a reasonable cost. Thus, supercontinuum sources were selected for broadband Mid-IR spectral imaging. For example, ZBLAN-fluoride-fiber-based supercontinuum sources, with a 2-4.5μm spectral range, were selected to be integrated into Mid-IR spectral imaging systems demonstrated in the past few years [46, 102, 103].

In 2012, Dupont et al presented, for the first time, a high-resolution contact-free infrared microscope. By using a 1900-nm fiber laser to pump 10 meters of ZBLAN fiber, the generated supercontinuum spanned from 1.4μm to 4.0μm. The system was tested by a mixture of oil and water and resolutions of 35 μm and 25 μm for the water absorption image and oil absorption image were obtained, respectively, as shown in Figure 1.15 [46].

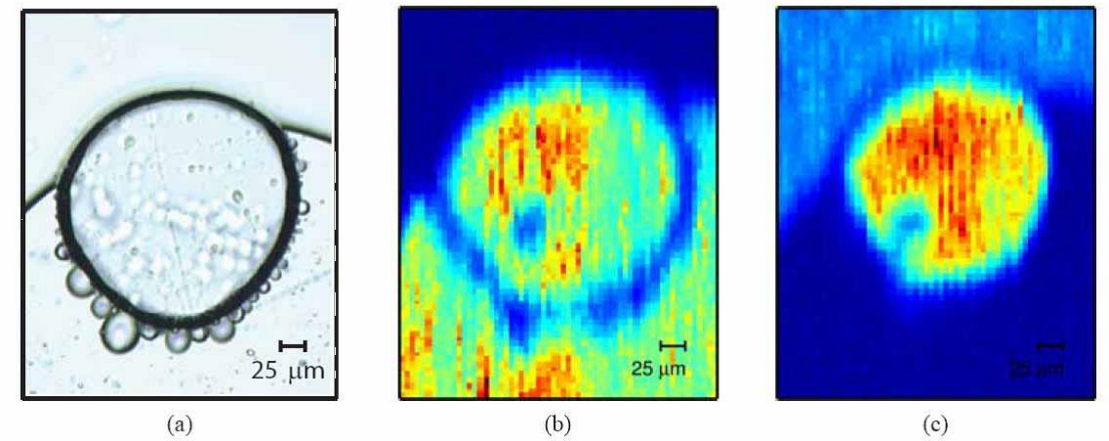

Figure 1.15 (a) Optical microscope image of oil–water mixture; (b,c) IR microscope image obtained at wavelengths corresponding to high absorption of water and oil, respectively[46]

In 2017, M. Farries et al. reported a mid-infrared spectral imaging system for rapid assessment of cells for cytological diagnosis, consisting of a ZBLAN-fiber-based supercontinuum source, a fast acousto-optic tunable filter (AOTF) and a high-resolution thermal camera. The AOTF enables the system to record a 100 wavelengths image cube and 300k pixels in 2 seconds, so that it can be used to test the

cells of living person. By comparison, the system proved to have a higher spectral resolution than Fourier transform infrared (FTIR) system. Restricted by the filter inside the thermal camera and the range of the supercontinuum source, collection of samples of colon cells could be imaged, nevertheless, in the 2.87-3.7 µm spectral range [103].

Hence, in the later studies, chalcogenide MOFs were chosen to replace ZBLAN fibers. In 2018, Peterson et al. designed the first Mid-IR spectral imaging system in the long-wavelength region using SC generation [47]. The system consisted of a point scanning device and a chalcogenide fiber-based supercontinuum. The supercontinuum source can deliver light from 2 to 7.5µm with an output power of 25mW, which enabled the system to collect sample information from 5.7 to 7.3µm, in the diagnostic fingerprint region. Figure 1.16 presents the first mid-IR spectral image obtained with a SC containing wavelengths longer that 4µm. The Mid-IR image obtained at 6.03µm (Figure 1.16c) is compared to classical histologic analysis (visible images, Figures 1.16a and 1.16b).

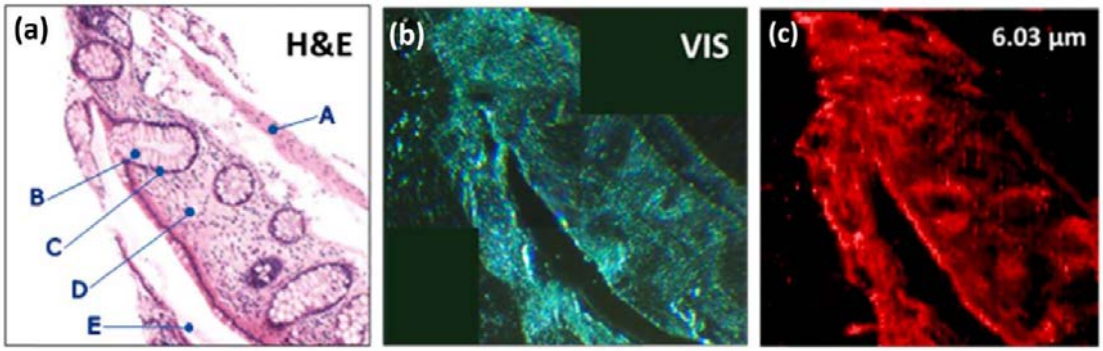

Figure 1.16 (a) Confocal image from histological analysis using gold standard hematoxylin and eosin (H&E); (b) visible light transmission image of the sample; (c) Mid-IR absorbance image[47]

References

[1]. J.-L. Adam, and X. Zhang, *Chalcogenide glasses: preparation, properties and applications* (Woodhead publishing, 2014).

[2]. K. A. Shore, "Electronic Processes in Non-crystalline Materials , by NF Mott and EA Davis: Scope: text book. Level: advanced undergraduate," (Taylor & Francis, 2014).

[3]. J. Nishii, and T. Yamashita, "Chalcogenide glass-based fibers," Infrared Fiber Optics, 143-184 (1998).

[4]. A. Feltz, *Amorphous inorganic materials and glasses* (VCH, 1993).

[5]. I. Inagawa, R. Iizuka, T. Yamagishi, and R. Yokota, "Optical and thermal properties of chalcogenide Ge-As-Se-Te glasses for IR fibers," Journal of Non-Crystalline Solids **95**, 801-808 (1987).

[6]. V. F. Kokorina, *Glasses for infrared optics* (CRC press, 1996).

[7]. V. Minaev, "Stekloobraznye poluprovodnikovye splavy (Vitreous Semiconductor Alloys), Moscow: Metallurgiya, 1991," Google Scholar.

[8]. D. Bletskan, "Glass formation in binary and ternary chalcogenide systems," Chalcogenide letters **3**, 81-119 (2006).

[9]. J. C. Phillips, "Topology of covalent non-crystalline solids I: Short-range order in chalcogenide alloys," Journal of Non-Crystalline Solids **34**, 153-181 (1979).

[10]. M. Thorpe, D. Jacobs, and B. Djordjević, "The structure and rigidity of network glasses," in *Insulating and Semiconducting Glasses*(World Scientific, 2000), pp. 95-145.

[11]. K. Tanaka, "Structural phase transitions in chalcogenide glasses," Physical Review B **39**, 1270 (1989).

[12]. P. Boolchand, D. Georgiev, and B. Goodman, "Discovery of the intermediate phase in chalcogenide glasses," Journal of Optoelectronics and Advanced Materials **3**, 703-720 (2001).

[13]. D. Bulla, R. Wang, A. Prasad, A. V. Rode, S. Madden, and B. Luther-Davies, "On the properties and stability of thermally evaporated Ge–As–Se thin films,"

Applied Physics A **96**, 615-625 (2009).

[14]. J. Sanghera, V. Nguyen, P. Pureza, R. Miklos, F. Kung, and I. Aggarwal, "Fabrication of long lengths of low-loss IR transmitting As/sub 40/S/sub (60-x)/Se/sub x/glass fibers," Journal of lightwave technology **14**, 743-748 (1996).

[15]. J. Harbold, F. Ilday, F. Wise, J. Sanghera, V. Nguyen, L. Shaw, and I. Aggarwal, "Highly nonlinear As–S–Se glasses for all-optical switching," Optics Letters **27**, 119-121 (2002).

[16]. G. Lenz, J. Zimmermann, T. Katsufuji, M. Lines, H. Hwang, S. Spälter, R. Slusher, S.-W. Cheong, J. Sanghera, and I. Aggarwal, "Large Kerr effect in bulk Se-based chalcogenide glasses," Optics Letters **25**, 254-256 (2000).

[17]. J. M. Harbold, F. O. Ilday, F. W. Wise, and B. G. Aitken, "Highly nonlinear Ge-As-Se and Ge-As-S-Se glasses for all-optical switching," IEEE Photonics Technology Letters **14**, 822-824 (2002).

[18]. A. Seddon, "Chalcogenide glasses: a review of their preparation, properties and applications," Journal of Non-Crystalline Solids **184**, 44-50 (1995).

[19]. J. A. Savage, "Optical properties of chalcogenide glasses," Journal of Non-Crystalline Solids **47**, 101-115 (1982).

[20]. M. Churbanov, "High-purity chalcogenide glasses as materials for fiber optics," Journal of non-crystalline solids **184**, 25-29 (1995).

[21]. T. A. Birks, J. C. Knight, and P. S. J. Russell, "Endlessly single-mode photonic crystal fiber," Optics letters **22**, 961-963 (1997).

[22]. G. Renversez, F. Bordas, and B. T. Kuhlmey, "Second mode transition in microstructured optical fibers: determination of the critical geometrical parameter and study of the matrix refractive index and effects of cladding size," Optics letters **30**, 1264-1266 (2005).

[23]. J. Ballato, H. Ebendorff-Heidepriem, J. Zhao, L. Petit, and J. Troles, "Glass and process development for the next generation of optical fibers: A review," Fibers **5**, 11 (2017).

[24]. S. Hocdé, C. Boussard-Plédel, G. Fonteneau, and J. Lucas, "Chalcogens based glasses for IR fiber chemical sensors," Solid State Sciences **3**, 279-284 (2001).

[25]. S. Danto, D. Thompson, P. Wachtel, J. D. Musgraves, K. Richardson, and B. Giroire, "A Comparative Study of Purification Routes for A s2 S e3 Chalcogenide Glass," International Journal of Applied Glass Science **4**, 31-41 (2013).

[26]. V. Shiryaev, and M. Churbanov, "Recent advances in preparation of high-purity chalcogenide glasses for mid-IR photonics," Journal of Non-Crystalline Solids (2017).

[27]. M. Churbanov, V. Shiryaev, I. Scripachev, G. Snopatin, V. Gerasimenko, S. Smetanin, I. Fadin, and V. Plotnichenko, "Optical fibers based on As–S–Se glass system," Journal of non-crystalline solids **284**, 146-152 (2001).

[28]. W. Kim, V. Nguyen, L. Shaw, L. Busse, C. Florea, D. Gibson, R. Gattass, S. Bayya, F. Kung, and G. Chin, "Recent progress in chalcogenide fiber technology at NRL," Journal of Non-Crystalline Solids **431**, 8-15 (2016).

[29]. J. Kobelke, J. Kirchhof, M. Scheffler, and A. Schwuchow, "Chalcogenide glass single mode fibres–preparation and properties," Journal of non-crystalline solids **256**, 226-231 (1999).

[30]. J. Ballato, H. Ebendorff-Heidepriem, J. Zhao, L. Petit, and J. Troles, "Glass and Process Development for the Next Generation of Optical Fibers: A Review," Fibers **5** (2017).

[31]. H. Patrick, S. Frédéric, C. Vincent, T. Johann, and G. Ludovic, "Selenide glass single mode optical fiber for nonlinear optics," Optical Materials **29**, 651-656 (2007).

[32]. J. Troles, Y. Niu, C. Duverger-Arfuso, F. Smektala, L. Brilland, V. Nazabal, V. Moizan, F. Desevedavy, and P. Houizot, "Synthesis and characterization of chalcogenide glasses from the system Ga–Ge–Sb–S and preparation of a single-mode fiber at 1.55 μm," Materials research bulletin **43**, 976-982 (2008).

[33]. F. Chenard, O. Alvarez, and A. Buff, "Mid-infrared chalcogenide fiber devices for medical applications," in *Optical Fibers and Sensors for Medical Diagnostics and Treatment Applications XVIII*(International Society for Optics and Photonics2018), p. 104880S.

[34]. C. Lafond, J.-F. Couillard, J.-L. Delarosbil, F. Sylvain, and P. de Sandro,

"Recent improvements on mid-IR chalcogenide optical fibers," in *Infrared Technology and Applications XL*(International Society for Optics and Photonics2014), p. 90701C.

[35]. T. M. Monro, Y. D. West, D. W. Hewak, N. Broderick, and D. Richardson, "Chalcogenide holey fibres," Electronics Letters **36**, 1998-2000 (2000).

[36]. L. Brilland, F. Smektala, G. Renversez, T. Chartier, J. Troles, T. N. Nguyen, N. Traynor, and A. Monteville, "Fabrication of complex structures of holey fibers in chalcogenide glass," Optics Express **14**, 1280-1285 (2006).

[37]. J. Le Person, F. Smektala, T. Chartier, L. Brilland, T. Jouan, J. Troles, and D. Bosc, "Light guidance in new chalcogenide holey fibres from GeGaSbS glass," Materials research bulletin **41**, 1303-1309 (2006).

[38]. P. Pureza, V. NGUYEN, F. Kung, and I. AGGARWAL, "Nonlinear properties of chalcogenide glass fibers," Journal of Optoelectronics and Advanced Materials **8**, 2148-2155 (2006).

[39]. L. Brilland, J. Troles, P. Houizot, F. Desevedavy, Q. Coulombier, G. Renversez, T. Chartier, T. N. Nguyen, J.-L. Adam, and N. Traynor, "Interfaces impact on the transmission of chalcogenides photonic crystal fibres," Journal of the Ceramic Society of Japan **116**, 1024-1027 (2008).

[40]. M. El-Amraoui, G. Gadret, J. Jules, J. Fatome, C. Fortier, F. Désévédavy, I. Skripatchev, Y. Messaddeq, J. Troles, and L. Brilland, "Microstructured chalcogenide optical fibers from As 2 S 3 glass: towards new IR broadband sources," Optics express **18**, 26655-26665 (2010).

[41]. Q. Coulombier, L. Brilland, P. Houizot, T. Chartier, T. N. N'guyen, F. Smektala, G. Renversez, A. Monteville, D. Méchin, and T. Pain, "Casting method for producing low-loss chalcogenide microstructured optical fibers," Optics Express **18**, 9107-9112 (2010).

[42]. R. Alfano, and S. Shapiro, "Emission in the region 4000 to 7000 Å via four-photon coupling in glass," Physical Review Letters **24**, 584 (1970).

[43]. R. R. Alfano, and S. Shapiro, "Observation of self-phase modulation and small-scale filaments in crystals and glasses," Physical Review Letters **24**, 592 (1970).

[44]. K. X. Liu, and E. Garmire, "Role of stimulated four-photon mixing and

efficient Stokes generation of stimulated Raman scattering in excimer-laser-pumped UV multimode fibers," Optics letters **16**, 174-176 (1991).

[45]. K. Ke, C. Xia, M. N. Islam, M. J. Welsh, and M. J. Freeman, "Mid-infrared absorption spectroscopy and differential damage in vitro between lipids and proteins by an all-fiber-integrated supercontinuum laser," Optics express **17**, 12627-12640 (2009).

[46]. S. Dupont, C. Petersen, J. Thøgersen, C. Agger, O. Bang, and S. R. Keiding, "IR microscopy utilizing intense supercontinuum light source," Optics Express **20**, 4887-4892 (2012).

[47]. C. R. Petersen, N. Prtljaga, M. Farries, J. Ward, B. Napier, G. R. Lloyd, J. Nallala, N. Stone, and O. Bang, "Mid-infrared multispectral tissue imaging using a chalcogenide fiber supercontinuum source," Optics letters **43**, 999-1002 (2018).

[48]. A. B. Seddon, "A prospective for new mid-infrared medical endoscopy using chalcogenide glasses," International Journal of Applied Glass Science **2**, 177-191 (2011).

[49]. B. J. Eggleton, B. Luther-Davies, and K. Richardson, "Chalcogenide photonics," Nature Photonics **5**, 141-148 (2011).

[50]. M. Kumar, M. N. Islam, F. L. Terry, M. J. Freeman, A. Chan, M. Neelakandan, and T. Manzur, "Stand-off detection of solid targets with diffuse reflection spectroscopy using a high-power mid-infrared supercontinuum source," Applied optics **51**, 2794-2807 (2012).

[51]. G. Qin, X. Yan, C. Kito, M. Liao, C. Chaudhari, T. Suzuki, and Y. Ohishi, "Ultrabroadband supercontinuum generation from ultraviolet to 6.28 μm in a fluoride fiber," Applied Physics Letters **95** (2009).

[52]. H. Shi, K. Liu, F. Tan, J. Liu, and P. Wang, "Mid-IR Supercontinuum Generation in ZBLAN fiber pumped by Diode-seeded Tm-doped MOPA," in *Conference on Lasers and Electro-Optics/Pacific Rim*(Optical Society of America2015), p. 27A22_22.

[53]. C. Xia, M. Kumar, O. P. Kulkarni, M. N. Islam, F. L. Terry Jr, M. J. Freeman, M. Poulain, and G. Mazé, "Mid-infrared supercontinuum generation to 4.5 μm in

ZBLAN fluoride fibers by nanosecond diode pumping," Optics letters **31**, 2553-2555 (2006).

[54]. J. Swiderski, M. Michalska, and G. Maze, "Mid-IR supercontinuum generation in a ZBLAN fiber pumped by a gain-switched mode-locked Tm-doped fiber laser and amplifier system," Optics express **21**, 7851-7857 (2013).

[55]. K. Liu, J. Liu, H. Shi, F. Tan, and P. Wang, "High power mid-infrared supercontinuum generation in a single-mode ZBLAN fiber with up to 21.8 W average output power," Optics express **22**, 24384-24391 (2014).

[56]. J. Picot-Clemente, C. Strutynski, F. Amrani, F. Désévédavy, J. Jules, G. Gadret, D. Deng, T. Cheng, K. Nagasaka, and Y. Ohishi, "Enhanced supercontinuum generation in tapered tellurite suspended core fiber," Optics Communications **354**, 374-379 (2015).

[57]. M. Liao, W. Gao, Z. Duan, X. Yan, T. Suzuki, and Y. Ohishi, "Supercontinuum generation in short tellurite microstructured fibers pumped by a quasi-cw laser," Optics letters **37**, 2127-2129 (2012).

[58]. P. Domachuk, N. Wolchover, M. Cronin-Golomb, A. Wang, A. K. George, C. Cordeiro, J. C. Knight, and F. Omenetto, "Over 4000 nm bandwidth of mid-IR supercontinuum generation in sub-centimeter segments of highly nonlinear tellurite PCFs," Optics Express **16**, 7161-7168 (2008).

[59]. H. Saghaei, M. K. Moravvej-Farshi, M. Ebnali-Heidari, and M. N. Moghadasi, "Ultra-wide mid-infrared supercontinuum generation in As 40 Se 60 chalcogenide fibers: solid core PCF versus SIF," IEEE Journal of Selected Topics in Quantum Electronics **22**, 279-286 (2016).

[60]. D.-P. Wei, T. Galstian, I. Smolnikov, V. Plotnichenko, and A. Zohrabyan, "Spectral broadening of femtosecond pulses in a single-mode As-S glass fiber," Optics express **13**, 2439-2443 (2005).

[61]. I. Kubat, C. S. Agger, U. Møller, A. B. Seddon, Z. Tang, S. Sujecki, T. M. Benson, D. Furniss, S. Lamrini, and K. Scholle, "Mid-infrared supercontinuum generation to 12.5 μm in large NA chalcogenide step-index fibres pumped at 4.5 μm," Optics express **22**, 19169-19182 (2014).

[62]. V. Shiryaev, and M. Churbanov, "Trends and prospects for development of chalcogenide fibers for mid-infrared transmission," Journal of Non-Crystalline Solids **377**, 225-230 (2013).

[63]. R. E. Slusher, G. Lenz, J. Hodelin, J. Sanghera, L. B. Shaw, and I. D. Aggarwal, "Large Raman gain and nonlinear phase shifts in high-purity As 2 Se 3 chalcogenide fibers," JOSA B **21**, 1146-1155 (2004).

[64]. L. B. Shaw, R. R. Gattass, J. Sanghera, and I. Aggarwal, "All-fiber mid-IR supercontinuum source from 1.5 to 5 μm," in *Fiber Lasers VIII: Technology, Systems, and Applications*(International Society for Optics and Photonics2011), p. 79140P.

[65]. R. R. Gattass, L. B. Shaw, V. Nguyen, P. Pureza, I. D. Aggarwal, and J. S. Sanghera, "All-fiber chalcogenide-based mid-infrared supercontinuum source," Optical Fiber Technology **18**, 345-348 (2012).

[66]. J. Geng, Q. Wang, and S. Jiang, "High-spectral-flatness mid-infrared supercontinuum generated from a Tm-doped fiber amplifier," Applied optics **51**, 834-840 (2012).

[67]. Y. Peng, W. Wang, X. Wei, and D. Li, "High-efficiency mid-infrared optical parametric oscillator based on PPMgO: CLN," Optics letters **34**, 2897-2899 (2009).

[68]. S. Desmoulins, and F. Di Teodoro, "Watt-level, high-repetition-rate, mid-infrared pulses generated by wavelength conversion of an eye-safe fiber source," Optics letters **32**, 56-58 (2007).

[69]. C. R. Petersen, U. Møller, I. Kubat, B. Zhou, S. Dupont, J. Ramsay, T. Benson, S. Sujecki, N. Abdel-Moneim, Z. Tang, D. Furniss, A. Seddon, and O. Bang, "Mid-infrared supercontinuum covering the 1.4–13.3 μm molecular fingerprint region using ultra-high NA chalcogenide step-index fibre," Nature Photonics **8**, 830-834 (2014).

[70]. B. Zhang, W. Guo, Y. Yu, C. Zhai, S. Qi, A. Yang, L. Li, Z. Yang, R. Wang, and D. Tang, "Low Loss, High NA Chalcogenide Glass Fibers for Broadband Mid-Infrared Supercontinuum Generation," Journal of the American Ceramic Society **98**, 1389-1392 (2015).

[71]. D. D. Hudson, M. Baudisch, D. Werdehausen, B. J. Eggleton, and J. Biegert,

"1.9 octave supercontinuum generation in a As 2 S 3 step-index fiber driven by mid-IR OPCPA," Optics letters **39**, 5752-5755 (2014).

[72]. Y. Yu, B. Zhang, X. Gai, C. Zhai, S. Qi, W. Guo, Z. Yang, R. Wang, D.-Y. Choi, and S. Madden, "1.8-10 μm mid-infrared supercontinuum generated in a step-index chalcogenide fiber using low peak pump power," Optics letters **40**, 1081-1084 (2015).

[73]. H. G. Dantanarayana, N. Abdel-Moneim, Z. Tang, L. Sojka, S. Sujecki, D. Furniss, A. B. Seddon, I. Kubat, O. Bang, and T. M. Benson, "Refractive index dispersion of chalcogenide glasses for ultra-high numerical-aperture fiber for mid-infrared supercontinuum generation," Optical Materials Express **4**, 1444-1455 (2014).

[74]. B. Luo, Y. Wang, S. Dai, Y. n. Sun, P. Zhang, X. Wang, and F. Chen, "Midinfrared Supercontinuum Generation in As 2 Se 3–As 2 S 3 Chalcogenide Glass Fiber With High NA," Journal of Lightwave Technology **35**, 2464-2469 (2017).

[75]. H. Ou, S. Dai, P. Zhang, Z. Liu, X. Wang, F. Chen, H. Xu, B. Luo, Y. Huang, and R. Wang, "Ultrabroad supercontinuum generated from a highly nonlinear Ge–Sb–Se fiber," Optics letters **41**, 3201-3204 (2016).

[76]. T. Wang, X. Gai, W. Wei, R. Wang, Z. Yang, X. Shen, S. Madden, and B. Luther-Davies, "Systematic z-scan measurements of the third order nonlinearity of chalcogenide glasses," Optical Materials Express **4**, 1011-1022 (2014).

[77]. W.-H. Wei, R.-P. Wang, X. Shen, L. Fang, and B. Luther-Davies, "Correlation between structural and physical properties in Ge–Sb–Se glasses," The Journal of Physical Chemistry C **117**, 16571-16576 (2013).

[78]. A. A. Wilhelm, C. Boussard-Pledel, Q. Coulombier, J. Lucas, B. Bureau, and P. Lucas, "Development of Far-Infrared-Transmitting Te Based Glasses Suitable for Carbon Dioxide Detection and Space Optics," Advanced Materials **19**, 3796-3800 (2007).

[79]. Z. Yang, and P. Lucas, "Tellurium-Based Far-Infrared Transmitting Glasses," Journal of the American Ceramic Society **92**, 2920-2923 (2009).

[80]. S. Danto, P. Houizot, C. Boussard-Pledel, X. H. Zhang, F. Smektala, and J.

Lucas, "A Family of Far-Infrared-Transmitting Glasses in the Ga–Ge–Te System for Space Applications," Advanced Functional Materials **16**, 1847-1852 (2006).

[81]. J.-C. B. Clément Conseil, Catherine Boussard-Plédel, Xiang-Hua Zhang, Pierre Lucas, Shixun Dai, Jacques Lucas, and Bruno Bureau, "Te-based chalcohalide glasses for far-infrared optical fiber," Optical Materials Express (2012).

[82]. X. Wang, Q. Nie, G. Wang, J. Sun, B. Song, S. Dai, X. Zhang, B. Bureau, C. Boussard, and C. Conseil, "Investigations of Ge–Te–AgI chalcogenide glass for far-infrared application," Spectrochimica Acta Part A: Molecular and Biomolecular Spectroscopy **86**, 586-589 (2012).

[83]. S. Kedenburg, T. Steinle, F. Mörz, A. Steinmann, and H. Giessen, "High-power mid-infrared high repetition-rate supercontinuum source based on a chalcogenide step-index fiber," Optics letters **40**, 2668-2671 (2015).

[84]. T. Cheng, K. Nagasaka, T. H. Tuan, X. Xue, M. Matsumoto, H. Tezuka, T. Suzuki, and Y. Ohishi, "Mid-infrared supercontinuum generation spanning 2.0 to 15.1 mum in a chalcogenide step-index fiber," Opt Lett **41**, 2117-2120 (2016).

[85]. B. Zhang, Y. Yu, C. Zhai, S. Qi, Y. Wang, A. Yang, X. Gai, R. Wang, Z. Yang, B. Luther-Davies, and Y. Xu, "High Brightness 2.2-12 μm Mid-Infrared Supercontinuum Generation in a Nontoxic Chalcogenide Step-Index Fiber," Journal of the American Ceramic Society **99**, 2565-2568 (2016).

[86]. J. Yao, B. Zhang, K. Yin, L. Yang, J. Hou, and Q. Lu, "Mid-infrared supercontinuum generation in step-index As 2 S 3 fibers pumped by a nanosecond shortwave-infrared supercontinuum pump source," Optics express **24**, 15093-15100 (2016).

[87]. Y. Wang, S. Dai, X. Han, P. Zhang, Y. Liu, X. Wang, and S. Sun, "Broadband mid-infrared supercontinuum generation in novelAs2Se3-As2Se2Sstep-index fibers," Optics Communications **410**, 410-415 (2018).

[88]. Z. Zhao, B. Wu, X. Wang, Z. Pan, Z. Liu, P. Zhang, X. Shen, Q. Nie, S. Dai, and R. Wang, "Mid-infrared supercontinuum covering 2.0-16 μm in a low-loss telluride single-mode fiber," Laser & Photonics Reviews **11** (2017).

[89]. I. D. A. J. S. Sanghera, L. B. Shaw, C. M. Florea, P. Pureza, V. Q. Nguyen, F.

Kung, I. D. Aggarwal, "Nonlinear properties of chalcogenide glass fibers," (2006).

[90]. J. M. Dudley, G. Genty, and S. Coen, "Supercontinuum generation in photonic crystal fiber," Reviews of Modern Physics **78**, 1135-1184 (2006).

[91]. M. El-Amraoui, J. Fatome, J. C. Jules, B. Kibler, G. Gadret, C. Fortier, F. Smektala, I. Skripatchev, C. F. Polacchini, Y. Messaddeq, J. Troles, L. Brilland, M. Szpulak, and G. Renversez, "Strong infrared spectral broadening in low-loss As-S chalcogenide suspended core microstructured optical fibers," Opt Express **18**, 4547-4556 (2010).

[92]. C. R. Petersen, P. M. Moselund, C. Petersen, U. Moller, and O. Bang, "Spectral-temporal composition matters when cascading supercontinua into the mid-infrared," Opt Express **24**, 749-758 (2016).

[93]. C. R. Petersen, R. D. Engelsholm, C. Markos, L. Brilland, C. Caillaud, J. Troles, and O. Bang, "Increased mid-infrared supercontinuum bandwidth and average power by tapering large-mode-area chalcogenide photonic crystal fibers," Opt Express **25**, 15336-15348 (2017).

[94]. T. Cheng, Y. Kanou, X. Xue, D. Deng, M. Matsumoto, T. Misumi, T. Suzuki, and Y. Ohishi, "Mid-infrared supercontinuum generation in a novel AsSe2-As2S5 hybrid microstructured optical fiber," Opt Express **22**, 23019-23025 (2014).

[95]. G. G. M. El-Amraoui, J. C. Jules, J. Fatome, C. Fortier, F. Désévédavy, I. Skripatchev, Y. Messaddeq, J. Troles, L. Brilland, W. Gao, T. Suzuki, Y. Ohishi, and F. Smektala, "Microstructured chalcogenide optical fibers from As2S3 glass towards new IR broadband sources," (2010).

[96]. O. Mouawad, J. Picot-Clemente, F. Amrani, C. Strutynski, J. Fatome, B. Kibler, F. Desevedavy, G. Gadret, J. C. Jules, D. Deng, Y. Ohishi, and F. Smektala, "Multioctave midinfrared supercontinuum generation in suspended-core chalcogenide fibers," Opt Lett **39**, 2684-2687 (2014).

[97]. P. Toupin, L. Brilland, C. Boussard-Plédel, B. Bureau, D. Mechin, J.-L. Adam, and J. Troles, "Comparison between chalcogenide glass single index and microstructured exposed-core fibers for chemical sensing," Journal of Non-Crystalline Solids **377**, 217-219 (2013).

[98]. R. Baker, K. Rogers, N. Shepherd, and N. Stone, "New relationships between breast microcalcifications and cancer," British journal of cancer **103**, 1034 (2010).

[99]. J. T. Kwak, A. Kajdacsy-Balla, V. Macias, M. Walsh, S. Sinha, and R. Bhargava, "Improving prediction of prostate cancer recurrence using chemical imaging," Scientific reports **5**, 8758 (2015).

[100]. D. C. Fernandez, R. Bhargava, S. M. Hewitt, and I. W. Levin, "Infrared spectroscopic imaging for histopathologic recognition," Nature biotechnology **23**, 469 (2005).

[101]. J. Nallala, M.-D. Diebold, C. Gobinet, O. Bouché, G. D. Sockalingum, O. Piot, and M. Manfait, "Infrared spectral histopathology for cancer diagnosis: a novel approach for automated pattern recognition of colon adenocarcinoma," Analyst **139**, 4005-4015 (2014).

[102]. F. Borondics, M. Jossent, C. Sandt, L. Lavoute, D. Gaponov, A. Hideur, P. Dumas, and S. Février, "Supercontinuum-based Fourier transform infrared spectromicroscopy," Optica **5** (2018).

[103]. M. Farries, J. Ward, I. Lindsay, J. Nallala, and P. Moselund, "Fast hyper-spectral imaging of cytological samples in the mid-infrared wavelength region," in *Optical Biopsy XV: Toward Real-Time Spectroscopic Imaging and Diagnosis*(International Society for Optics and Photonics2017), p. 100600Y.

Chapter II Photo-inscription of Chalcogenide waveguides

2.1 Introduction

Femtosecond laser micro-machining, determined by its inherited features, can be employed for removing small subjects or altering the structure and properties of materials [1]. In 1994, femtosecond laser micro-machining was displayed for the first time in removing micrometer-sized objects from the surface of silica and silver [2, 3]. The ability of femtosecond laser macro-machining to change the properties of materials, normally referred to as "Photo-inscription", has become an ideal candidate for fabrication of photonic devices in transparent bulk substrates and other applications in the past few decades. Different types of substrates, like glasses, crystals and polymers, have been chosen for this technique. Due to their high purity and wide transparency, glasses are normally selected to be the base materials. Compared with other photonic-device fabrication techniques, femtosecond laser macro-machining possess a few advantages. For example, the nonlinear quality of the absorption provides a better confinement of the induced modification to the focal volume, which would be beneficial for building complicated three-dimensional structures. And wider choices of compositions could be accomplished with different combinations of chalcogenide elements. Therefore, this technique has been applied to a variety of industrial and scientific domains, like photonic-crystal templates for telecommunications [4], integrated photonic lanterns for spectrograph [5], optical guiding applications [6] and etc.

However, as the increase of demands for devices and facilities operating in longer wavelengths, mid-infrared region for example, silica based materials are no longer suitable. Meanwhile, Chalcogenide glasses, with its intrinsic photosensitivity, high nonlinearities and large transparent window, have drawn plenty of attentions. When the femtosecond laser pulse with high enough intensity is focused into glasses, the optical breakdown occurs. The laser pulse energy is partially transferred to the electrons and the lattice in the short duration of the pulse. The highly excited electrons thermalize with the ions and alter the material permanently. As a result of the femtosecond laser irradiation, the material can go through a phase or structural

modification, resulting in a localized permanent change in the refractive index or even a void. In the case of Chalcogenide glasses, the subsequent local elevation of the temperature can induce eventually thermodynamic and hydrodynamic phenomena of matter modification and rearrangement. And the permanent change is normally represented by a local modification of the refractive index of the glass, which can be either positive (local densification, type I) or negative (local expansion, type II). Particularly interesting for photonic applications is the case of positive index change, where by translating the sample during the irradiation process a structure can be generated that is able to guide light. Therefore, Chalcogenide glasses have been studied and applied in various spheres in the last decade, such as photonic saturable absorber [7], spectro-interferometer for spatial and drone applications [8], three-dimensional mid-infrared photonic circuits [9], waveguides inscription with different structures and methods [10-18], and also mid-infrared supercontinuum generation in waveguides made of chalcogenide glasses [19-24].

In previous works [18], it has been discovered that the thermal history during glass preparation of chalcogenide glasses plays an essential part in determine of the refractive index contrast caused by ultrafast laser photo-inscription. Samples of chalcogenide glasses with a short annealing and a long annealing process respectively exhibited quite different responses to the laser irradiation which proved that the glass matrix could be affected by thermal annealing treatment. Therefore, in this chapter, we tested the impact of numbers of annealing cycles on the laser induced refractive contrast in chalcogenide glasses in static conditions and dynamic conditions. Based on the behaviors of the glass samples, further verifications and discussions were given.

2.2 Material preparation and bulk glasses synthesis

The three chalcogenide glasses compositions used in the experiments are: Gallium-Lanthanum-Sulfide (GLS) with a stoichiometry of $70Ga_2S_3{:}24La_2S_3{:}6La_2O_3$, $Ge_{20}As_{20}S_{60}$, and $Ge_{15}As_{15}S_{70}$. The GLS material is particularly interesting for laser photo-inscription technique as it indicate robust processing windows for both positive

(type I) and negative (type II) refractive index changes, resulting from structural and hydrodynamic effects, respectively. In addition, the limited nonlinear response in comparison to other chalcogenide materials is compensated by a relatively high laser modification threshold. And for GeAsS glasses, it has been proved that [18], the addition of Ge into the AsS glass matrix plays a determinant role in generating high-contrast positive index changes by setting various degrees of the matrix connectivity.

The GLS glasses were purchased from ChG Southampton Ltd. The bulk glass of $Ge_{20}As_{20}S_{60}$ and $Ge_{15}As_{15}S_{70}$ were synthesized in the laboratory. The method used for synthesis is the traditional "melt and quench" method. First, the raw elements with high purity (Germanium5N, Arsenic5N, and Sulfur5N) are measured in adequate portions based on the calculation in a glovebox filled with Argon. Then the elements were inserted into a silica ampoule and connected to a vacuum pump for a few hours. The silica ampoule was cleaned with Hydrofluoric acid in advance to remove any impurity stuck on the inside surface (mainly silica dust) and the vacancy provided by the vacuum pump (10^{-5} millibar) would get rid of the remaining oxygen and water inside the ampoule that might interact with the chalcogenide elements during synthesis. Afterwards, the silica ampoule was sealed under vacuum condition and put into the rocking furnace for homogenization, as is shown in Figure 2.1.

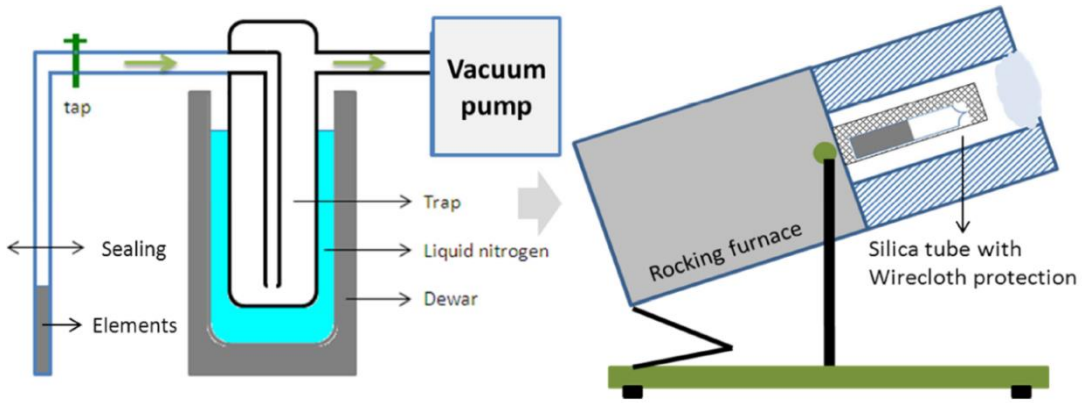

Figure 2.1 The Schematic diagram of glass preparation process.

During the homogenization process, the silica ampoule and the raw elements were heated up to 850℃ with a heating rate no more than 2℃/min to avoid any

potential explosions caused by the increase of inner pressure. Subsequently, the samples were maintained at 850℃ for 8 hours and gradually decrease to 550℃ in 4 hours. Then, the melted elements were quenched in water and annealed at around glass transition temperature (T_g) for 30 minutes and slowly cool down to room temperature to remove the structural stress induced by the quenching. The thermal profile of $Ge_{20}As_{20}S_{60}$ and $Ge_{15}As_{15}S_{70}$ glasses are shown in Figure 2.2 and Figure 2.3.

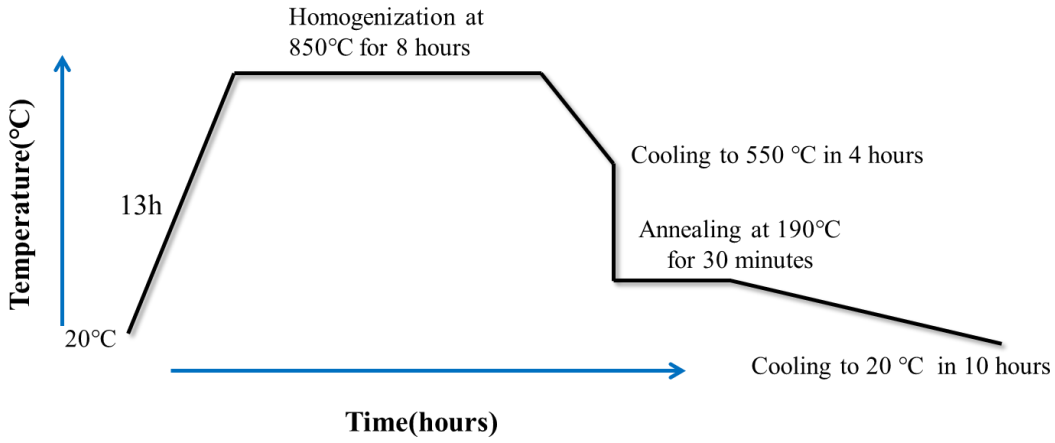

Figure 2.2 Thermal profile of the synthesis of $Ge_{15}As_{15}S_{70}$ glass

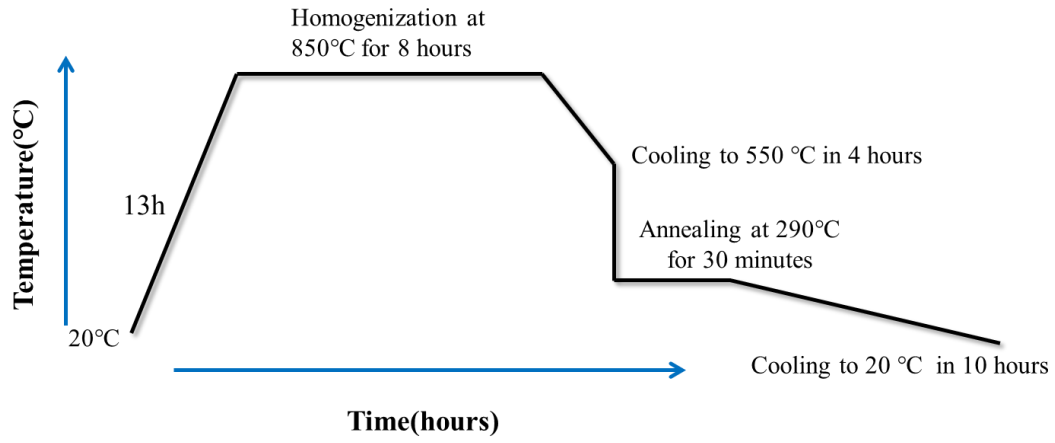

Figure 2.3 Thermal profile of the synthesis of $Ge_{20}As_{20}S_{60}$ glass

In order to better focus the laser beam into the glasses, high quality parallelepipedic samples without surface defect need to be obtained. The method used for polishing bulk glasses is mechanical polishing. The bulk glasses were first cut into pieces with approximate diameters by a cutting machine. Then we used polishing

papers with 1200 to 4000 grits to further reduce the deviations from the demanded size and alumina powder of 1.5μm was utilized at last to finalize the polishing. The samples obtained were illustrated in Figure 2.4.

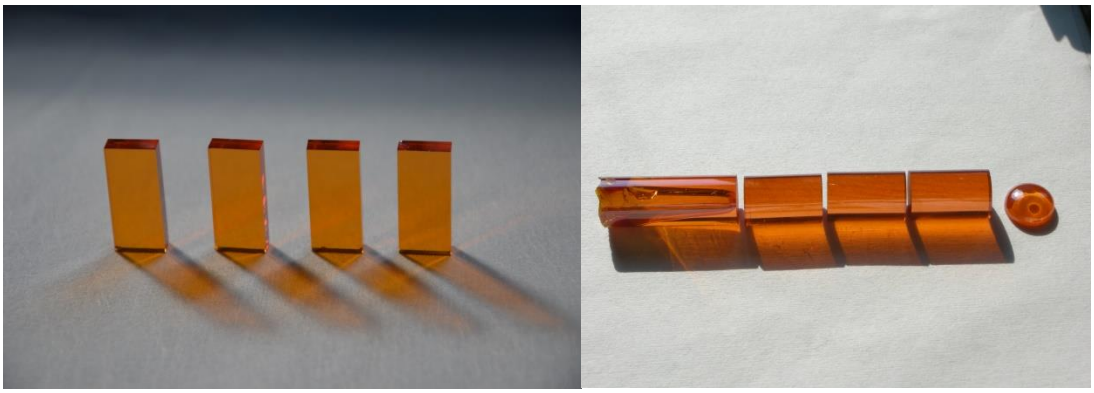

Figure 2.4 Examples of cut and well-polished samples of $Ge_{15}As_{15}S_{70}$

2.3 Photo-inscription in static condition

In order to investigate the influence of the thermal history of chalcogenide glasses on the response of the glasses to the ultrafast laser irradiation, the photo-inscription of the three samples were firstly conducted in the static condition. In the static condition, the ultrafast laser beam was focused into the glasses through a 20×-0.3NA microscope objective to generate refractive index modifications and the samples were kept in static position during the whole experiment procedures. So, by changing the time of exposure to laser irradiation, permanent positive modifications with different index contrast (in general the index contrast ranges between 10^{-4} and 10^{-3}) in relation to the received laser energetic dose. To evaluate the degrees of the refractive modifications, Phase Contrast Microscopy (PCM) was used to measure in the experiments, as positive permanent refractive index changes (type I) appear as dark traces in PCM images and negative refractive changes (type II) appear as light traces. The samples used in the experiments were thermally annealed for several cycles and photo-inscribed after each annealing cycle. Then, we record and analyze PCM images of the photo-induced positive index modification in order to evaluate the relative variation of the index contrast as a function of the exposure time.

2.3.1 Experimental Setup

The laser irradiation was provided by an amplified Ti:Sapphire chain, which can deliver 150 fs laser pulses with a repetition rate of 100 kHz and a maximum energy per pulse of 6μJ. The pulse temporal profile and in particular its duration can be changed by means of a pulse-shaper mounted between the oscillator and the amplifying regenerative cavity (RegA 9000). The laser irradiation conditions are fixed for a given sample, and the induced index contrast is evaluated by measuring the grey level of the transverse profile of the trace obtained in PCM images.

The single thermal annealing cycle designed for the experiments is as shown in Figure 2.5. The samples were heated up to the temperatures that are slightly lower than T_g, and then cooled down to room temperature in a long period. The positive ramp for reaching the maximum temperature is set to 20 °C/min, then the sample is cooled down to the room temperature with a slow rate of about 0.3 °C/min, in order to relax the mechanical stress eventually accumulated during the fast heating process. The peak temperature (T_{max}) is set to be different for each samples and it is set under the glass transition temperature value (T_g) respectively, as follow: 250°C for $Ge_{20}As_{20}S_{60}$ (T_{max}/T_g = 0.82), 175°C for $Ge_{15}As_{15}S_{70}$ (T_{max}/T_g = 0.85) and 400 °C for GLS (T_{max}/T_g = 0.7). Afterwards, the three samples were annealed one after another cycle, and the impact of this procedure on the laser induced refractive index contrast was collected and compared. The glass samples were cut and polished into pieces with diameters of 1.5cm*2cm*0.5cm.

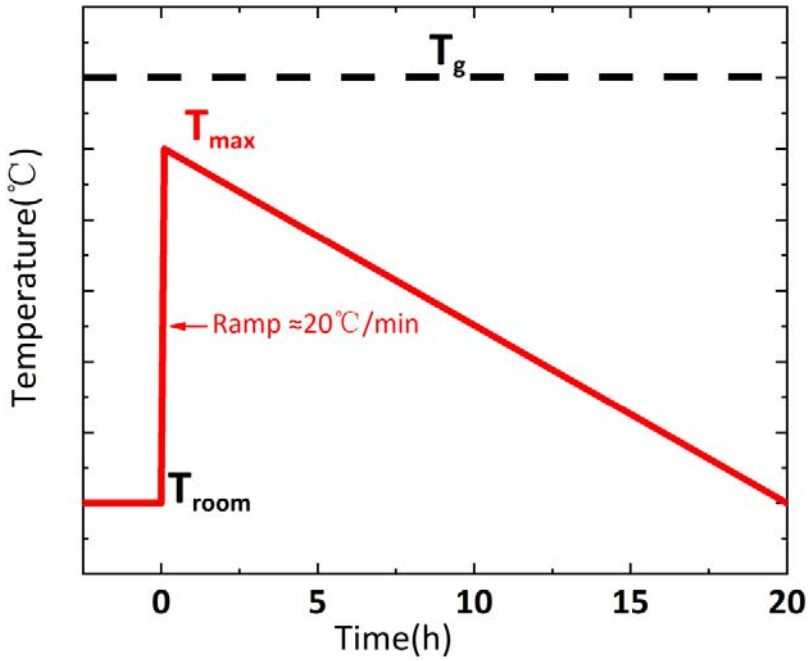

Figure 2.5 The variation of temperature along time in single annealing cycle

2.3.2 Results and analysis

The relative variation of the index contrast induced by the laser irradiation after each annealing cycle is plotted as a function of the number of annealing cycles in figure 2.6.

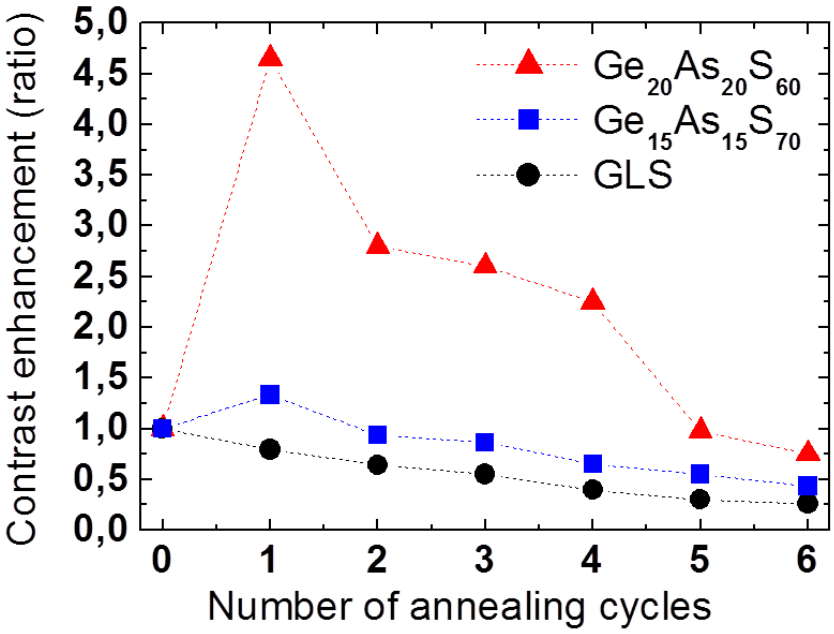

Figure 2.6 The relative variation of refractive index contrast after each annealing cycles of $Ge_{20}As_{20}S_{60}$ and $Ge_{15}AS_{15}S_{70}$ and GLS samples

It can be seen from the results that, the three glass compositions showed quite different responses to the laser irradiation, especially after the first annealing cycle. In the case of GLS glass, the refractive index contrast enhancement was consistently decreasing after each annealing cycle. Whereas, the $Ge_{20}As_{20}S_{60}$ glass exhibited an enormous enhancement of the refractive index contrast after the first annealing cycle, which was about 4.7 times higher than before, and then decreased as the annealing cycle went on. It has to be underlined that the experimental conditions (focusing geometry and laser parameters) are maintained constant during the experiment; this means that the efficiency of the process by which the focused laser beam induces local positive index changes (local densification) can be considerably enhanced by thermal annealing under T_g. Also, similar trend could be observed in the case of $Ge_{15}As_{15}S_{70}$ glass, only the enhancement was not as high as the $Ge_{20}As_{20}S_{60}$ glass, which was about 1.3 times of the sample before thermal annealing treatment. In the GLS glass case, we also verified that increasing the peak temperature up to T_{max} = 450 °C, in order to reach a ratio value (T_{max}/T_g = 0.78) close to the values used for the other two samples, would speed up the degradation of the laser-induced densification process as a function of the number of annealing cycles. Furthermore, for all the samples, we verified that the effect induced by thermal annealing was stable in the time, and we found the thermally induced effect unaltered by photo-inscribing again the samples months later, with the same experimental conditions.

2.4 Photo-inscription in dynamic condition

Since the three compositions of glasses showed quite different responses to laser induced photo-inscription in static conditions, it is necessary to verify the results with a different method. Therefore, we performed the photo-inscription of single-mode waveguides in the dynamic conditions. In the dynamic conditions, the samples were translated along the propagation direction of the laser source, in a given range of translation speeds between 40μm/s and 160μm/s，as is shown in Figure 2.7. By fixing the laser pulse energy, the quality of the inscribed single mode waveguides would be

determined solely by the translation speed. Since The V-number parameter of a waveguide reflects its guiding quality (guided mode confinement) and, for fixed diameter and wavelength, it is proportional to the square-root of the waveguide refractive index contrast. Therefore, the confinement and the intensity of the guided mode can reflect the degree of refractive index contrast of the waveguide.

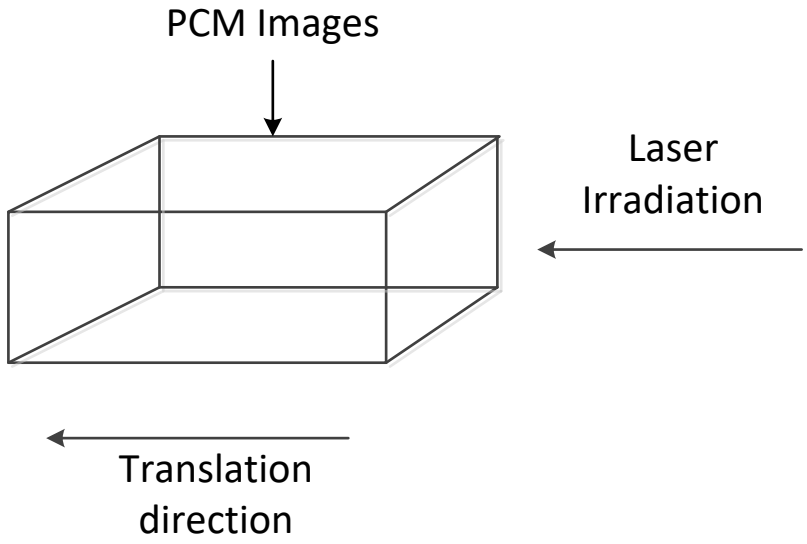

Figure 2.7 schematic diagram of the dynamic conditions

We performed then guiding tests on the samples and measured the guided mode intensity at the end of the waveguide (near field mode).The same laser system with a central wavelength at 800nm was applied to inject light into the waveguides in the samples. The near filed image coming out of the waveguides were collected with a imaging system assembled with CCD camera. Then, we analyzed the relative mode intensity variation after annealing cycles for fixed photo-inscription conditions (pulse energy and translation speed).

2.4.1 Verification of GLS glass samples in dynamic conditions

According to the different behaviors of the three glass compositions in the static conditions, we first analyzed the case of GLS glass.

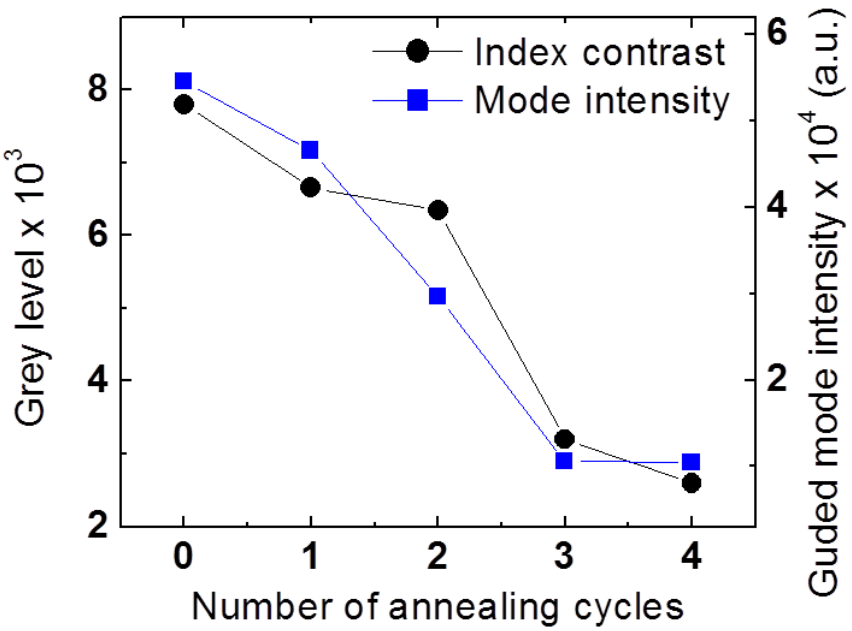

Figure 2.8 The evolutions of the refractive index contrast (dark solid circles) of photo-inscription and guided mode intensity (blue solid squares) with the increase of the annealing cycles in GLS glass in dynamic conditions

The trends of variation of refractive index contrast and guided mode intensity after each annealing cycle is shown in Figure 3.8. The laser energy and translation speed for the experiment was fixed at 200nJ and 30μm/s respectively. It can be seen from the figure that as the annealing cycles increase, both the refractive index contrast and the guided mode intensity decreased. At the same time, we also recorded the PCM images and the near filed mode of the waveguides inscribed in the GLS glass, shown in Figure 2.9. It was also clear that the effect of the refractive index contrast and the intensity of the guided mode were weakened by thermal annealing. Combining the results obtained in the cases of dynamic and static photo-inscription, we can give therefore the following conclusion for the GLS sample: the photo-inscription process of positive index modifications (densification) in GLS is degraded by thermal annealing under T_g.

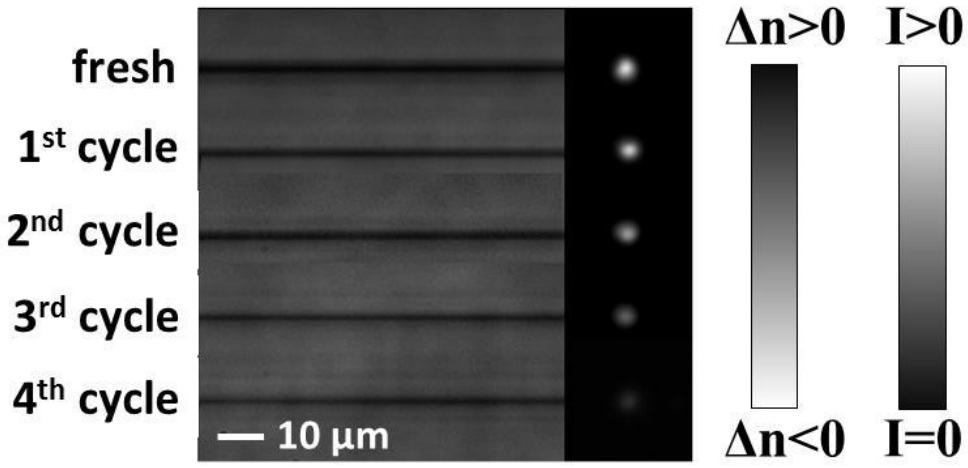

Figure 2.9 The PCM images (left) and near-field mode (right) images of the waveguides photo-inscribed in GLS at 800nm.

2.4.2 Verification of Ge-As-S glass samples in dynamic conditions

As in the static condition, the glass samples of $Ge_{20}As_{20}S_{60}$ and $Ge_{15}As_{15}S_{70}$ showed the opposite results from the GLS case, we made a comparison between laser-induced index modifications of photo-inscribed waveguides in a "fresh" $Ge_{20}As_{20}S_{60}$ sample which was not annealed at all (Figure 2.9a) and in the same sample after the first annealing cycle (Figure 2.9b) with two different laser energetic doses. For the photo-inscription of the waveguides, we set the pulse duration to 2ps and the other experimental conditions were maintained unaltered before and after the annealing cycle. The only difference was that during the experiment, the translating speed of the sample was set to be 40µm/s as before in the "fresh sample" and the translating speed of the sample after one annealing cycle was set to be 160µm/s. which was 4 times higher than the "fresh sample". The comparison of the PCM images, near filed mode intensities and grey scales of the two samples were depicted in Figure 2.10.

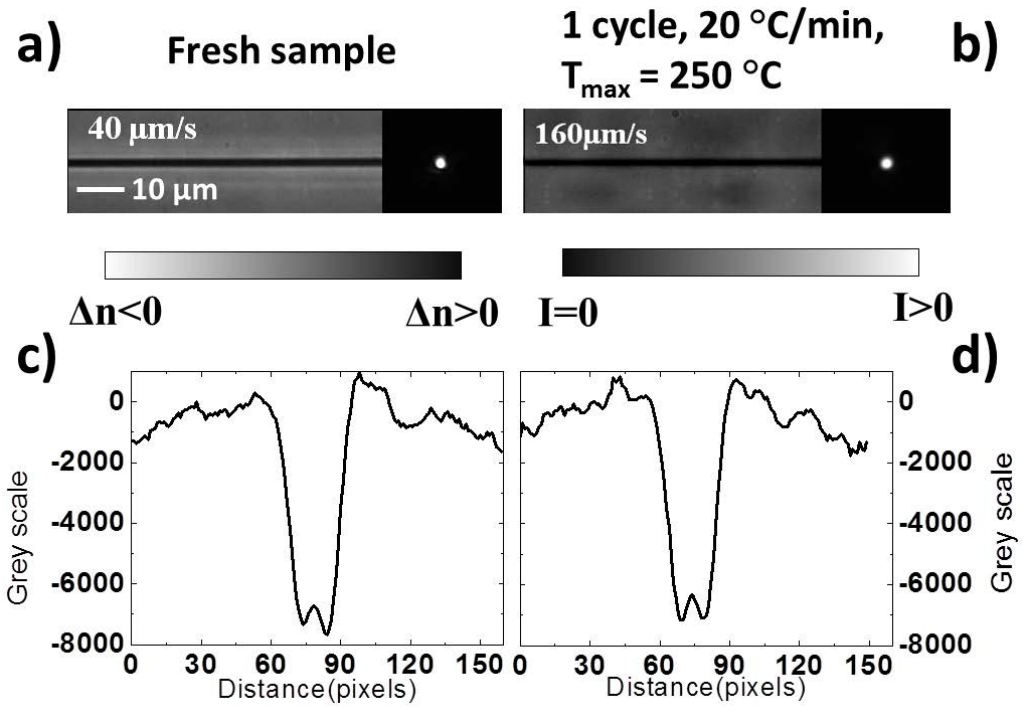

Figure 2.10 Waveguides photo-inscribed by ultrashort laser in (a) "fresh" $Ge_{20}As_{20}S_{60}$ sample and in (b) the same sample after the first annealing cycle. The grey level transvers profiles of the traces in the figures (a) and (b) are shown respectively in (c) and (d).

From the results, we can see that even with a higher translating speed of the sample after one annealing cycle, the refractive index contrast caused by photo-inscription and the intensity of the guided mode is basically the same as the "fresh sample". And also the grey levels of both samples are in good agreement with the results. Since higher translating speed means less exposure time and received laser irradiation, it can be implied that same degree of refractive index modification can be achieved in the sample after one annealing cycle with less laser irradiation. In other words this means that in this case, after thermal treatment, the same result can be obtained by reducing the laser dose by 4 times, and therefore the waveguide photo-inscription process can be speeded-up by 4 times. Therefore, the enhancement of the photo-inscription process after the thermal annealing cycle is confirmed also in the case of dynamic condition.

2.4.3 Results discussion

A photo-induced refractive index change is associated with dominantly a local change in its density: positive type I and negative type II refractive index modifications are linked respectively to local densification and expansion of the glass matrix. While laser-induced local expansion can have a thermodynamic origin, as the local temperature increases sufficiently to melt the glass or drive a thermal expansion in solid phase [18, 25, 26], this is presumably not the case of ultrafast laser-induced local densification. It has been reported in the literature [18] that a process that does not allow structural relaxation would generate a glass sample with high enthalpy and volume, and the density of the glass will decrease. However, re-annealing enables a structural relaxation that corresponds closely to a structural equilibrium at the annealing temperature, which is little affected by the cooling time as the relaxation times becomes prohibitively long [27]. In other words, from a standard normal thermodynamic behavior of a chalcogenide glass, the longer the annealing time at temperatures under T_g, the lower its final volume will be, and the higher its density becomes [28]. The refractive index of the glass, which mainly depends on its density, will depend therefore on its thermal history. A glass annealed long time at a temperature close to T_g will have therefore a higher refractive index than a glass annealed during a short time. Global refractive index variations of the order of 10^{-4} to 10^{-3} can be reached by annealing [29, 30]. The enthalpy represents a first evaluation of structural flexibility allowing evaluating the strength of additional laser-induced modification on a structure with different degrees of relaxation, up to the point where in principle no further structural changes and relaxation can be induced. The structural state reached by controlled annealing will play therefore a role in additional laser-assisted processes as the laser excitation can relaunch a heating-cooling cycle or additional molecular reorganization. In re-annealed samples, where the glass structure is relaxed, it should be much harder to induce photo-contraction, and furthermore the opposite effect of photo-expansion should be observed, especially at higher intensities [31], as is shown in Figure 2.11.

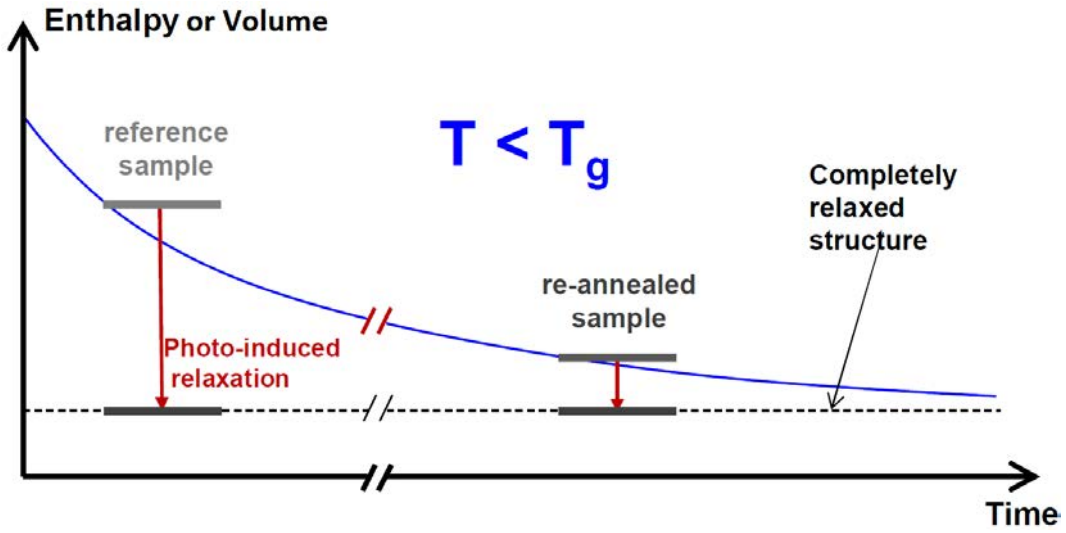

Figure 2.11 Schematic of the thermal history of annealed chalcogenide glasses and its influence on the enthalpy of the microscopic glass structure [18].

Thus, based on the theories introduced above, in our cases, the non-relaxed Ge-As-S glasses' volume was expected to decrease as a function of the annealing time when the glass was annealed at a given temperature under T_g [18], and the relaxation process gets faster as the annealing temperature is closer to T_g. This leaves fewer possibilities for the laser radiation to further densify as the material is already in a higher density state. Now a typical structural relaxation of the glass matrix is expected to be monotonic as a function of the annealing time; this is the reason why, if the behavior observed for GLS glass was expected, the non-monotonic evolutions observed in $Ge_{15}As_{15}S_{70}$ and in $Ge_{20}As_{20}S_{60}$, which clearly showed a trend inversion during the structural relaxation, is an unexpected result.

2.5 The impact of the laser dose on the ultrafast laser induced local modification

To further investigate the mechanism leading to the results obtained above, we considered the impact of the laser irradiation dose received by glass samples on the refractive index change caused by photo-inscription. The experiments were carried out under the static condition and the laser pulse energy was kept constant. In this way,

the laser dose was directly proportional to the laser exposure time of the irradiated region. The laser source employed had pulse duration of 150fs with a repetition rate of 100 kHz and pulse energy of 30nJ.

The variation of the laser-induced index contrast as a function of the exposure time was listed below for $Ge_{20}As_{20}S_{60}$ sample in Figure 2.12.

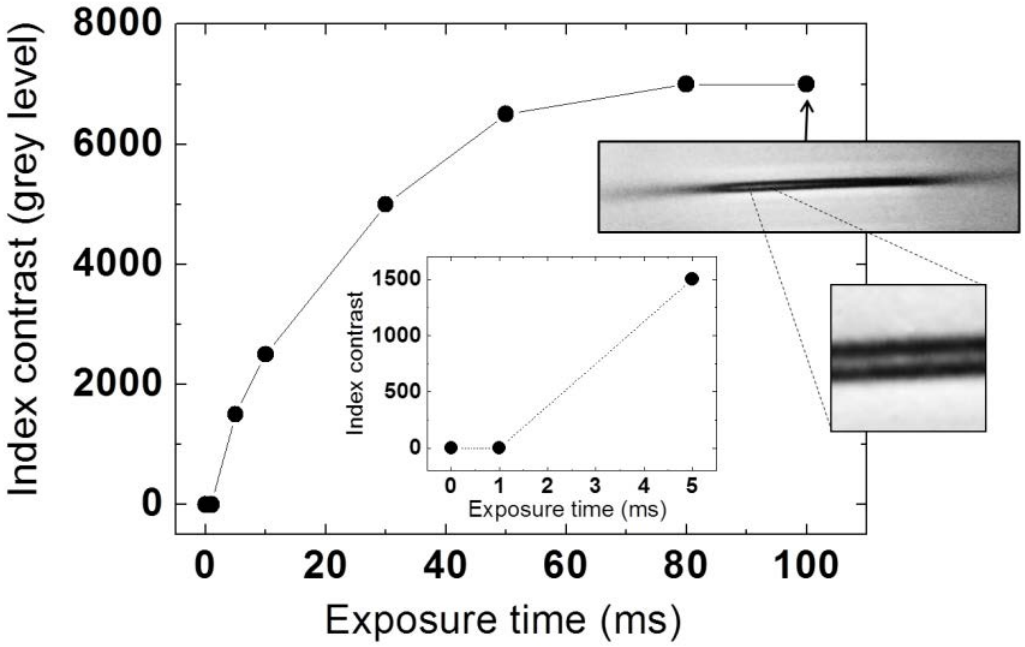

Figure 2.12 Elevation of the index contrast in $Ge_{20}As_{20}S_{60}$ glass as a function of exposure time. The inset graph shows a threshold behavior in terms of exposure time. The inset picture shows the inversion of the response of the glass to laser radiation in the region where the positive index contrast is saturated for high laser doses.

The figure showed the trend of the refractive index change as the exposure time increased and a more detailed figure of the trend in the first few microseconds were placed inside. Besides, two PCM images were added to vividly describe the variation. From the results, it can be concluded that there existed an obvious threshold around 1ms to 5ms for the laser-induced refractive index contrast to be able collect the PCM images. Also, when the laser dose accumulated to a certain saturated value, the positive type I modification would turn into negative type II modification. We attribute this phenomenon to a trend inversion of the response of the material: in correspondence of the regions where the positive index contrast reached the

maximum saturated value the glass cannot furtherly densify and it started to expand instead. It has been tested [14, 18] that the saturated value of the refractive index contrast depends on the glass compositions and, in particular, on the structural flexibility of the glass matrix. Furthermore we can reasonably state that the existence of a threshold (in terms of laser dose) for laser-induced densification is rather related to the efficiency by which the laser pulses couple with the glass matrix. This is a crucial point because it implies that, as a consequence of any glass pre-treatment, a variation of the saturated value of the index contrast would mean a variation of the glass structural flexibility (volume, enthalpy …), as can be obtained for example by glass structural relaxation within a thermal annealing process under T_g (thermally induced physical ageing), while a variation of the laser dose threshold at which the induced local densification becomes visible by PCM would mean a modification of the efficiency of the interaction between the ultrafast laser pulses and the glass structure and, potentially, the inset of new interaction mechanisms.

Thus, to further investigate testify the outcomes obtained above, we compared the positive local refractive index changes which was induced by the laser beam focused into the $Ge_{20}As_{20}S_{60}$ sample before and after the first thermal annealing cycle, and showed the results in Figure 2.13. In the experiments, the “fresh sample” and the sample after one annealing cycles were photo-inscribed under with the laser irradiation dose of 1ms, which was lower than the threshold and 100ms. The effect can be observed on the PCM images obtained. And the evolution of the contrast enhancement against the numbers of annealing cycles of the two exposure time was presented.

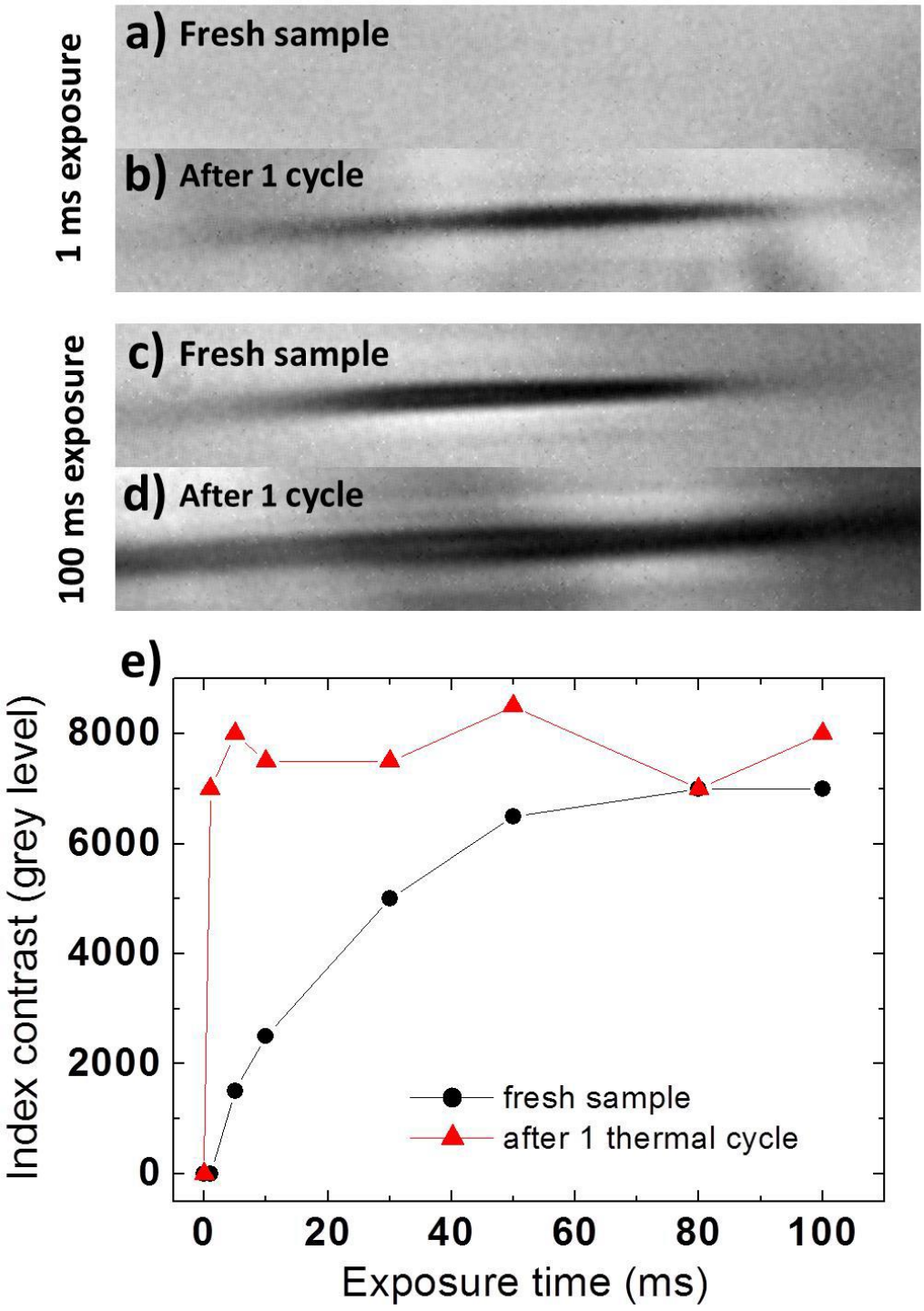

Figure 2.13 Refractive index enhancements of $Ge_{20}As_{20}S_{60}$ samples with and without annealing cycles under 1ms and 100ms of laser irradiation. And the evolution of index contrast enhancement against exposure time.

It can be seen from the figure that an obvious positive local index change can be induced by the laser after the first annealing cycle, while no observable index

changes could be generated, in the same experimental conditions (1ms exposure time at 100 kHz repetition rate, which corresponds to 100 laser pulses), in the "fresh" sample. This means the threshold of the laser induced local densification can be reduced by annealing cycles. And when the laser dose was increased to 100ms, the saturation mentioned above also happened in this experiment. Furthermore, the variation of the contrast of the laser-induced local index modification as a function of the exposure time (laser dose) was plotted for the same $Ge_{20}As_{20}S_{60}$ sample before (dark solid circles) and after (red solid triangles) the first annealing cycle. The change of the response of the sample to the laser radiation, before and after the thermal treatment, was evident. It can be concluded in this graph how the response of two samples were different at low laser doses while the saturation value of the index contrast at higher laser doses remained almost the same. In other words, after the first annealing cycle, the response of the sample to the laser radiation (in terms of induced index contrast) saturated much faster as a function of the laser dose but the saturation value of the index contrast remained almost unchanged. Combining the results mentioned above, we can give the following conclusion: the first annealing cycle does not increase the structural flexibility of the glass matrix (volume of the glass structure) but rather enhances the interaction efficiency between the glass matrix and the laser pulses.

2.6 Conclusion

In this chapter, the influence of thermal annealing treatment on the enhancement of the refractive index contrast of three different chalcogenide glasses (GLS, $Ge_{20}As_{20}S_{60}$, and $Ge_{15}As_{15}S_{70}$) was investigated. The bulk glasses were synthesized using conventional "melt and quench" method and cut into demanded sizes and well-polished.

The experiments were conducted in the static conditions first. By keeping the samples unmoved and injecting laser irradiation into the samples, the impact of the thermal annealing can be reflected on the index contrast enhancement. The three glass samples exhibited different reaction to the laser irradiation, where the refractive index contrast in GLS glass was decreasing with the annealing cycle number increase and the $Ge_{20}As_{20}S_{60}$ and $Ge_{15}As_{15}S_{70}$ glasses had enhancement of 4.7times and 1.3 times after the first annealing and then decreased as the annealing cycle increase.

To verify the results obtained in static conditions, the three samples were also tested in the dynamic conditions (waveguides photo-inscription with translating samples). In the case of GLS glass, both the refractive index contrast PCM images and the near field mode intensity coming out of the waveguide photo-inscribed by in the GLS glasses showed a trend of decreasing after each annealing cycle. And for the case of Ge-As-S glasses, by comparing the reactions of the sample without thermal treatment and the sample after one annealing cycle under different translating speed, the two samples acquired approximately the same degree of refractive index contrast and intensity of the near field mode. Thus, the results from the static conditions are all verified.

Therefore, in order to find the mechanism behind the results, the relationships between the laser doses received by the samples (i.e. exposure time of samples) and the index contrast were investigated. It was discovered that there existed a threshold in terms of laser dose at which the photo-induced index contrast started to be measurable by PCM and the laser-induced index contrast started to go into a saturation status when the laser dose reached certain amount. Subsequently, by comparing samples

with and without annealing cycles in the same experiments, it was found out that the first annealing cycle did not increase the structural flexibility of the glass matrix (volume of the glass structure) but rather enhanced the interaction efficiency between the glass matrix and the laser pulses.

Based on all the comparisons and date collected, it is still not enough to determine the real mechanism of the results obtained in static and dynamic conditions for the Ge-As-S glass samples. Further experiments and testing are required in the future.

Reference

[1]. Rafael R. Gattass, and a. e. MazuR, "Femtosecond Laser Micromachining in Transparent Materials," Nature Photonics (2008).

[2]. D. Du, X. Liu, G. Korn, J. Squier, and G. Mourou, "Laser-induced breakdown by impact ionization in SiO2 with pulse widths from 7 ns to 150 fs," Applied physics letters **64**, 3071-3073 (1994).

[3]. P. Pronko, S. Dutta, J. Squier, J. Rudd, D. Du, and G. Mourou, "Machining of sub-micron holes using a femtosecond laser at 800 nm," Optics communications **114**, 106-110 (1995).

[4]. M. Deubel, G. von Freymann, M. Wegener, S. Pereira, K. Busch, and C. M. Soukoulis, "Direct laser writing of three-dimensional photonic-crystal templates for telecommunications," Nat Mater **3**, 444-447 (2004).

[5]. N. Cvetojevic., N. Jovanovic., S. Gross., B. Norris., I. Spaleniak., C. Schwab., M. J. Withford., M. Ireland., P. Tuthill., O. Guyon., F. Martinache., and J. S. Lawrence., "modal noise in an integrated photonic lantern fed diffraction-limited spectrograph," Opt Express (2017).

[6]. C. Mauclair, G. Cheng, N. Huot, E. Audouard, A. Rosenfeld, I. V. Hertel, and R. Stoian, "Dynamic ultrafast laser spatial tailoring for parallel micromachining of photonic devices in transparent materials," Optics express **17**, 3531-3542 (2009).

[7]. S. Minardi, G. Cheng, C. D'Amico, and R. Stoian, "Low-power-threshold photonic saturable absorber in nonlinear chalcogenide glass," Opt Lett **40**, 257-259 (2015).

[8]. G. Martin, M. Bhuyan, J. Troles, C. D'Amico, R. Stoian, and E. Le Coarer, "Near infrared spectro-interferometer using femtosecond laser written GLS embedded waveguides and nano-scatterers," Opt Express **25**, 8386-8397 (2017).

[9]. A. Rodenas, G. Martin, B. Arezki, N. Psaila, G. Jose, A. Jha, L. Labadie, P. Kern, A. Kar, and R. Thomson, "Three-dimensional mid-infrared photonic circuits in chalcogenide glass," Opt Lett **37**, 392-394 (2012).

[10]. O. Caulier, D. Le Coq, E. Bychkov, and P. Masselin, "Direct laser writing of

buried waveguide in As2S3 glass using a helical sample translation," Opt Lett **38**, 4212-4215 (2013).

[11]. O. Caulier, P. Masselin, E. Bychkov, and D. L. Coq, "[INVITED] Tailoring the morphology of photowritten buried waveguides by helical trajectory in As2S3 glass," Optics & Laser Technology **78**, 56-61 (2016).

[12]. R. Stoian, C. D'Amico, M. K. Bhuyan, and G. Cheng, "[INVITED] Ultrafast laser photoinscription of large-mode-area waveguiding structures in bulk dielectrics," Optics & Laser Technology **80**, 98-103 (2016).

[13]. B. McMillen, M. Li, S. Huang, B. Zhang, and K. P. Chen, "Ultrafast laser fabrication of Bragg waveguides in chalcogenide glass," Opt Lett **39**, 3579-3582 (2014).

[14]. C. D'Amico, G. Cheng, C. Mauclair, J. Troles, L. Calvez, V. Nazabal, C. Caillaud, G. Martin, B. Arezki, E. LeCoarer, P. Kern, and R. Stoian, "Large-mode-area infrared guiding in ultrafast laser written waveguides in sulfur-based chalcogenide glasses," Opt Express **22**, 13091-13101 (2014).

[15]. I. Blonskyi, V. Kadan, O. Shpotyuk, M. Iovu, P. Korenyuk, and I. Dmitruk, "Filament-induced self-written waveguides in glassy As4Ge30S66," Applied Physics B **104**, 951-956 (2011).

[16]. T. H. Xin Gai, Amrita Prasad, Steve Madden, Duk-Yong Choi, Rongping Wang, Douglas Bulla and Barry Luther-Davies, "Progress in optical waveguides fabricated from chalcogenide glasses," Opt Express (2010).

[17]. W. Y. M. Hughes, and D. Hewak, "Fabrication and characterization of femtosecond laser written waveguides in chalcogenide glass," Applied Physics Letters (2007).

[18]. C. D'Amico, C. Caillaud, P. K. Velpula, M. K. Bhuyan, M. Somayaji, J. P. Colombier, J. Troles, L. Calvez, V. Nazabal, A. Boukenter, and R. Stoian, "Ultrafast laser-induced refractive index changes in Ge_15As_15S_70 chalcogenide glass," Optical Materials Express **6** (2016).

[19]. M. Sinobad, C. Monat, B. Luther-davies, P. Ma, S. Madden, D. J. Moss, A. Mitchell, D. Allioux, R. Orobtchouk, S. Boutami, J.-M. Hartmann, J.-M. Fedeli, and

C. Grillet, "Mid-infrared octave spanning supercontinuum generation to 85 μm in silicon-germanium waveguides," Optica **5** (2018).

[20]. Y. Yu, X. Gai, P. Ma, K. Vu, Z. Yang, R. Wang, D.-Y. Choi, S. Madden, and B. Luther-Davies, "Experimental demonstration of linearly polarized 2–10 μm supercontinuum generation in a chalcogenide rib waveguide," Optics letters **41**, 958-961 (2016).

[21]. L. Carletti, P. Ma, Y. Yu, B. Luther-Davies, D. Hudson, C. Monat, R. Orobtchouk, S. Madden, D. Moss, and M. Brun, "Nonlinear optical response of low loss silicon germanium waveguides in the mid-infrared," Optics express **23**, 8261-8271 (2015).

[22]. Y. Yu, X. Gai, P. Ma, Z. Yang, R. Wang, D.-Y. Choi, S. Madden, S. Debbarma, and B. Luther-Davies, "A broadband mid-infrared supercontinuum generated in a short chalcogenide glass waveguide," in *Photonics Society Summer Topical Meeting Series, 2014 IEEE*(IEEE2014), pp. 39-40.

[23]. Y. Yu, X. Gai, P. Ma, Z. Yang, R. Wang, D.-Y. Choi, S. Madden, S. Debbarma, and B. Luther-Davies, "A two-octave broadband quasi-continuous mid-infrared supercontinuum generated in a chalcogenide glass waveguide," in *Lasers and Electro-Optics (CLEO), 2014 Conference on*(IEEE2014), pp. 1-2.

[24]. X. Gai, D.-Y. Choi, S. Madden, Z. Yang, R. Wang, and B. Luther-Davies, "Supercontinuum generation in the mid-infrared from a dispersion-engineered As 2 S 3 glass rib waveguide," Optics letters **37**, 3870-3872 (2012).

[25]. P. K. Velpula, M. Bhuyan, F. Courvoisier, H. Zhang, J.-P. Colombier, and R. Stoian, "Spatio-temporal dynamics in nondiffractive Bessel ultrafast laser nanoscale volume structuring," Laser & Photonics Reviews **10**, 230-244 (2016).

[26]. M. K. Bhuyan, M. Somayaji, A. Mermillod-Blondin, F. Bourquard, J. P. Colombier, and R. Stoian, "Ultrafast laser nanostructuring in bulk silica, a “slow” microexplosion," Optica **4** (2017).

[27]. H. Hisakuni, and K. Tanaka, "Giant photoexpansion in As2S3 glass," Applied Physics Letters **65**, 2925-2927 (1994).

[28]. J. Zarzycki, *Glasses and the vitreous state* (Cambridge University Press,

1991).

[29]. L. Boesch, A. Napolitano, and P. Macedo, "Spectrum of volume relaxation times in B2O3," Journal of the American Ceramic Society **53**, 148-153 (1970).

[30]. P. Macedo, and A. Napolitano, "Effects of a distribution of volume relaxation times in the annealing of BSC glass," J Res Natl Bur Stand **71**, 231-238 (1967).

[31]. Laurent Calvez, Zhiyong Yang, and a. P. Lucas, "Reversible giant photocontraction in chalcogenide glass," Opt Express (2009).

Chapter III Innovative Chalcogenide Fiber designs for Mid-Infrared Supercontinuum Generation

3.1 Introduction

Chalcogenide glass fibers based on sulfide, selenide, telluride and their rare earth doped compositions are being actively investigated worldwide. Chalcogenide glass fibers possess the superiority of chalcogenide glass, such as photosensitivity, high nonlinearities (several orders of magnitude higher than silica), wide transparent window in the mid-infrared region (sulphides transmit to ~7μm, selenides to ~12μm and tellurides to beyond 15μm) and high linear refractive index, and the advantages of optical fibers, like compactness, high efficiency and easy to cool down. With these outstanding qualities, chalcogenide fibers have been studied and utilized in a variety of domains, for example chemical sensing [1-7], imaging [8, 9], spectro-microscopy [10] and the aim of our work: the mid-infrared supercontinuum generation (SCG) [8, 11-20].

One of the aims of Mid-infrared supercontinuum generation is to extend the wavelengths coverage. It requires the fiber to be able to transmit light in the mid-infrared region with acceptable losses. Similar intentions were proposed in "Terrestrial Planet Finder" project led by National Aeronautics and Space Administration (NASA) and "Darwin Project" led by European Space Agency (ESA) which aimed at detecting extra solar terrestrial planets. To fulfill the goals, a step-index fiber covering the fingerprint region of most chemical and biological molecules has to be developed. Therefore, Tellurium-based glass was selected due to the wide transparent range caused by its heavy atomic masses and smaller bonding force constants. As it has been reported, Tellurium-based bulk glass is able to transmit infrared light beyond 35μm [19, 21-24]. However, melt Tellurium has a strong metallic character which makes it quite difficult to vitrify, different methods have been applied by adding Gallium [21], Iodine [22], silver iodide [25, 26] or selenium [27-29]. And it has been discovered that addition of silver iodine as a form of salt not only solved the problem of the volatility of iodine but also improved the thermal stability of the glass obtained, as the DSC curves of glass with 10,15 and 20% of

silver iodine showed no obvious crystallization peak [25]. Thus, in the first section of this chapter, the three compositions mentioned above were synthesized with a two-step purification procedure. By analyzing the thermal and optical properties of the bulk glass, compositions for the core and cladding of the step-index fiber was selected. With the assistance of a modified casting method, the preform of the cladding was fabricated and the final preform of the step-index fiber was assembled and drawn into fibers for light guiding test.

Besides the wavelengths extension of mid-infrared supercontinuum generation, the efficiency of the interaction between the pump source and the chalcogenide fiber is essential as well. This mainly concerns the dispersion status of the chalcogenide fiber and the central wavelength of the pump source. It has been convicted that SCD in normal dispersion regime requires engineered, flattened curve of dispersion for a higher efficiency [30, 31].However, up to date , few commercially available laser source with high peak power can be utilized for the SCG. Therefore, it is necessary to find a solution of fiber dispersion engineering. For the conventional step-index structure fibers, there is limited space preserved for dispersion modification. As for photonic crystal fiber (PCF), higher degree of dispersion modification can be achieved by altering the diameter of the air holes and the distance between them, but the fabrication desire fine fabrication. Thus, grade-index fiber was chosen for realizing dispersion engineering for high efficiency generation of supercontinuum [32, 33].Through numerical simulations, it was discovered that broader and more flatten spectrum could be generated in the graded-index fiber with designed dispersion profile compared with step-index fibers. A novel technique was put forward for the fabrication of such type graded-index fiber. In the second part of this chapter, two glass compositions selected to be the high and low refractive index rods were synthesized and characterized. A stacked preform of the fiber was assembled with the glass rods and the optical property of the graded-index fiber obtained was measured.

The advent of micro-structured fibers gave access to a wide range of fiber geometries and associated optical properties non-accessible with conventional optical fibers. Initially focused in the optical fibers made of high purity silica glass, this

research field has then rapidly been extended to other more exotic glasses that were not easy to exploit in conventional optical fiber geometry due to the difficulty there exists, for non-silica materials, in realizing a core/cladding structure made of two similar materials with perfectly controlled refractive index difference. Chalcogenides, fluorides and other oxides glasses have been used to obtain new photonic devices. As different optical fiber platforms have focused on silica micro-structured fiber with wide range of geometries or non-silica optical fibers with novel glass compositions, it is of great interest to develop on hybrid fiber structures containing different types of glass. Studies on the hybrid structure fiber glass have been carried out in the last few years [34-36] , and more attention was payed to the generation of supercontinuum sources [37-42]. So, in the last section of this chapter, a hybrid fiber made with inclusion of silica PCF with TAS glass was attempted and the factors influencing the obtained results were collected and analyzed.

3.2 Te_4GeAgI chalcogenide step-index fiber

3.2.1 Glass composition selection

It has been discovered in previous research [43] that the $(Te_4Ge)_{100-x}AgI_x$ (TG-AgI) glass system appeared to have a better thermal stability than the other types of Tellurium-based glass systems, which makes it potential candidate for step-index fiber fabricating. To explore the thermal stability evolution of TG-AgI glasses, compositions of $(Te_4Ge)_{100-x}AgI_x$ with X=5,10,15,20,25 and 30 had been synthesized and tested in [19]. The Differential scanning calorimetry (DSC) curves of all the compositions were measured and the results are presented in Figure 3.1

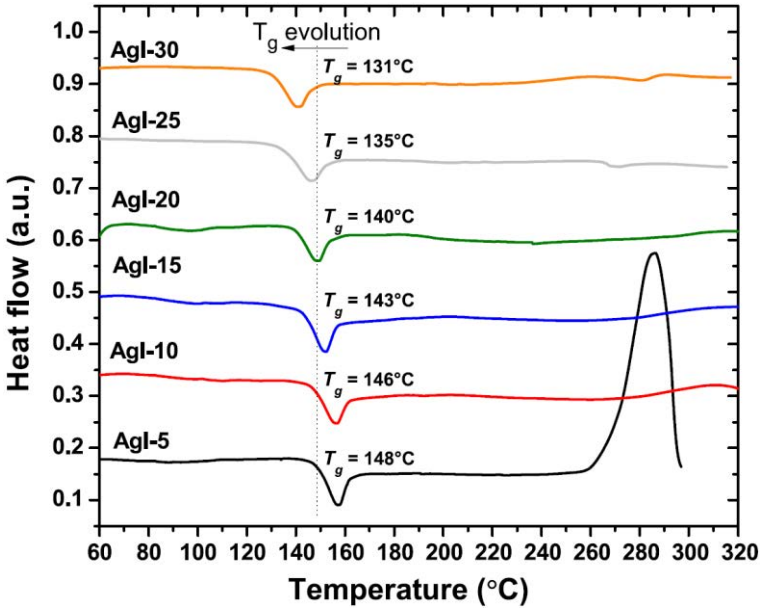

Figure 3.1 DSC curves of the $(Te_4Ge)_{100-x}(AgI)_x$ glasses (x=5, 10, 15, 20, 20, 25, and 30).

From the Figure 3.1, we can see that as the increase of AgI content, the glass transition temperature (T_g) of the glass gradually reduced. The TG-AgI glasses started to show no visible crystallization peak when the AgI content reached more than 10%, which is in consistent with previous results [25, 44]. And when the AgI content reached 30%, a small crystallization peak can be observed in the curve. Of all the measured DSC curves of the glasses, compositions with 10, 15 and 20% content of AgI showed no visible crystallization, which proved the thermal stability of the three compositions. Therefore, in this section, the three glass compositions namely $(Te_4Ge)_{90}AgI_{10}$, $(Te_4Ge)_{85}AgI_{15}$, $(Te_4Ge)_{80}AgI_{20}$ were chosen to be the material for the fabrication of the single index fiber.

3.2.2 Bulk glass synthesis and characterization

3.2.2.1 Purification of tellurium

Due to the long distance of propagation of light in the fiber, the defect on the surface or the absorption caused by the impurities existing in the fiber can cause serious losses. So it is of great importance to fabricate high quality fibers.

In order to obtain fiber with high purity, it is necessary to purify the raw elements used for synthesis. As for germanium, the purification is difficult to be carried out duo to the high melting temperatures of both Ge and GeO_2, further purification will be illustrated in the process of glass synthesis. And also, Silver iodine is unlikely to interact with oxygen and water compared with germanium and tellurium, there is no need for purification based on its intrinsic 5N purity. Hence, only the purification of tellurium (Te) will be presented here.

The mechanism of the distillation of tellurium is to make use of the difference of the vapor pressures. Indeed, metallic tellurium is more volatile than tellurium oxide. In addition the distillation process permits to remove other refractory elements (Carbon, silicon oxide, other refractory oxides …) that can be embedded in the raw materials. (The distillation process is illustrated in Figure3.2)

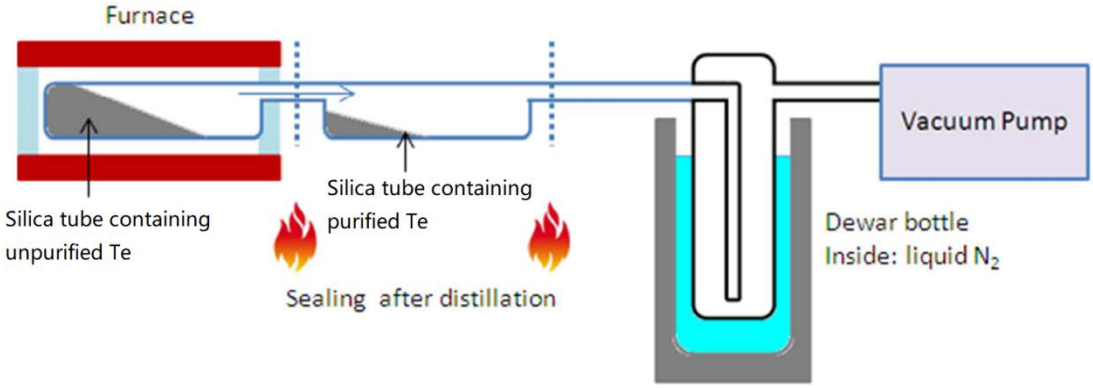

Figure 3.2 Schematic explanation of tellurium purification

The silica chamber containing unpurified tellurium was inserted into a furnace and heated up to 500 ° C in 3 hours. Then, the temperature was gradually increased to 550 ° C. At this temperature, the vapor pressure of the liquid state tellurium was about 100 Pa [45, 46], which made it easy to the vaporize and condense in the cold chamber. Thus, due to the difference in vapor pressure caused by the melting temperature difference between Te and refractory impurities can be separated from Te. The tellurium bulk is then sealed in both end and placed horizontally at 500 ℃ for 30 minutes and cooled down to room temperature.

3.2.2.2 Synthesis of Te_4Ge glass

The method used for the fabrication of bulk glass is still traditional melt and quench technique, and for a better quality of the glass, "two-steps purification process" were utilized. For the synthesis of Te_4Ge glass, the silica ampoule used for had an inside diameter of 10 mm and an outside diameter of 13 mm. The silica ampoule was first cleaned with hydrofluoric acid (HF) to remove the silica dust and cleaned thoroughly with distilled water. Then it was connected to a vacuum pump (10^{-3} mbar) for a few hours to erase the residual water and oxygen. To avoid oxidation and contamination, the raw elements were weighted in a glovebox under the protection of argon and added to the silica ampoule which was sealed by a tap. Except for Tellurium and Germanium, 100ppm of Aluminum was also inserted into the silica ampoule. The aim of adding Aluminum was to let it react with the oxide impurities contained in the raw elements during the first step of chemical purification. The tube was then connected back to the trap immersed in liquid nitrogen and evacuated (10^{-5} mbar) for another several hours.

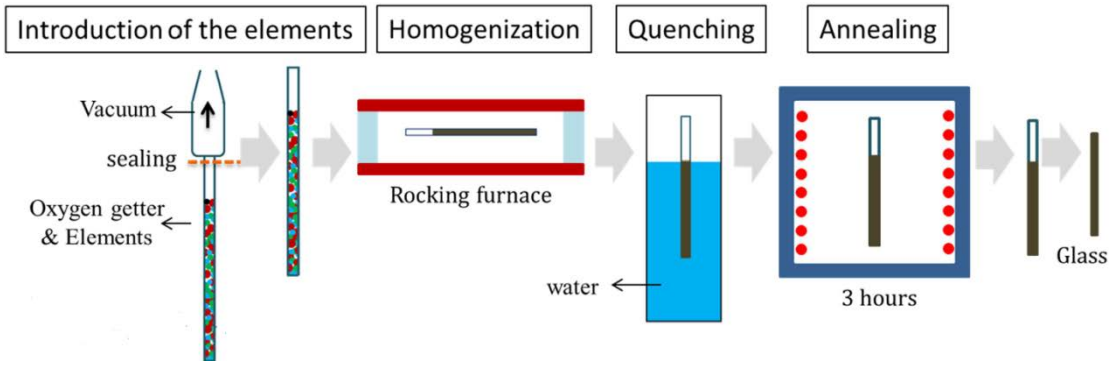

Figure 3.3 Schematic diagram of the synthesis of Te_4Ge glass

After that, the silica ampoule containing the raw elements was sealed under hydrogen flame and put into a rocking furnace for homogenization. During the homogenization, the raw elements were heated up to 800℃ with a heating rate no more than 2℃/min and kept at this temperature for 10 hours. Afterwards, the temperature was decreased to 450℃ in 2 hours and quenched in water. After quenching, the formed glass was transferred into an annealing furnace for 3 hours slightly lower than the T_g to release the stress inside the glass and then cooled down to

room temperature in 10 hours. The schematic diagram of the synthesis and the thermal treatment of the Te_4Ge glass are presented in Figure 3.3 and Figure 3.4 respectively.

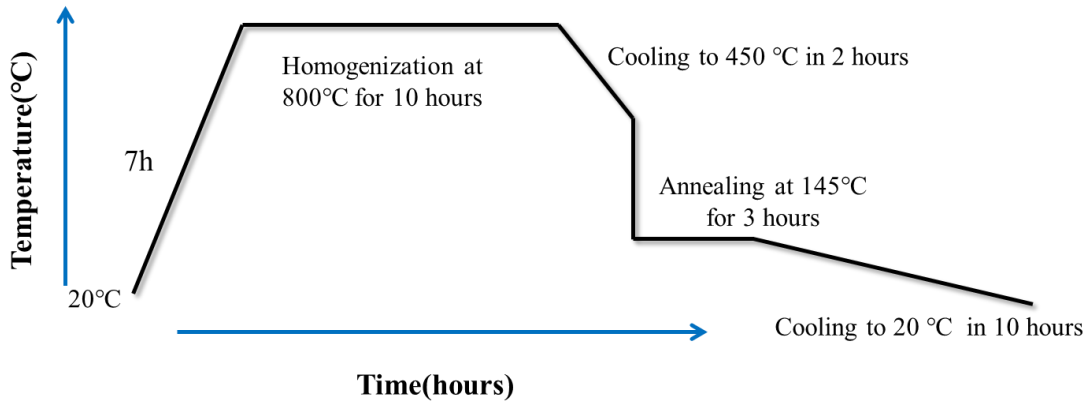

Figure 3.4 Thermal profile for the synthesis of Te_4Ge glass

4.2.2.3 Distillation of Te_4Ge glass and synthesis of Te-Ge-AgI glass

As mentioned above, for an ideal bulk glass synthesis, the "two-steps distillation" method was applied in our experiment. The inserted 100ppm Aluminum was the first step of chemical distillation, so as to react with the oxide came with the raw elements of Tellurium and Germanium.

In the second step of the distillation, a silica ampoule with a different design structure was elaborated. Indeed, the silica set-up is composed of a filter with a cannula on the top and a straight tube at the bottom. To maximize the elimination of contaminations inside the silica ampoule, it was also washed in hydrofluoric acid and thoroughly cleaned with distillated water. Then, it was connected to a vacuum pump and put under vacuum for at least 2 hours. After being introduced into a glovebox filled with Argon, the bulk glass of Te_4Ge previously synthetized with the addition of the metallic aluminum as an oxygen getter, was put in the filter chamber and the AgI was weighted in calculated portion and inserted to the bottom of the silica ampoule. Followed by reconnecting to the vacuum pump and placed under accelerated vacuum

overnight, the sample was sealed and put into a distillation furnace.

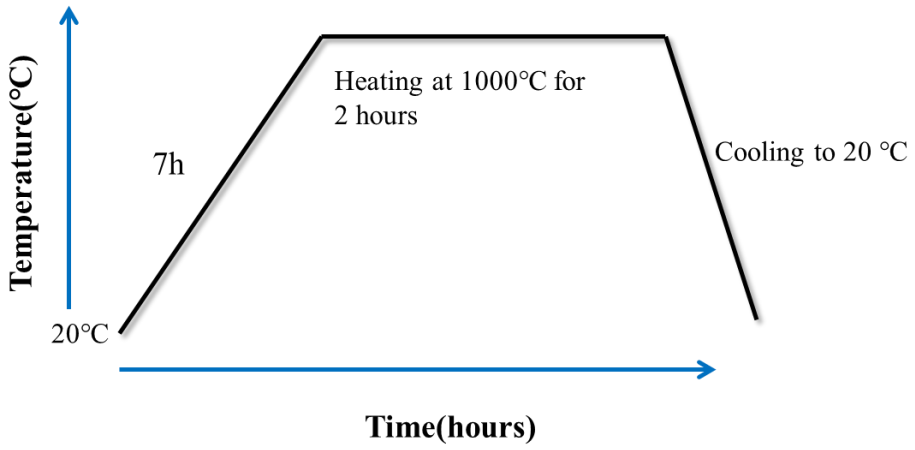

Figure 3.5 Thermal profile of the distillation process

The thermal profile of the distillation is displayed above in Figure 3.5. During the distillation process, the furnace was heated up to 1000℃ in 7hours, and maintained for 2 hours. In this period, the Tellurium and Germanium would be melted and vaporized. As the only part of the silica ampoule positioned in the furnace was the filter chamber, the Tellurium and Germanium vapor finally cooled down at the bottom of the ampoule where the AgI was placed, leaving the Al_2O_3 and all the other refractory impurities behind in the filter chamber, due to the different melting point and boiling point of them. The bottom of the ampoule was then sealed and went through the last step of homogenization. The schematic diagram of the distillation is shown in Figure 3.6. Same as the procedure before, the furnace was heated up to 800℃ with a heating rate no more than 2℃/min and maintained for 10 hours for homogenization. After cooling to 450℃ in 2 hours, the Te-Ge-AgI glass was quenched in water and annealed at 145℃ for 3 hours. The temperature of the annealing furnace was gradually decreased to 20℃ in 10 hours.

One more thing to notice is that, in order to avoid bubbles inside or on the surface of the bulk glass, the rocking furnace was put statically in the vertical position for one hour in the homogenization at 800℃ and the rest of the time before reaching the temperature for quenching. The schematic diagram of the distillation of Te_4Ge glass and the Te-Ge-AgI synthesis are illustrated in Figure 3.6 and the thermal profile for

the synthesis of Te-Ge-AgI glass in Figure 3.7. As a result, the obtained bulk glass could be used for fiber drawing.

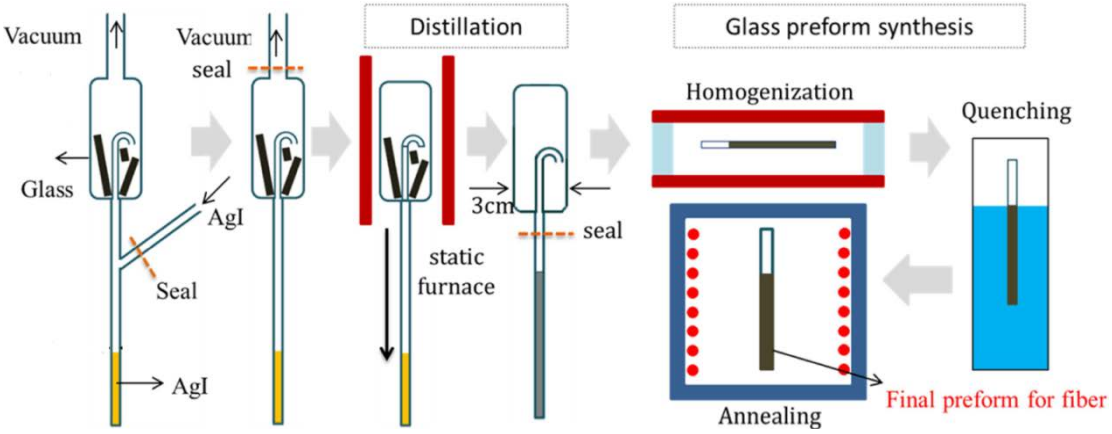

Figure 3.6 Schematic diagram of the distillation process and the synthesis of Te-Ge-AgI glass

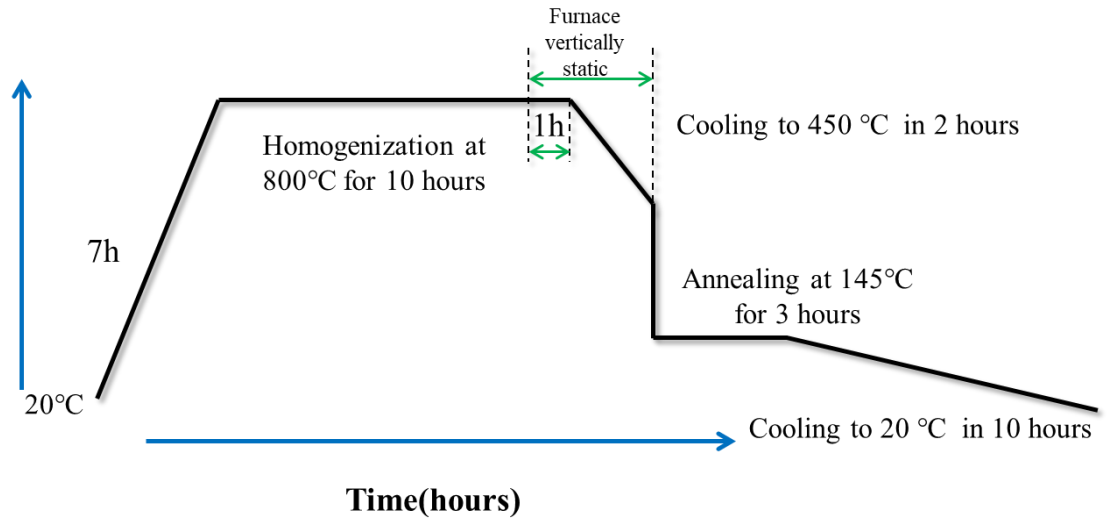

Figure 3.7 Thermal profile for the synthesis of Te-Ge-AgI glass

4.2.2.4 Thermal stability of Te-Ge-AgI glass

After the synthesis of the Te-Ge-AgI glass, it is necessary to measure the thermal stability of the glass to verify the thermal property of the glass. The glass composition of Te_4GeAgI_{10} was tested as an example. The DSC test was carried out with a heating rate of 10℃/min on a TA instruments Auto Q20 from 50℃ to 290℃. The results are shown in Figure 3.8. From the result, it can be seen that the estimated T_g of the glass

was about 148℃ and no obvious T_x was found in the test range, which verified the thermal stability of the glass.

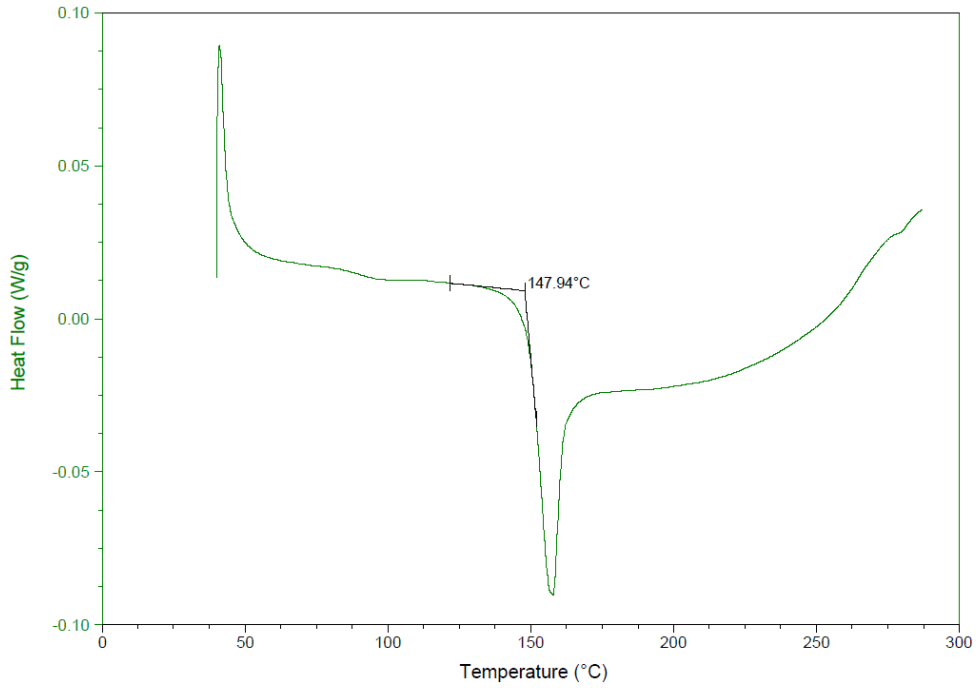

Figure 3.8 DSC curves of $(Te_4Ge)_{90}AgI_{10}$ glass

3.2.2.5 Optical transmittance of Te-Ge-AgI glass

For the fabrication of high quality fibers, it is essential to measure the optical transmission property of the bulk glass. A piece of the bulk glass cut from the bulk glass with a thickness of 1.5mm was well-polished as instructed in Chapter I, as is depicted in Figure 4.2.9(a).

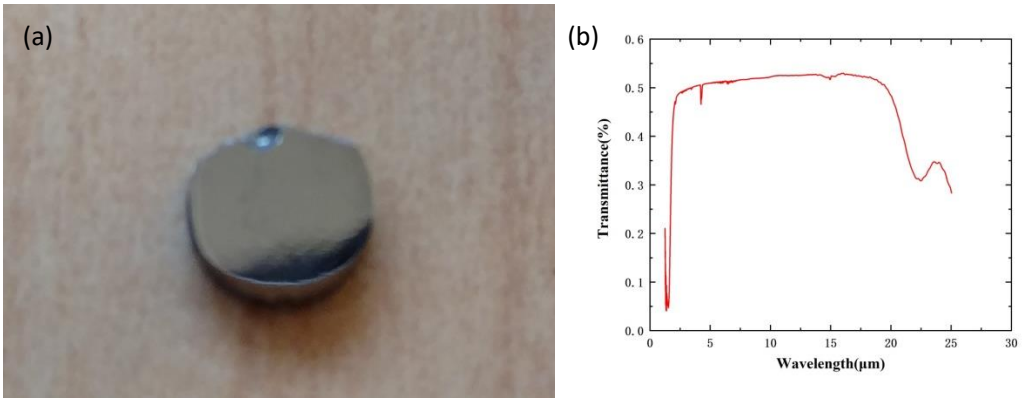

Figure 3.9 (a) Photo of well-polished glass piece for transmission measurement (b) Transmittance curve of Te_4GeAgI_{10} glass sample

The optical losses of the sample were measured using a Bruker vector 27 FT-IR Spectrometer and the curve was shown in Figure 3.9(b).

The transmittance of the $(Te_4Ge)_{90}AgI_{10}$ glass sample was smooth from 3μm to 20μm (the absorption band at 4.26μm, comes from atmospheric CO_2 detected during the transmission measurement).

3.2.3 Preparation and characterization of single index fiber

3.2.3.1 Fiber drawing process

Subsequent to the thermal and optical analysis of the bulk glass is the single index fiber drawing process. Same as mentioned above, the facility utilized for the fabrication of the fibers was a home-made fiber tower the photograph of the fiber drawing tower and schematic diagram of fiber drawing process are shown in Figure 3.10.

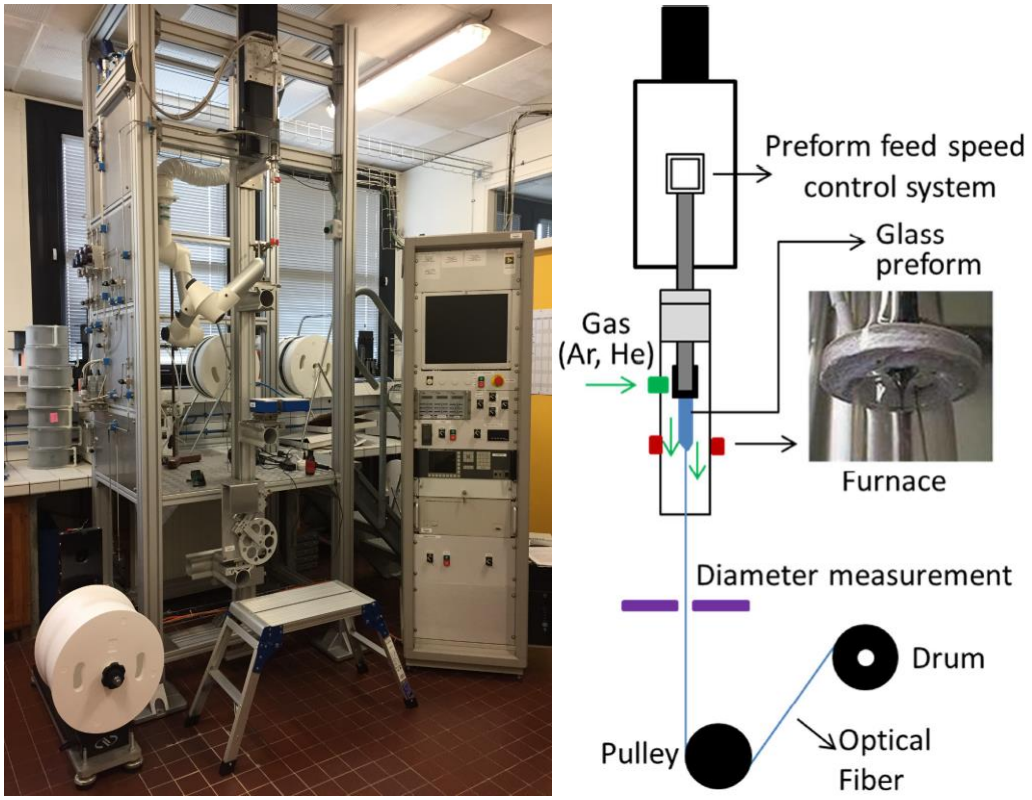

Figure 3.10 Photograph of the drawing tower (left) and the illustration of the fiber drawing process

In the fiber drawing process, the glass preform obtained from previous step was vertically fixed close to the ring furnace chamber and cleaned with pressured Argon so as to remove the dust on the surface of the glass preform. In order to prevent the influence of oxidation caused by the presence of H_2O and O_2 in the atmosphere, the furnace chamber was purged under a flow of Argon with a speed of 3 L/min for at least 2 hours. And then, the Argon flow was replaced by Helium with the same flow rate of 3 L/min to provide better thermal conductivity.

At the beginning of the fiber drawing process, the furnace was firstly heated up to a temperature to the glass softening point and by the effect of its own weight a glass drop was generated. Then the fiber is stretched and taped on the rotating drum (Figure 3.10). Therefore, the fiber was drawn under the heat of the furnace and the pulling force from the rotation of the drum. Normally, by changing the processing parameters such as preform descent speed (V_p) and drum rotation speed (V_d), fibers with various diameters can be prepared. The relationship between the V_p and V_d can be described with the equation 4.2.1.

$$\frac{\pi \emptyset_p^2}{4} V_p = \frac{\pi \emptyset_f^2}{4} V_d \tag{3.1}$$

In the equation, $\emptyset_p$ and $\emptyset_f$ represented the diameters of the preform and the fiber respectively. Thus, in the process of fiber drawing, the fiber diameter could be controlled by fixing V_p and adjusting V_d.

In a first step, a single index fiber with a composition of $(Te_4Ge)_{90}AgI_{10}$ has been elaborated to be further applied in forming the core of a step-index fiber. The diameter of the preform after polishing was measured to be around 8.736 mm. the polishing of the preform permits to remove all the surface defects that can induce crystallization during the drawing. The final diameters of the fiber obtained were around 350µm and 490 µm, for attenuation measurements and step index fiber fabrication respectively. An image of the preform after drawing, the first drop and the obtained fiber is displayed below in Figure 3.11.

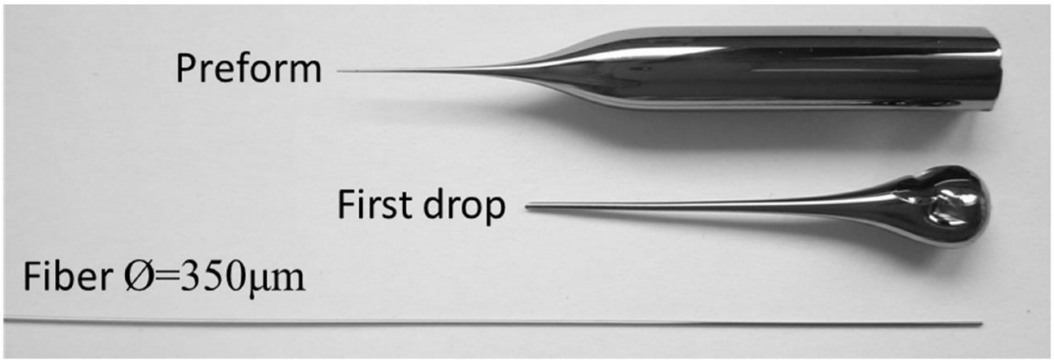

Figure 3.11 Image of the preform, first drop and fiber after drawing

4.2.3.2. Attenuation measurements of the single index fiber

The optical loss is an essential factor to evaluate the quality of fibers. Normally, the losses are induced by several reasons, such as the intrinsic absorption of the materials, impurities, scattering losses and bending losses. Of all the reasons, losses caused by impurities and scattering are considered to be more influential. Therefore, due to the high sensitivity of optical fibers to the existence of any impurity, optical attenuation measurement is the most efficient method to evaluate the glass quality.

Cut-back technique

The cutback technique is a destructive technique for determining optical fiber transmission characteristics. Also, it is normally considered to be the most common way to measure the attenuation. The measurement technique consists of:

1. performing the desired measurements on a long length of the fiber under test
2. cutting the fiber under test at a point near the launching end
3. repeating the measurements on the short length of fiber
4. subtracting the results obtained on the short length to determine the results for the residual long length.

Following the rules above, the attenuation of the fiber α (in dB / m) as a function of the wavelength λ using the following equation:

$$\alpha(\lambda) = \frac{10}{L_1 - L_2} \log_{10} \frac{I_2(\lambda)}{I_1(\lambda)} \tag{3.2}$$

In the equation, L_1 and L_2 represent the lengths of the fiber before and after the

cut respectively, I_1 and I_2 represent the output power before and after respectively. The schematic diagram of cutback technique is shown in Figure 3.12. In our case, measurements were performed using a Tensor 37, Bruker Fourier Transform Spectrometer. For each fiber length considered, several measurements are executed and the calculation of the resulting attenuation was obtained from an average of the spectra obtained.

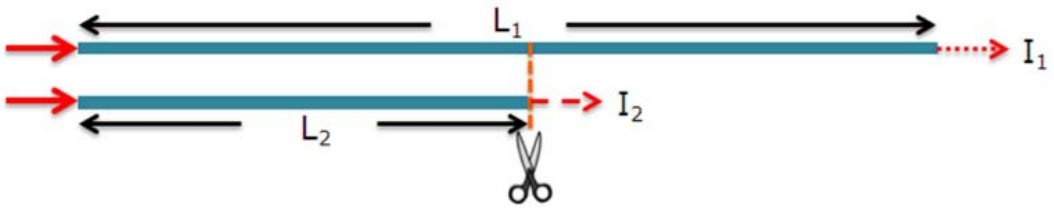

Figure 3.12 Schematic diagram of cutback technique used for fiber attenuation measurement

Using the cutback technique introduced in front, the measurement of the attenuation of the $(Te_4Ge)_{90}AgI_{10}$ optical fiber is shown in Figure 3.13. The optical losses were measured thanks to a Bruker Vector 27 FT-IR Spectrometer and the output signal of the fiber is focused on a mercury cadmium telluride (MCT) detector cooled by liquid nitrogen.

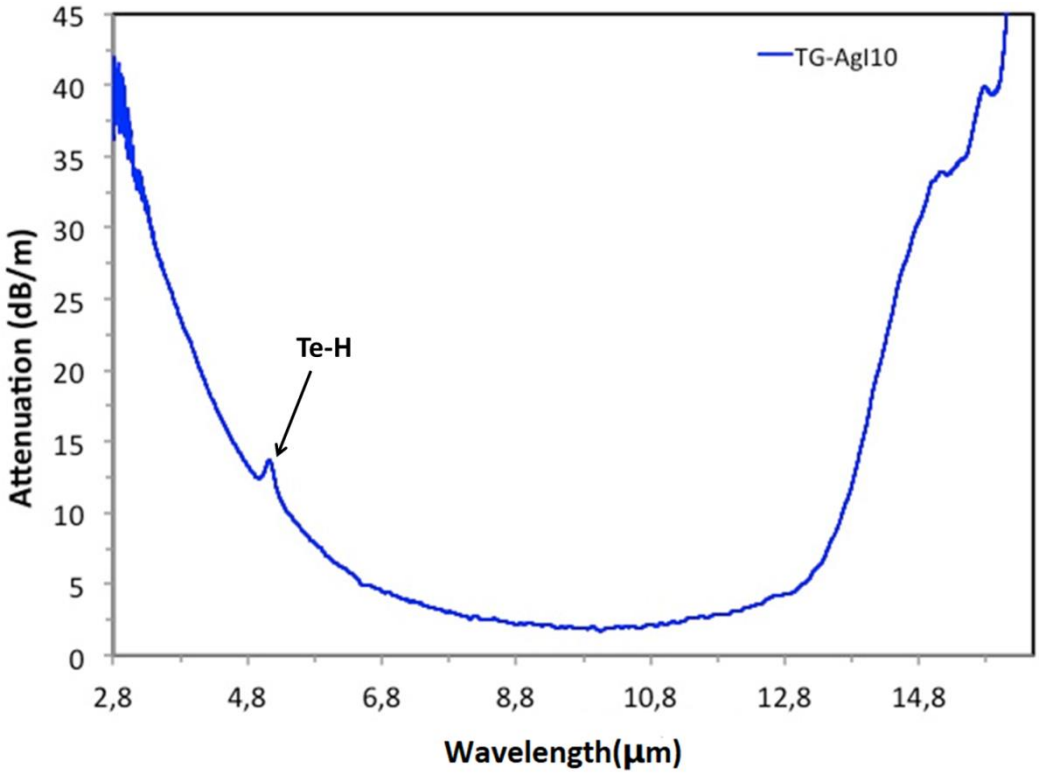

Figure 3.13 Attenuation curve of single index $(Te_4Ge)_{90}AgI_{10}$ fiber

As can be observed from the figure, the minimum attenuation in the range of measurement is 2dB/m at 10µm. The absorption peak located at 5µm is due to Te-H bonds. The possible cause could be that the hydrogen was absorbed by the silica in the form of OH during the manufacture of the tube and the cleaning process. This type of impurity is also often observed in selenide glasses (Se-H bonds) and it is difficult to eliminate completely simply by vacuum drying.

4.2.3.3 Refractive index measurements

The refractive index contrast between the core and cladding of a fiber is the essential guarantee of the light propagation in the fiber. Therefore, it is indispensable to measure the refractive index of the compositions selected for fabricating the fiber. With the assistance of our colleague in Florida, the measurements were carried out at 22℃ at 10.6µm. For each composition, the measurements were taken 5 times and averaged. The composition glass $(Te_4Ge)_{90}AgI_{10}$ has a refractive index of 3.1143 (± 0.0003) and the composition glass $(Te_4Ge)_{85}AgI_{15}$ has a refractive index of 3.1132 (±

0.0003). Therefore, the step-index fiber will be made with a core composition of $(Te_4Ge)_{90}AgI_{10}$ and a cladding of $(Te_4Ge)_{85}AgI_{15}$ ($\Delta n \approx 10^{-3}$).

3.2.4 Preparation and characterization of step index fiber

3.2.4.1 Casting method introduction

Defects of rod-in-tube method

As the strong metallic property of Tellurium, Te-based glasses possess high crystallization tendency. Thus, it is necessary to develop a method to successfully produce the glass preform without crystallization. Based on previous experiments on chalcogenide fibers, the commonly used method to design double index fiber is the so-called "rod in tube" technique. This method normally consists of several steps, including drawing of the rod, preparation of the tube by rotational casting, and drawing of the preform with rod inside the tube. Depending on the desired final dimensions, the second and third steps can be repeated several times. However, as "rod in tube" technique requires several times of casting and drawing before achieving the desired core diameter (Figure 3.14) for single mode propagation, it is not suitable for the glass having a high tendency to crystallize. In a previous study, it has been found that after the rotational casting process, crystals appear on the surface of telluride glass tube.

In addition, also due to high crystallization tendency of the Te rich glasses, fiber cannot be elaborated by the double crucible method. (Method used for the commercial step index chalcogenide fibers from core active and IR Flex companies). Hence, a new technique needs to be developed to decrease the tendency of crystallization during preform preparation and fiber drawing proceeds for Te-based glasses.

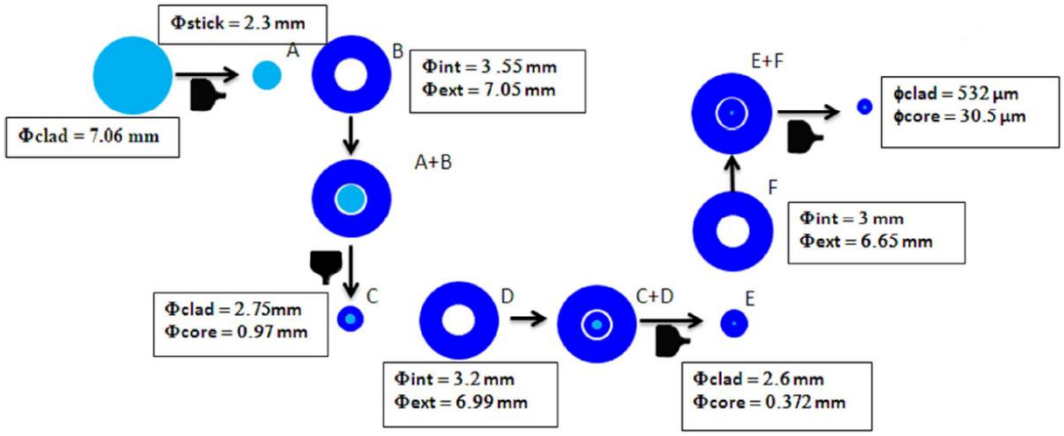

Figure 3.14 Schematic diagram of "rod-in-tube" method

Introduction of casting method

Casting method was originally developed for the fabrication of micro-structured optical fibers. In this method, by placing array of silica capillaries in the mold and purge melted chalcogenide glass into it, a micro-structure fiber preform could be obtained after removing the silica capillaries with an hydrofluoric acid treatment.

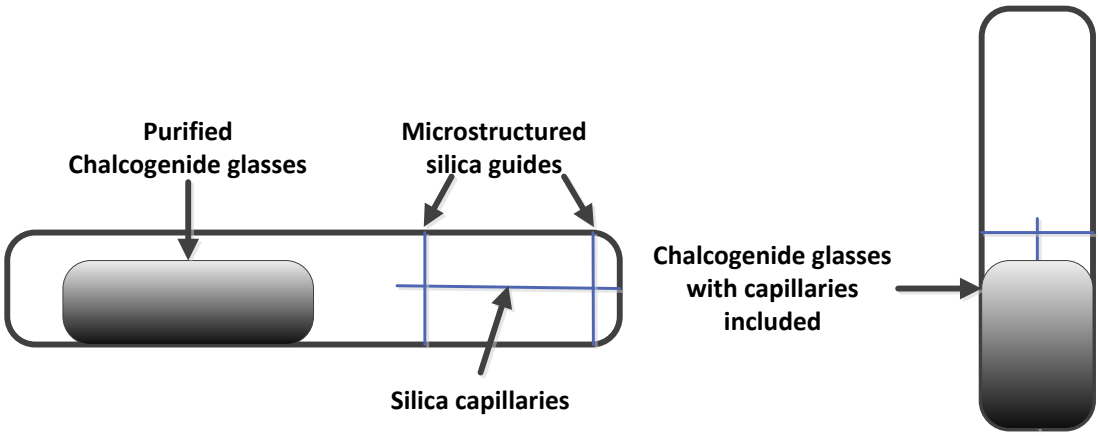

Figure 3.15 Schematic diagram of the modified casting method

Similar to the casting method for chalcogenide micro-structured fiber fabrication, a modified casting method is applied in our case (Figure 3.15). The $(Te_4Ge)_{85}AgI_{15}$ glass which was chosen to be the cladding was cast on a mold made entirely of silica. The mold consisted of a silica ampoule, two structured guides and a capillary in the center of the ampoule. The capillary was threaded through the two guides and the latter were torch-welded about 5cm apart from each other at the bottom of the silica ampoule.

To start with, the purified glass preform was inserted into the silica ampoule

containing the mold. The sample was placed in a rocking furnace in a horizontal position at 500℃. Once the glass softening temperature was reached, the furnace was then switched to the vertical position so that the glass flows into the mold (see Figure 3.15). Then the molded preform was quenched in water and annealed 145℃ for 4 hours and cooled down to room temperature in 10 hours. After the annealing, the mold is removed by soaking in hydrofluoric acid, the silica capillary is dissolved in less than an hour. Once the preform was washed with deionized water and dried, the composition of $(Te_4Ge)_{90}AgI_{10}$ for the fiber core was inserted. The preform is thus ready for fiber drawing. The steps for obtaining a double index fiber preform with this modified casting method are shown schematically in Figure 3.16. Since the diameter of the capillary used for molding was 500μm, the internal diameter of the cladding was therefore around 500μm.

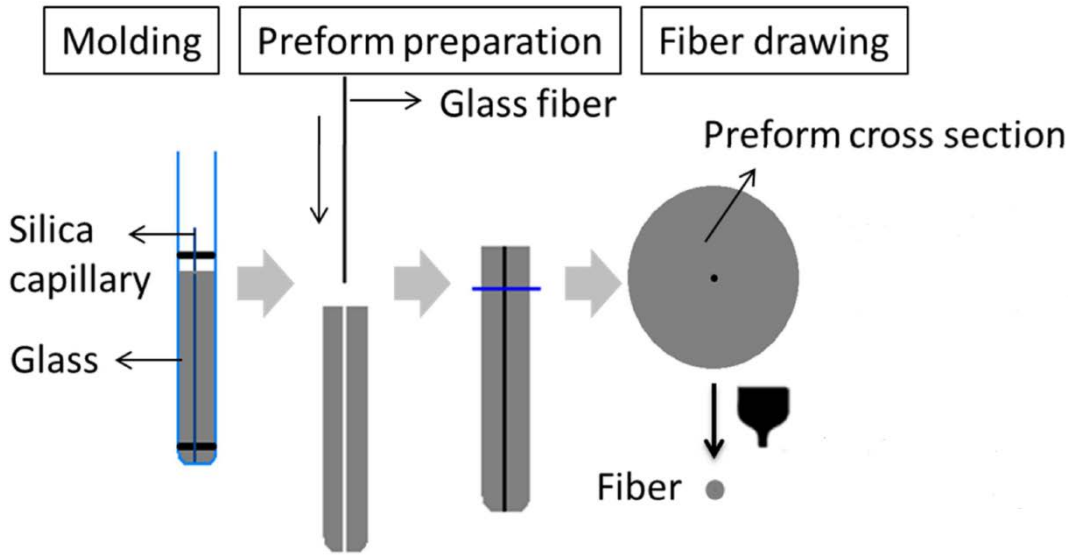

Figure 3.16 Schematic diagram of the steps of step-index fiber preform fabrication

3.2.4.2 Chemical durability of Te-Ge-AgI glass in hydrofluoric acid

As described before in the casting method, a Hydrofluoric acid treatment was used to remove the silica capillary to form the cladding tube. The reaction between

HF and SiO_2 is normally described as follows:

$$4HF + SiO_2 = SiF_4 + 2H_2O \quad (3.3)$$

However, due to the strong causticity of HF, the impact of the HF on the cladding preform needs to be studied to confirm that the no erosion or surface defect happened during the 1 hour soaking period. Then, we tested the stability of the $(Te_4Ge)_{90}AgI_{10}$ glass and $(Te_4Ge)_{80}AgI_{20}$ glass with respect to the Hydrofluoric acid. The pieces of the glasses were cut into a thickness of 2mm and well-polished firstly, and then immersed in the HF for a period of time ranging from 0 to 4 hours. The infrared transmittances of the glasses were measured after each immersion and the spectra are shown in Figure 3.17.

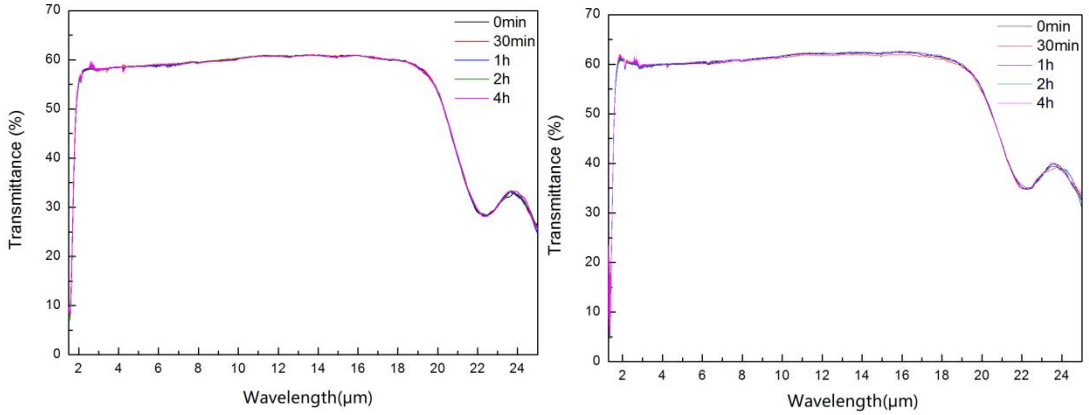

Figure 3.17 Infrared transmittance spectra of $(Te_4Ge)_{90}AgI_{10}$ (left)and $(Te_4Ge)_{80}AgI_{20}$ (right) glass before and after immersion in hydrofluoric acid for different time.

From the obtained results, it can be seen that the transmission of the bulk glass was not affected by immersion in hydrofluoric acid even when the time was as long as four hours and the observation could be well applied in both the glass composition of $(Te_4Ge)_{90}AgI_{10}$ and $(Te_4Ge)_{80}AgI_{20}$. In addition, the cutoff wavelengths as well as the value of the short wavelength transmittance that were sensitive to microscopic size defects, showed no variation. Thus, it can be concluded that the $(Te_4Ge)_{90}AgI_{10}$ and $(Te_4Ge)_{80}AgI_{20}$ glass could behave relatively stable against hydrofluoric acid.

To confirm this conclusion, the surfaces of the glasses were photographed under an optical microscope after the different reaction times with HF. The images of the

composition glass $(Te_4Ge)_{90}AgI_{10}$ are shown in Figure 3.18 and the images of the composition glass$(Te_4Ge)_{80}AgI_{20}$ are presented in the Figure 3.19. In correspondence with previous result, no surface damage or erosion were found in the images when soaked in HF for no more than 4 hours. So, it will be possible to remove the silica capillary from the glass $(Te4Ge)_{85}AgI_{15}$ without the risk of damaging the chalcogenide glass.

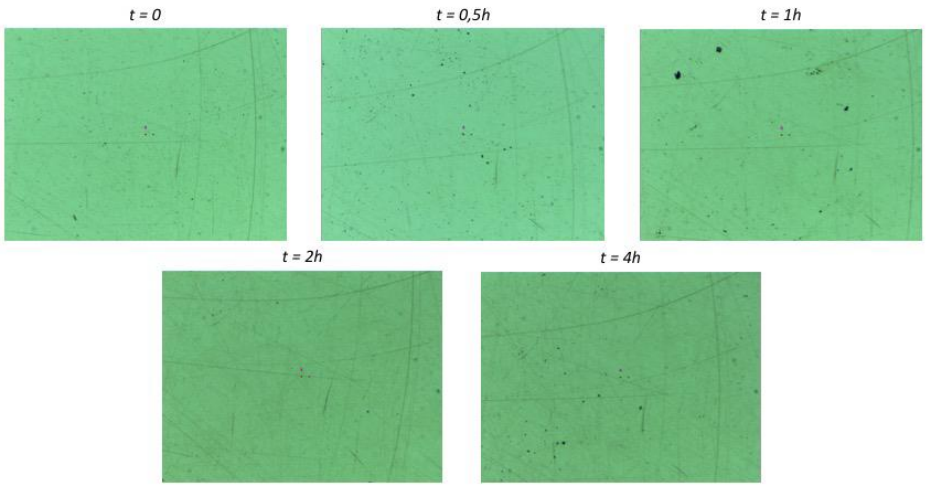

Figure 3.18 Images of the surface of $(Te_4Ge)_{90}AgI_{10}$ glass after being immersed in hydrofluoric acid from 0 to 4 hours

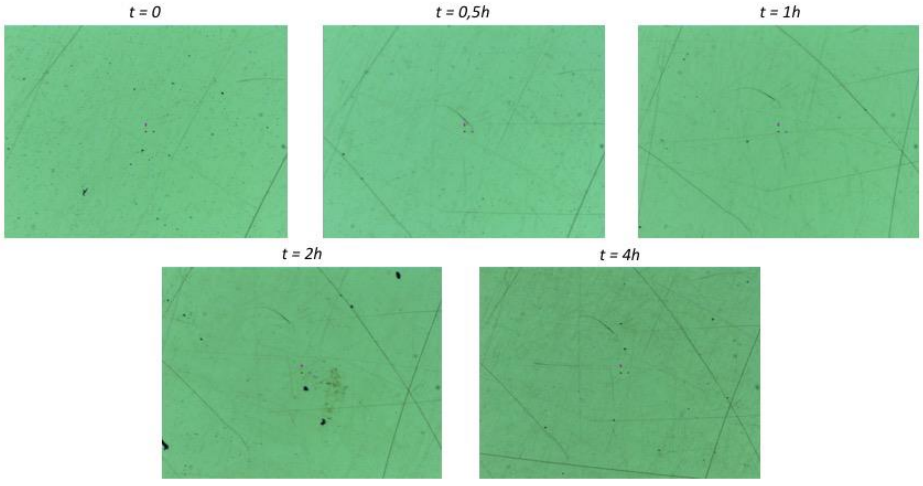

Figure 3.19 Images of the surface of $(Te_4Ge)_{80}AgI_{20}$ glass after being immersed in hydrofluoric acid from 0 to 4 hours

3.2.4.3 Assembly and characterization of the step-index Te-Ge-AgI fiber

To verify the transmittance of the $(Te_4Ge)_{85}AgI_{15}$ cladding preform before assembly of the final preform, a photo was taken in front of the infrared camera to observe the state of the tube (see Figure 3.20). The preserved space for inserting the core could be clearly observed and the bubbles on the surface of the glass were generated during the quenching.

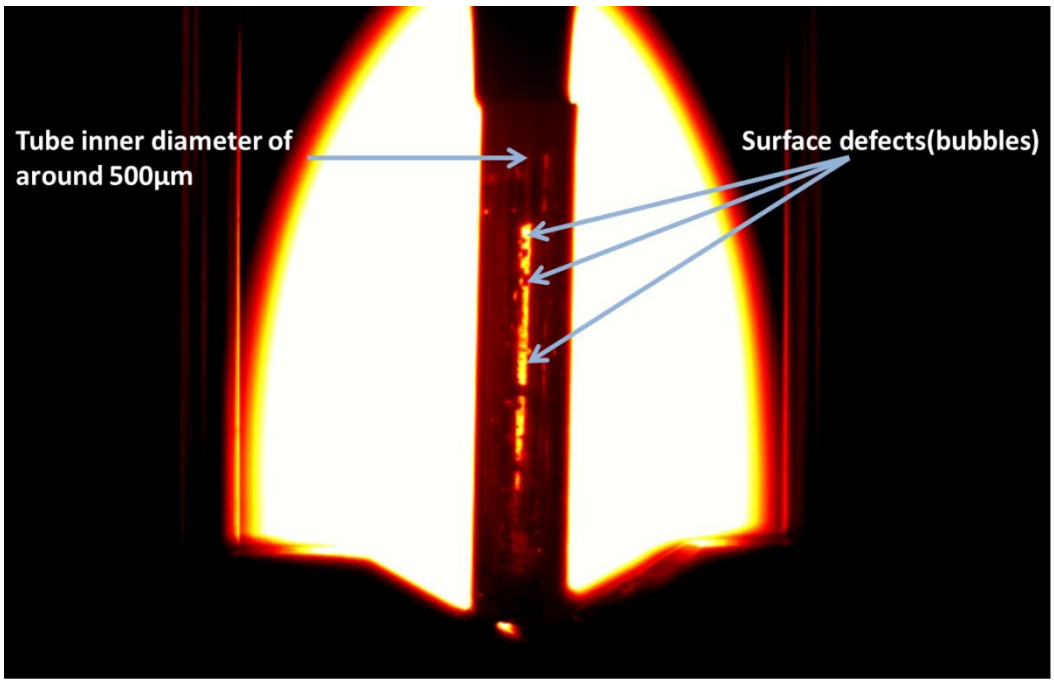

Figure 3.20 Image of the preform of cladding in infrared camera

The diameter of the $(Te_4Ge)_{90}AgI_{10}$ core fiber was measured to be 491µm and for the molded cladding, it was 9.91 mm with an inner diameter around 0.5 mm. Once the core fiber was inserted into the preform and installed, the step-index fiber preform was finally assembled. The drawing procedure and conditions were maintained the same as the previous steps. In addition, in order to well collapse the core clad interfaces a negative pressure is applied at the top of the rod in tube preform. As a result of fiber drawing, crystallization on the surface of the fiber was observed. We believe this surface crystallization comes mainly from the $(Te_4Ge)_{85}AgI_{15}$ tube due to the lack of polishing before the fiber drawing.

Following the fiber drawing procedure, a section of the fiber obtained was made and observed under an optical microscope. The diameter of the core was measured to be 16μm and for the cladding it was 294μm, which is in accordance with the parameters that were calculated before the fiber drawing, as is shown in Figure 3.21.

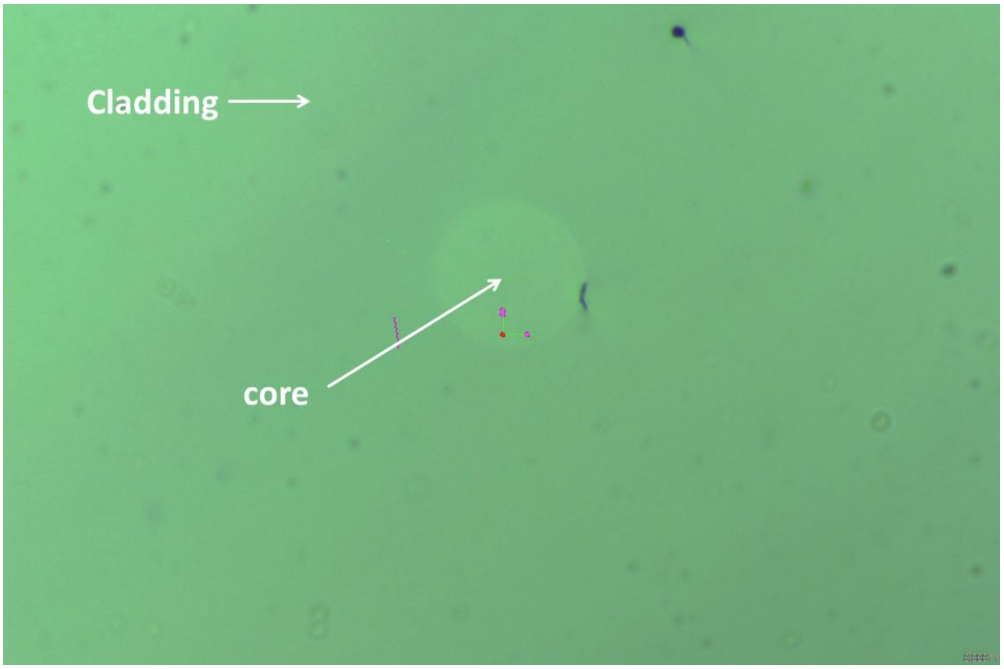

Figure 3.21 Cross section of the step-index fiber

A near field measurement was performed to verify if the fiber was able to allow light propagation. The light source used was a CO_2 laser operating at 10.6μm. The laser beam, after being focused by a germanium lens, was injected into the fiber and the signal was collected at the output with a detector of an IR camera. Light propagation could be observed in the camera. Then, in order to verify that the core of the fiber transmits light, carbon was deposited on the fiber in order to remove the light propagating in the cladding. However, no light beam was detected at the output of the core of the fiber this time. In our explanation the result can be attributed to the small difference between the refractive index of the core and the cladding. In addition, influenced by the volatility of iodine, the fiber drawing process might induced a modification of the composition of the fiber and further decreased the refractive index contrast between the core and the cladding, preventing the guiding of light in the core.

For the next fiber drawing, it will be necessary to choose two glass compositions with more contrasting refractive index to avoid this problem. From another point of view, considering the high tendency of crystallization of Tellurium, the result could also be caused by the crystallized fiber core.

3.3 Graded-index chalcogenide fiber design

3.3.1 Glass composition selection

As we know, silica graded index fibers are normally fabricated with the method of vapor deposition techniques, the MCVD technique permits to realize graded-index fiber by increasing layer after layer the amount of GeO_2 [33]. However, chalcogenide glasses and fibers are not suitable for being manufactured with current vapor deposition techniques. Therefore, we used a new approach to make graded-index chalcogenide fibers which was reported in [32]. In this method, the gradient refractive index distribution is achieved by using nano-structurization, in which effective medium theory is utilized.

In order to realize the fabrication of the graded-index fiber structure, the two glass compositions chosen for the core and the cladding need to be thermally and rheological compatible with each other, which means the thermal expansion coefficient and viscosity of the two glass compositions must be close so that the fiber structure can be maintained during the fiber drawing process. Thus, in our experiments, we selected $As_{38}Se_{62}$ and $Ge_{10}As_{22}Se_{68}$ for the core and cladding of the designed grade-index profile as the refractive index difference of these two glasses are distinguishable enough ($\triangle n \approx 0.2$ @1.55μm) and the glass transition temperatures of the two glasses are 175℃ for $As_{38}Se_{62}$ and 165℃ for $Ge_{10}As_{22}Se_{68}$ respectively.

3.3.1.1 Refractive index measurements

As previously introduced in reference [47], by measuring the refractive index of a particular sample at several wavelengths and applying the data to appropriate model

which will interpolate the data points, the characteristics could be displayed in as few coefficients as possible. In our case, we applied the Sellmeier model,

$$n^2 - 1 = A_0 + \sum_{n=1}^{N} \frac{A_n \lambda^2}{\lambda^2 - a_n^2} \quad (3.4)$$

where: A_0 and A_n are dimensionless coefficients; a_n are the material resonant wavelengths; N denotes the number of resonance terms; λ is wavelength.

As for the chalcogenide glasses, the Sellmeier model is not only simple in concept but also material dispersion may be obtained from the second derivatives of equation (4.3.1). Plus, the Sellmeier model can only be applied to the non-absorbing spectral region of the material, which can be considered here as the transparent window region. Moreover, the Sellmeier model has been shown to provide accuracy for As-(Ge)-Se glass compositions in representing the real part of the refractive index in the useable window, for which the extinction coefficient was more negligible[48, 49].

For our glass samples, an empirical refractive index dispersion curve for $As_{38}Se_{62}$ was determined by fitting the values of n measured at different wavelengths to the Sellmeier equation in the two poles approximation, the results are shown in Figure 3.22. As can be seen in Figure 3.22, the fitting points converge very well to the experimental data.

As for $Ge_{10}As_{22}Se_{68}$, due to the lack of experimental data, an estimation of the Sellmeier coefficient was obtained shifting the Sellmeier curve for a similar composition ($Ge_{10}As_{23.4}Se_{66.6}$) obtained from literature [32] in order to match it with our measurement of n at 1.55 and 1.31μm. The resulting curve and coefficients can be found respectively in Figure 3.23 and Table 3.1.

Table 3.1 the resulting coefficients obtained for two glass compositions

	$As_{38}Se_{62}$	$Ge_{10}As_{22}Se_{68}$
A_0	2.7134	2.8060
A_1	3.9387	2.7938
a_1	0.40574	0.41025
A_2	1.0693	0.77098
a_2	42.395	39.463

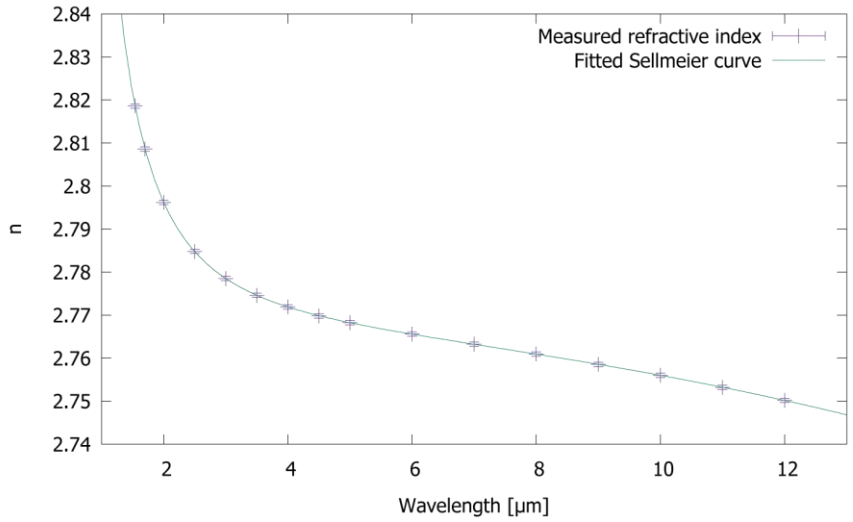

Figure 3.22 Measurement of the refractive index of $As_{38}Se_{62}$ compared to fitted Sellmeier curve

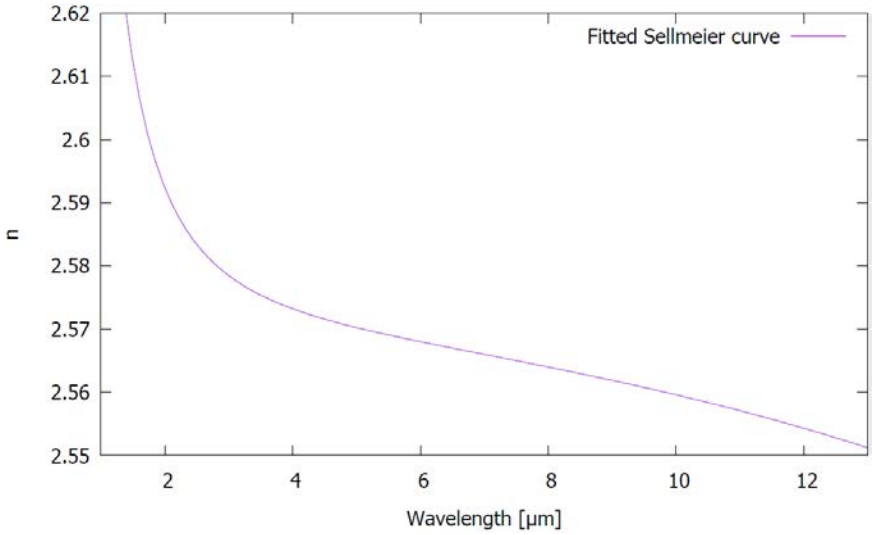

Figure 3.23 Fitting of the Sellmeier curve of $Ge_{10}As_{22}Se_{68}$ glass

3.3.1.2 Attenuation measurements

To obtain ideal graded-index chalcogenide fibers, the transmission of the bulk glass is of great importance. Therefore, we measured the attenuations of the two glasses with high purity and the results are displayed in Figure 3.24. It can be seen from the figure that the two purified fibers showed flat attenuation curves from 2μm to 9μm with an average loss lower than 1dB/m except for a strong absorption around 4.57μm which can be attributed to the vibration of the Se-H band due to the residual impurities from the glass synthesis process.

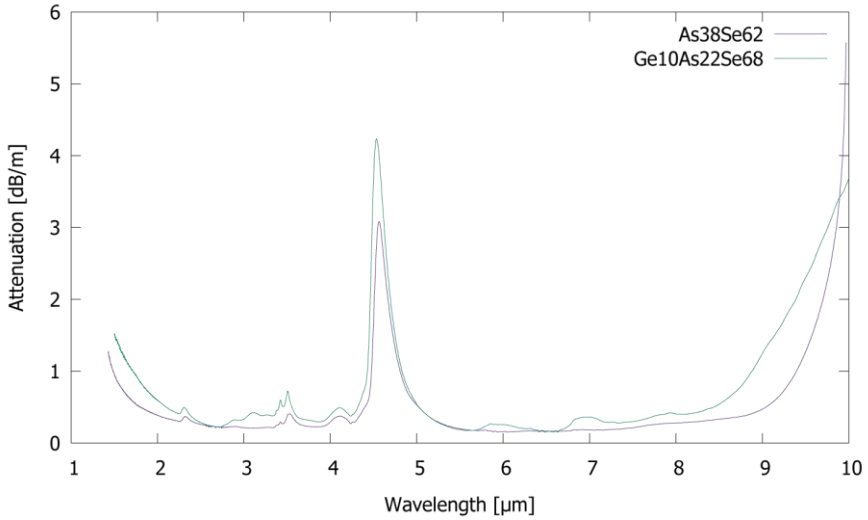

Figure 3.24 Attenuation curves of purified single index fibers with compositions of $As_{38}Se_{62}$ and $Ge_{10}As_{22}Se_{68}$

And since this is our first attempt of assembling this kind of grade-index fiber, the main purpose is to go through the whole procedure and discover the potential problems and difficulties. So, in this experiment, we used the non-purified glasses to produce fibers for stacking in order to simplify the process. In below, a typical attenuation curve of non-purified $As_{38}Se_{62}$ is reported as example in Figure 3.25.

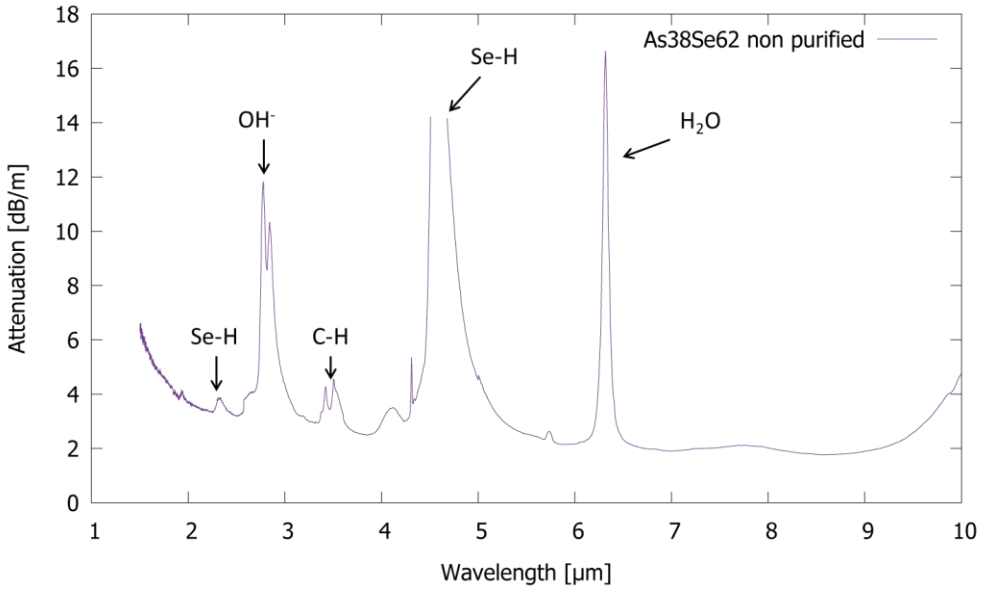

Figure 3.25 Typical attenuation curve of a single index fiber made from non-purified $As_{38}Se_{62}$ glass

3.3.2 Bulk glass synthesis

According to the plan for the graded-index fiber fabrication, the weight of different elements needed for the glass synthesis was calculated based on the diameter and length of the rods to be drawn in the next step, the inner diameter of the silica ampoule used for synthesis and the densities of the two glasses.

The same method utilized in chapter III (schematic gram see Figure 2.1), which is known as “melt and quench”, was also used here for the bulk glass synthesis. The raw elements which already had high purity of 5N were weighted in a glovebox protected by Argon and then added into the silica ampoule which had been washed with hydrofluoric acid in advance. Afterwards, to eliminate the existing impurities, the silica ampoule containing the raw elements was connected to the vacuum pump with a degree of 10^{-5} mbar for several hours. When the remaining oxygen and water inside were basically removed, the silica ampoule was sealed with hydrogen flame under vacuum condition and then inserted into the rocking furnace for homogenization.

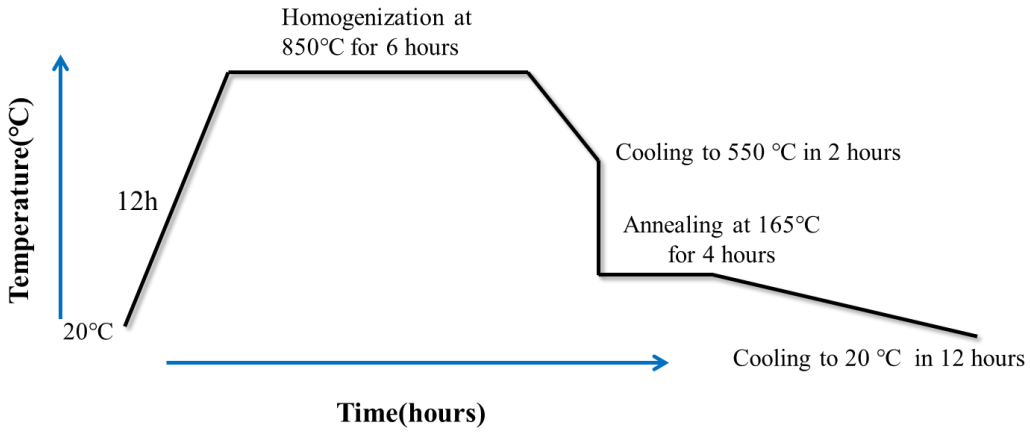

Figure 3.26 Program set for the homogenization of $As_{38}Se_{62}$ glass

Due to the different elements used for the two compositions, proper homogenization programs of the furnaces were needed so as to obtain bulk glasses with high qualities. For the case of $As_{38}Se_{62}$ glass, as is shown in figure 4.3.5, the elements were heated up to 850℃ with a rate no faster than 2℃/min and kept at this temperature for 6 hours. Then the temperature of the furnace was decreased to 550℃ in two hours. After quenching at 550℃, the glass were put into an annealing furnace to release the inner stress at a temperature of 165℃ for 4 hours and then cooled down naturally to room temperature, see Figure 3.26.

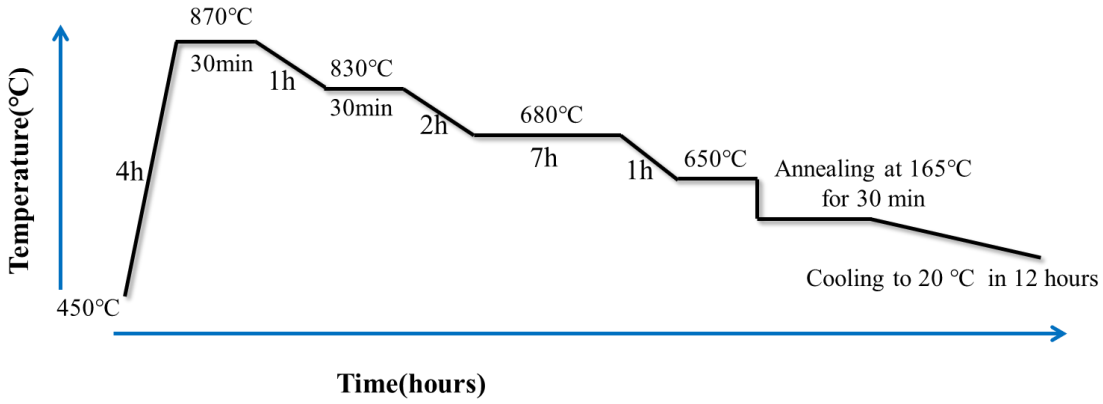

Figure 3.27 Program set for the homogenization of $Ge_{10}As_{22}Se_{68}$ glass

And for $Ge_{10}As_{22}Se_{68}$ glass, it was required to heat the furnace up to 450℃ before inserting the silica ampoule. After this, the temperature of the furnace was increased to 870℃ in four hours and maintained for 30 minutes. Then the temperature was decreased to 830℃, 680℃, 650℃ gradually and maintained for 30 minutes, 30 minutes and 7 hours respectively. Then, the glass was annealed at 170℃

for 30 minutes and cooled down to room temperature in 6 hours.

Consequently, the two obtained bulk glass were ideally fabricated, fulfilling the demanded weight and diameter, so as to be firstly draw into rods.

3.3.3 Rods preparation

For the first attempt of preparing rods for graded index fiber with stack and draw technique, the length of the rods were set to be around 10 cm long, and the diameter is selected to be around 450μm. Due to the existence of disturbance during the drawing process, we decided to accept the rods with a diameter of 450±20μm.

3.3.3.1 Drawing of the rods

The facility used for the drawing process was a home-made drawing tower introduced in previous section 3.2. Before actual starting to heat the preform, a 30-min long purge of the furnace with argon was performed. After this, the gas used for purging was switched from Argon to Helium, with a flow rate of 1.5 L/min, and the furnace was heated up to drawing temperature, which was 310℃ to 315℃ for $Ge_{10}As_{22}Se_{68}$ and 385℃ to 390℃ for $As_{38}Se_{62}$. The glass rods were drawn using a capstan. The drawing speed was set to be 0.73m/min with a preform motion speed of 1mm/min, as calculated from the preform diameter (12.07 mm).

During the first attempt of drawing rods of $Ge_{10}As_{22}Se_{68}$ glass, obvious dots and voids inside the rods can be observed from the beginning of the experiment (when the real-time monitored diameter of the rods went towards stability) until the end. Also, breaking of the rods caused by dots and voids inside the bulk glass occurred several times during the drawing process. As a consequence, the experiment had to be terminated as the bulk glass left in the furnace was not enough to make the numbers of rods needed. So, after the attempt failed due to the high instability in the diameter exhibited during the drawing by non-purified $Ge_{10}As_{22}Se_{68}$, we chosen to use high purity preforms for this composition.

In the second attempt of drawing, where high purity $Ge_{10}As_{22}Se_{68}$ glass was used,

the stability of the diameter and the quality of the rods were obviously improved, which proved that for this composition the purification had a great impact on the stability of the process, i.e. the stability of the glass. With no obvious existence of dots and voids and fluctuation of diameter, we collected over 400 pieces of rods with appropriate diameter as demanded in the end.

As for the drawing of $As_{38}Se_{62}$ bulk glass, similar phenomenon was observed during the experiment since the $As_{38}Se_{62}$ glass was also synthesized without purification. However, the diameter fluctuation and the fiber breaking were not as serious as in the case of non-purified $Ge_{10}As_{22}Se_{68}$ glass and also about 700 pieces of rods were successfully obtained.

3.3.3.2 Graded-index preform stacking

Since we fabricated enough rod pieces of the two glass compositions, it was necessary to find a suitable method for the stacking of the designed preform matrix.

The preform was stacked based on the previously designed matrix from[32](see Figure 3.28) which was done in collaboration with ITME in Poland and the final shape of the preform was shown in Figure 3.29.

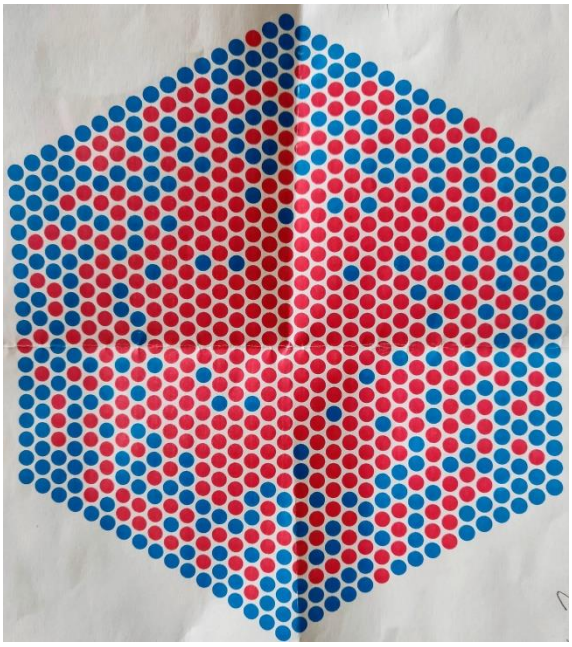

Figure3.28 Designed matrix of the preform, where red dots represent the high refractive index rods ($As_{38}Se_{62}$) and blue dots represent the low refractive index rods ($Ge_{10}As_{12}Se_{68}$)

Figure 3.29 Stacked preform for fabrication of the graded-index fiber

3.3.4 Cane drawing and characterization

3.3.4.1 Cane fabrication

The procedures of the cane fabrication are illustrated in Figure 3.30. As can be seen, the rods of both compositions were firstly stacked together and then drawn into the cane and finally inserted into the cladding tube to assemble the final fiber preform.

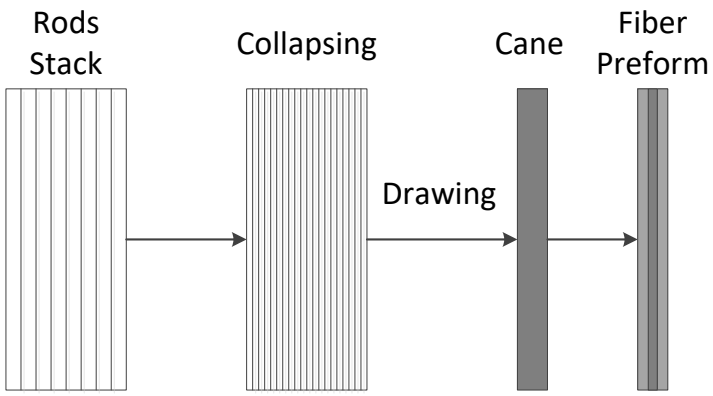

Figure 3.30 procedures of the cane fabrication

Although the preform of the cane was stacked following the designed matrix, there was still interspace between the rods. In order to obtain a preform as described from the previous part, two steps are needed: partial collapsing and drawing. The purpose is to use high temperature to melt the preform so that different layers can be stick together, or at least to stick the external layers of the preform, so as to keep it in a condition of airtight during the drawing process. To make this happen, the stacked preform has been thermally treated in the drawing tower. Indeed, when temperature of the furnace reached 360℃, collapsing of the stack could be observed by eye in the hot zone, and therefore the preform motion was started with a speed of 5mm/min, which allowed to collapse the whole preform The resulting partially collapsed preform can be seen in Figure 3.31.

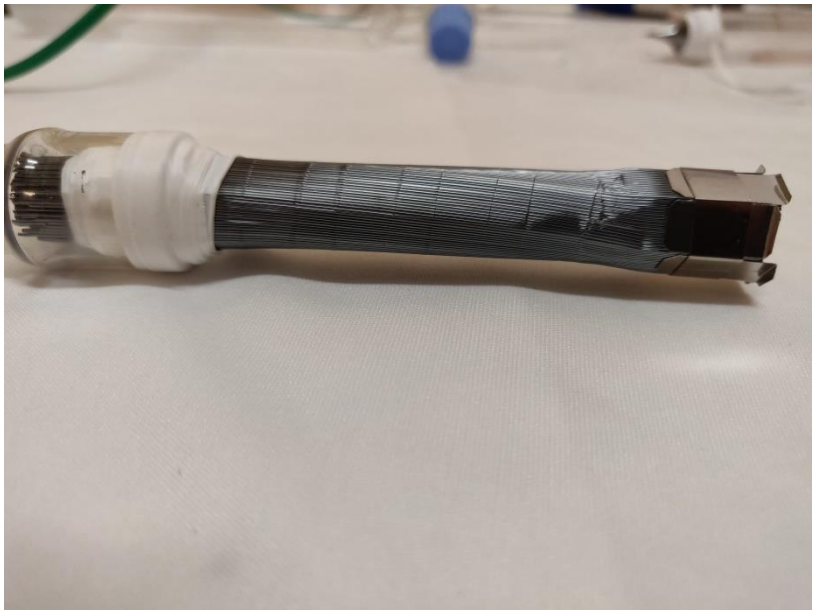

Figure 3.31 partially collapsed preform

The partially collapsed preform was then, with the help of the capstan, drawn into rods to be used as the core for our graded-index fiber. During this procedure, vacuum on the top of the preform was applied in the attempt to get rid of the remaining interstitial holes. Three different diameters of canes were made with the diameters of 1, 2 and 3μm.

The final cross section of the fiber obtained is illustrated in figure 3.32. As is shown in the picture, the structure was conserved on the whole during the drawing process and the distribution of the refractive index is similar to the designed matrix. Even though, some interspace between the rods still existed, further steps of fiber drawing would help to eliminate it.

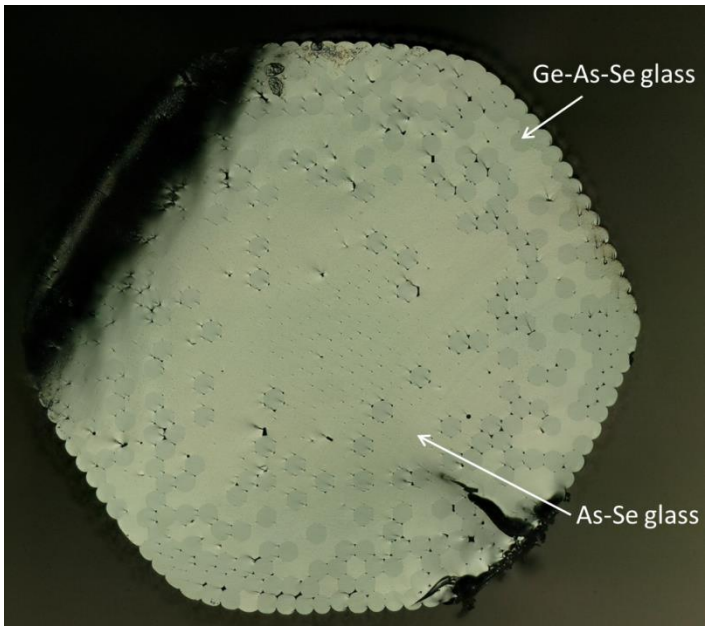

Figure 3.32 Cross section of the core rod

3.3.4.2 Cane characterization

As the preform for the core of the graded-index fiber had been obtained, it was necessary to measure the optical property of it. The light source applied was centered at 10.6μm and a single index $Ge_{10}As_{22}Se_{68}$ fiber was used to inject the light into the Cane. We used a section of 60mm-long core rod with a diameter of 1mm as an example. It can be seen from Figure 3.33 that the output near field image of the Cane seemed to have an even distribution although the $Ge_{10}As_{22}Se_{68}$ fiber was multimode

and the alignment between the $Ge_{10}As_{22}Se_{68}$ fibers and cane was not ideal.

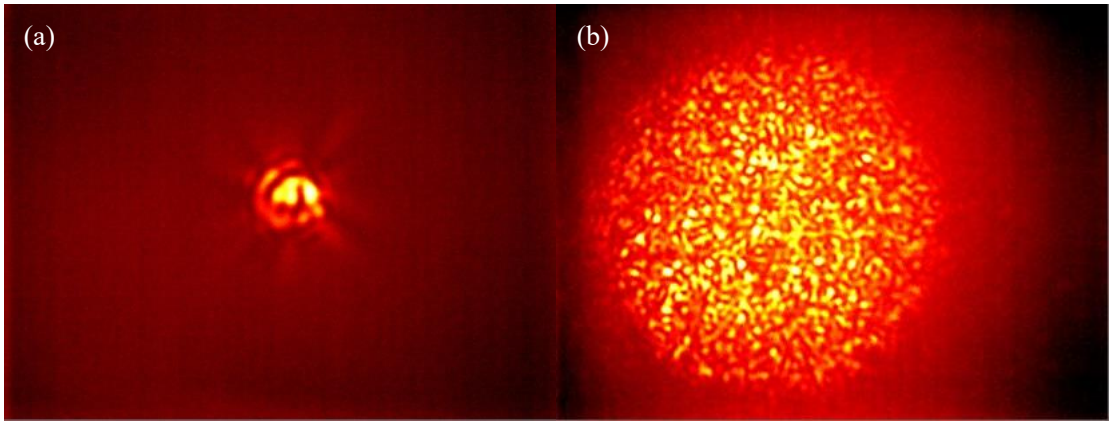

Figure 3.33 Near field images of (a) single index $Ge_{10}As_{22}Se_{68}$ fiber and (b) cane when injected with light centered at 10.6μm

Meanwhile, we also collected the radiance intensity information of the single index $Ge_{10}As_{22}Se_{68}$ fiber and the cane. As can be seen in Figure 3.34 and Figure 3.35, the results of the radiance intensity further indicated the difference in output light quality between the two fibers which means that the cane is suitable for the propagation of mid-infrared light.

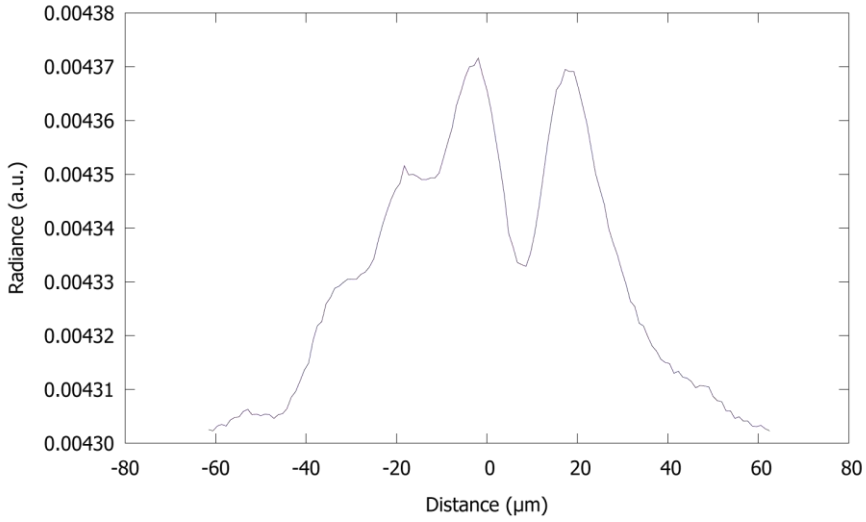

Figure 3.34 Radiance intensity of the near field light from single index $Ge_{10}As_{22}Se_{68}$ fiber

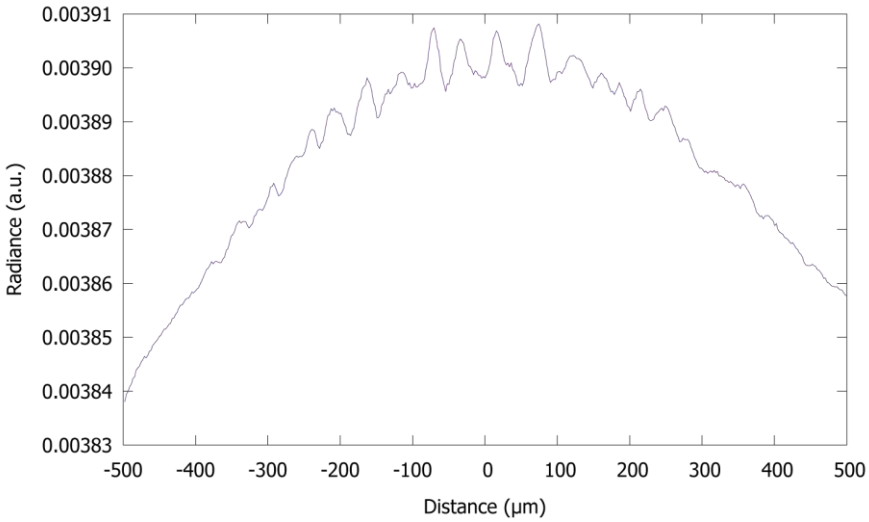

Figure 3.35 Radiance intensity of near field light from the cane

Although the ability to transmit mi-infrared light of the cane was guaranteed, the transmission loss was also not negligible. As is shown in Figure 3.36(a), by taking an infrared picture of the rod, a large leak of light due to scattering was quite obvious along the side of the cane. Concerning the previous results, this could be caused by the interface between the rods.

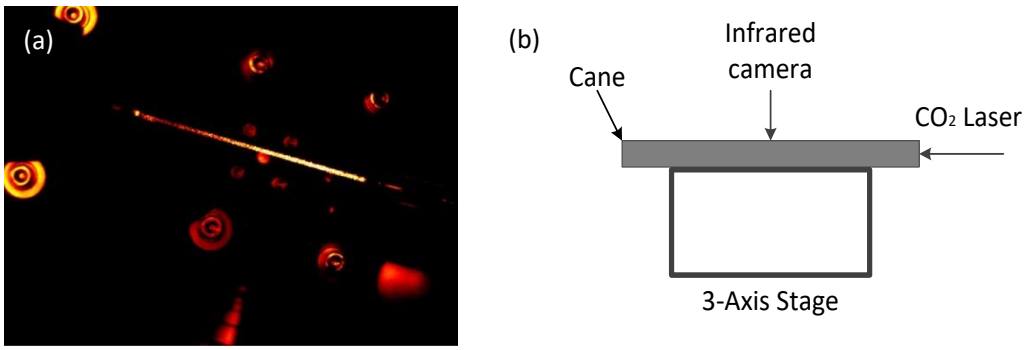

Figure 3.36 (a) Infrared image of light scattering from the side of the cane (b) Schematic diagram of the image collecting

Thus, an estimation of the losses ensuing from this phenomenon had been made by plotting the logarithm of the radiance against the distance from the injection point, and fitting it with a straight line. The losses estimated in this way were around 20±5dB/m, see Figure 3.37.

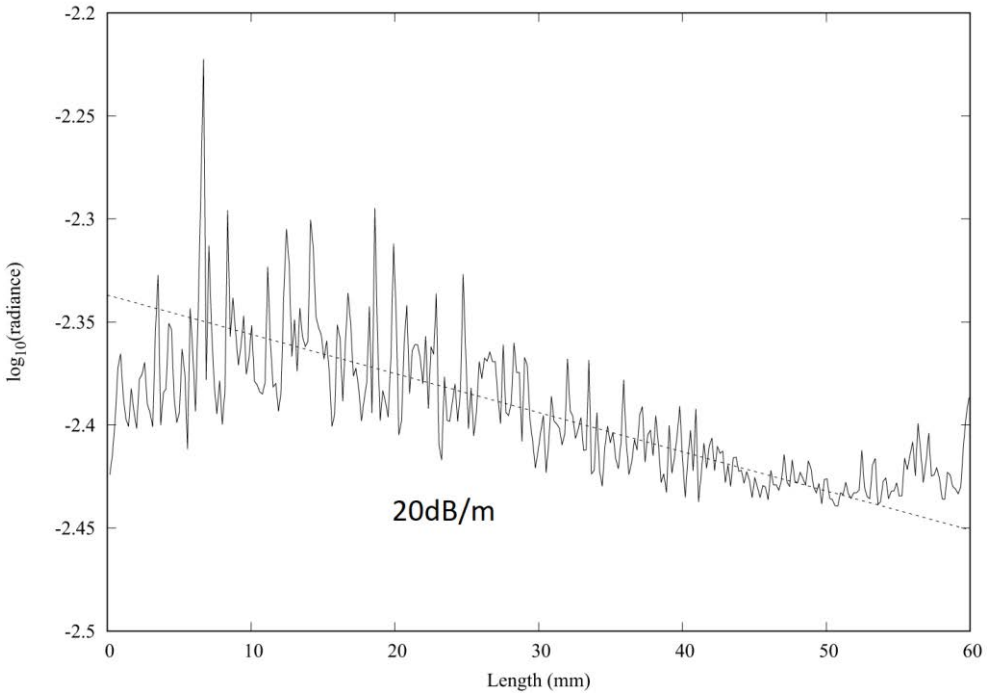

Figure 3.37 logarithm of radiance along the cane longitudinal profile, plotted against the distance from the light injection point, with the linear fit used to estimate scattering losses

3.3.5 Graded-index fiber drawing and characterization

3.3.5.1 Cladding preparation

After the fabrication of the cane and the verification of the ability to propagate mid-infrared light, the following step was to prepare the cladding in order to complete the graded-index fiber structure. The cladding tubes for the fiber drawing attempts were prepared by rotational casting technique during which shards of high purity $Ge_{10}As_{22}Se_{68}$ were placed in a 10 cm-long silica tubes with an internal diameter of 12 mm, and sealed under high vacuum. The glass was afterwards fully melted at 550℃ and put into a rotation device subsequently. By spinning the melted glass at a speed of 3000 rpm as it cooled down to a temperature slightly higher than T_g , the cladding tube were forged in 6.5min. The tube was then annealed at 170℃ for 30minutes.

3.3.5.2 Grade-index fiber drawing

With the well manufactured cane and cladding tube, the first attempt of the graded-index fiber drawing was conducted. The diameter chosen for the cane was 1mm and the selected cladding tube had an external diameter of 12.1mm and an internal diameter of 5.5mm. However, it turned out that the geometry of the cane of the final fiber could not be maintained very well with the parameter applied. Reducing the drawing temperature allowed for a good core shape, but it made it impossible to collapse the holes around it, whereas increasing the drawing temperature caused complete collapse of the holes at the price of destroying the core.

Therefore, in the second attempt, we selected a cane with a diameter of 3mm and the cladding tubes with external and internal diameters of 12mm and 3.9mm respectively. With this configuration, we finally achieved a fiber of 125µm with a good cross section and completely collapsed holes, see Figure 3.38. And based on the previous data and diameters of rods, cane and the cladding tube, the final diameter of the core of the graded-index fiber was around 30µm and the single rod diameter could be as small as around 1µm.

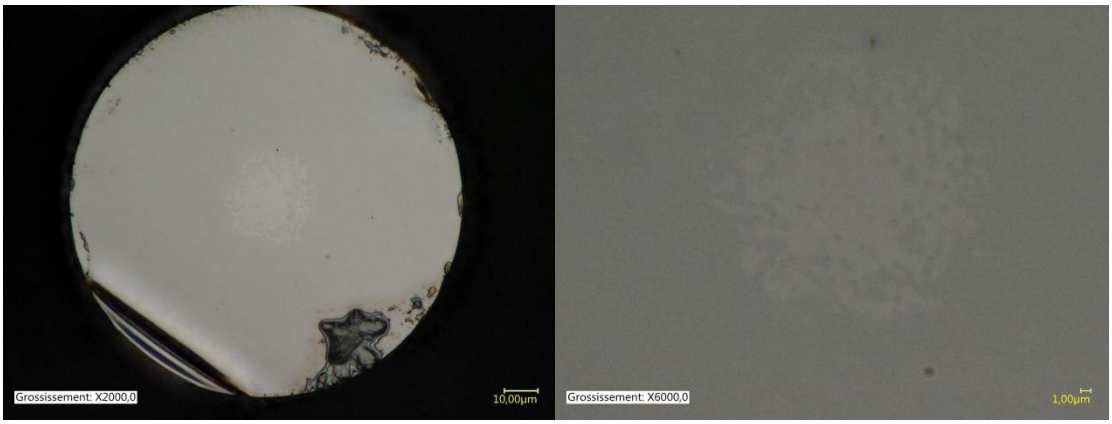

Figure 3.38 (a) The cross section of the obtained graded-index fiber and (b) the zoomed image of the core

Unfortunately, it was not possible to see any light propagation inside the graded-index cane. The optical losses observed inside the cane were around 20dB/m. This value has probably increased in the last step of drawing and this increasing could

be mainly attributed to a strong crystallization of the chalcogenide glass. Maybe for the next attempt, the As-Se glass which can crystalize after numerous thermal treatments would be substituted with another Ge-As-Se glass composition. Although the first attempt was not successful, it did prove that it can be possible to realize a graded-index chalcogenide fiber.

3.4 Inclusion of silica PCF with chalcogenide glass

3.4.1 Introduction of SPICY project

As it has been introduced in previous section, hybrid optical fibers made of silica and silicon have been a research interest for almost a decade. The new hybrid optical fibers not only brought new geometry structures but also various optical properties which were not accessible with conventional optical fibers. Due to the intrinsic characteristics of silicon, such as being a semiconductor for applications in photonics, transparency in the 1-7μm region, large third-order nonlinearity, high refractive index and high damage threshold, the understanding of the physical and optical properties of this new glass of fibers has been investigated and new demonstrations have been proposed by a number of groups [50, 51].Therefore, the aim of the SPICY project is to explore totally new hybrid structures and investigate the potential of more conventional geometries for nonlinear applications in the infrared region. Then, the interest would be to propose new optical fibers that could answer to the quest for specific designs like silicon-core fibers and “photon cages” as proposed in [52].

The photon cages concept was proposed in the context of the development of high-Q optical micro-resonators to enhance light-matter interaction for various phenomena as nonlinear effect, stimulated emission, or optical sensing. Indeed, by increasing the photon lifetime and consequently the interaction path length, resonance phenomena increase the probability of interaction. Yet, a milestone towards further development of these optical devices is to achieve strong light confinement directly in the air, or in low index media, that contain the particles of interest. Photon cages are

good candidates since they not only maximize the 3D light confinement but also enforce maximal overlap between localized field and the environment. One way to confine light in a low index media is to exploit monolayer diffracting structures, called Photonic Crystal Membrane, as broadband efficient reflectors. In this way, highly selective one dimensional air vertical micro-cavities can be fabricated by associating two suspended photonic crystal membrane. The first attempt to exploit these membranes to confine light in the more than one direction was to fold virtually one dimensional photonic crystal membrane in order to define a cylindrical two dimensional micro0cavity (see Figure 3.39), or two dimensional photon cage.

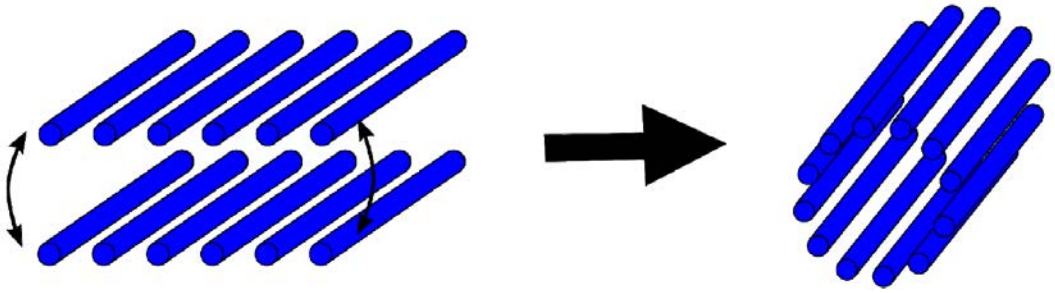

Figure 3.39 Schematic views of (left) a photonic crystal membrane based vertical micro cavity and (right) a cylindrical 2dimensional photon cage[52]

The geometry of such a structure is defined by an array of high refractive index pillars periodically arranged on a cylinder, embedded in a low refractive index environment. The aims of this project are to confine light inside the core of the cylinder and its optical properties are determined by the radius of the cavity and by the reflectivity properties of the arrangement of pillars. Considering that the reflectivity properties of the cylindrical pillars arrangements are close to those of its planar counterpart, the reflectivity of the cylindrical mirror is optimized by an appropriate design of the shape and dimensions of the pillars, and by the length of the arc of circle between each pillar.

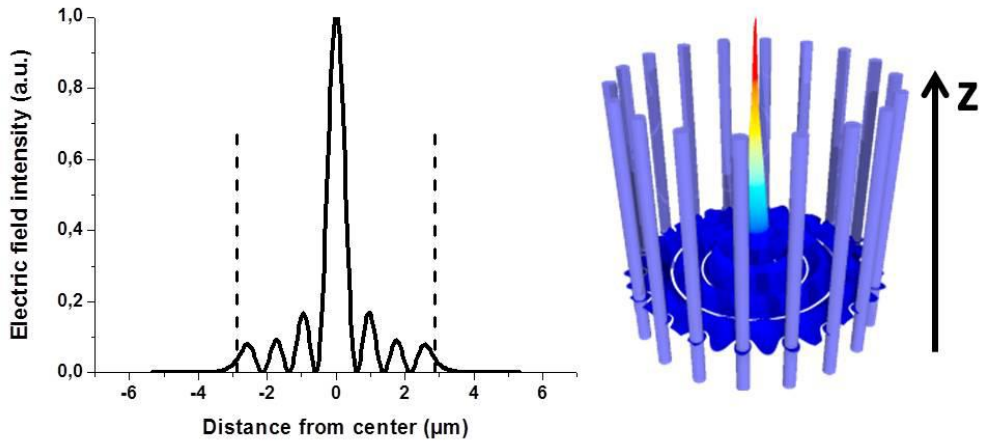

Figure 3.40 (left) Electric field intensity along a diameter of the cage, (Right) 3D view of this distribution.[52]

Calculation demonstrated that under certain conditions, the cylindrical structure was able to support resonant modes, similar to those of a circular cavity and extremely high concentration of the mode field was reached at the center of the cage although the cavity is composed of more than 95% of air, as is illustrated in Figure 3.40.

In the SPICY project, two structures are targeted:

- The first one consists in a Silicon/Silica photon cage designed to present resonant mode around 1.5µm. It will serve to evaluate the properties of the resonant mode in the photon cage.
- The second one consists in Silicon/Silica photon cages containing a hollow cylinder. This configuration, closer to applications, would allow inserting a low index fluid containing NIR emitters as PbS quantum dots and evaluate the capacity of the device to enhance light emission.

In our part of work, chalcogenide glasses will be exploited in replace of Silicon to enhance the nonlinearity of the final fiber and maintain the confinement effect of the photon cage structure at the same time.

3.4.2 Inclusion of silica PCF with TAS glass

In order to promote the realization of the “photon-cage” structure in the end, we

picked Tellurium-Arsenic-Selenium (TAS) ternary glass composition as the filling of silica photonics crystal fibers (PCF) due to the high refractive index and the high stability it poses[53, 54], a table of the comparison of transmission window and refractive index at 2μm and 5μm between different chalcogenide glass compositions are listed in Table 3.2. The TAS glass has been also chosen for its low crystallization tendency.

Table 3.2 Bulk Transmission Window and Refractive Index of Different Chalcogenide Glass Compositions

Composition	Transmission window	n at 2 μm	n at 5 μm
$As_{40}S_{60}$ (As_2S_3)	0,5 – 12 μm	2,426	2,407
$As_{38}Se_{62}$	0,8 – 16 μm	2,796	2,768
$Ge_{10}As_{22}Se_{68}$	0,8 – 16 μm	≈ 2,61	≈ 2,59
$Te_{20}As_{30}Se_{60}$	2 – 18 μm	2,959	2,920
$Ge_{20}Te_{78}Se_2$*	4 – 25 μm	-	≈ 3,42

The experimental setup is displayed in Figure 3.41. The TAS glass was synthesized and inserted to the bottom of a silica ampoule and the other side of the ampoule was connected to a vacuum pump with a plastic tube through a plug. The silica PCF utilized in the experiment was firstly dipped in Dichloromethane to remove most part of the polymer coating. Then, the fiber was sealed to the end of the plastic tube with the plug to introduce perfect vacuum in the fiber. In the end, the fiber was slightly inserted into the silica ampoule and the ampoule was closed with the plug.

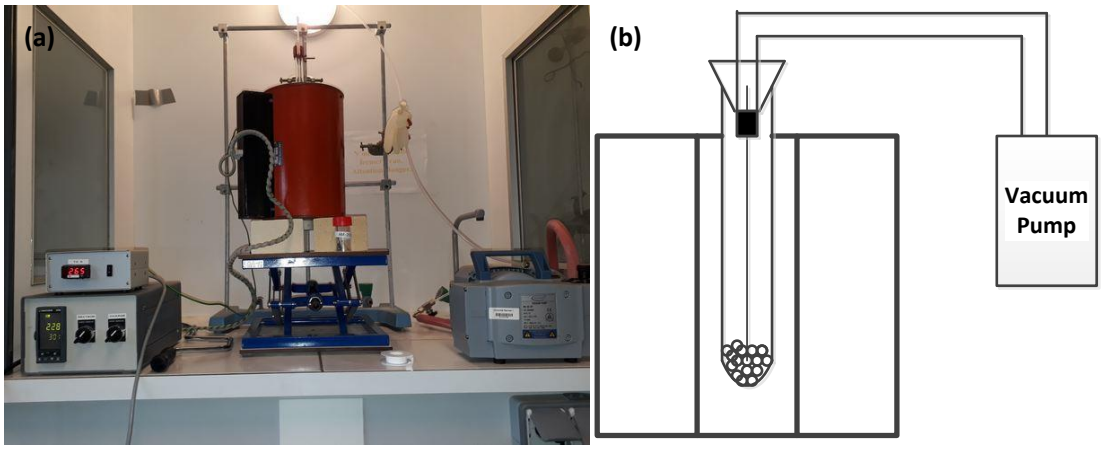

Figure 3.41 (a) Experimental setup of the filling of chalcogenide in to silica PCF (b) Schematic setup of the experiment

3.4.2.1 First attempt of filling

In the first attempt of the experiment, as the TAS glass had already been synthesized, the furnace was heated up to 450℃ in one hour and the vacuum pump was started the same time as the heating. The fiber length was preserved a little bit longer than the distance from the TAS glass to the top of the ampoule so that when the TAS glass was fully melted the fiber end could be completely sank in the melted TAS glass. To obtain a better result of filling, the fiber was kept in the melted glass for one hour under vacuum before taking out for examination. The cross section of the obtained fiber was checked with an optical microscopic. And since the bottom of the PCF was fully covered by TAS glass, it was impossible to get a view of the cross section of the bottom without damaging the fiber structure. Thus, we cleaved the fiber with a ceramic blade at every 5mm position from the bottom of the PCF and took the images of the cross section to compare the filling effect. The results of the cross section images obtained are listed below in Figure 3.42.

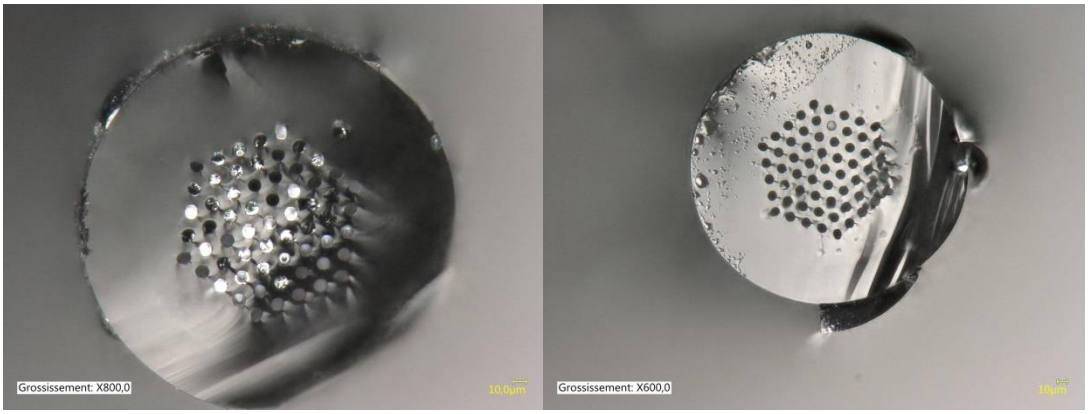

Figure 3.42 The images of the cross section of the PCF filled with TAS glass at the position of (left) 5mm and (right) 10mm to the bottom of the fiber

From the images, it can be seen that 1) part of the air holes of the silica PCF were successfully filled with TAS glass but not all of them 2) the filled air holes could be barely observed when the distance to the bottom was only 10mm. The results, in our explanation, can be attributed to the following factors. First, starting the vacuum pump at the same time as the heating process could reduce the pressure inside the ampoule which made the filling process more difficult to be carried out. Then higher

temperature of the furnace and longer time under vacuum might improve the result. And for the last, the cross section of the bottom of the PCF could be damaged or blocked before the TAS glass is fully melted. Hence, we tested the impact of the touching of TAS glass on the cross section of the bottom of PCF fiber. In the test, two section of PCF fiber were perfectly cleaved with ceramic blade and one was slightly scratched with the TAS glass and the other one was heavily scratched with the TAS glass. The obtained results in comparison with PCF cross section without scratching are listed in Figure 3.43.

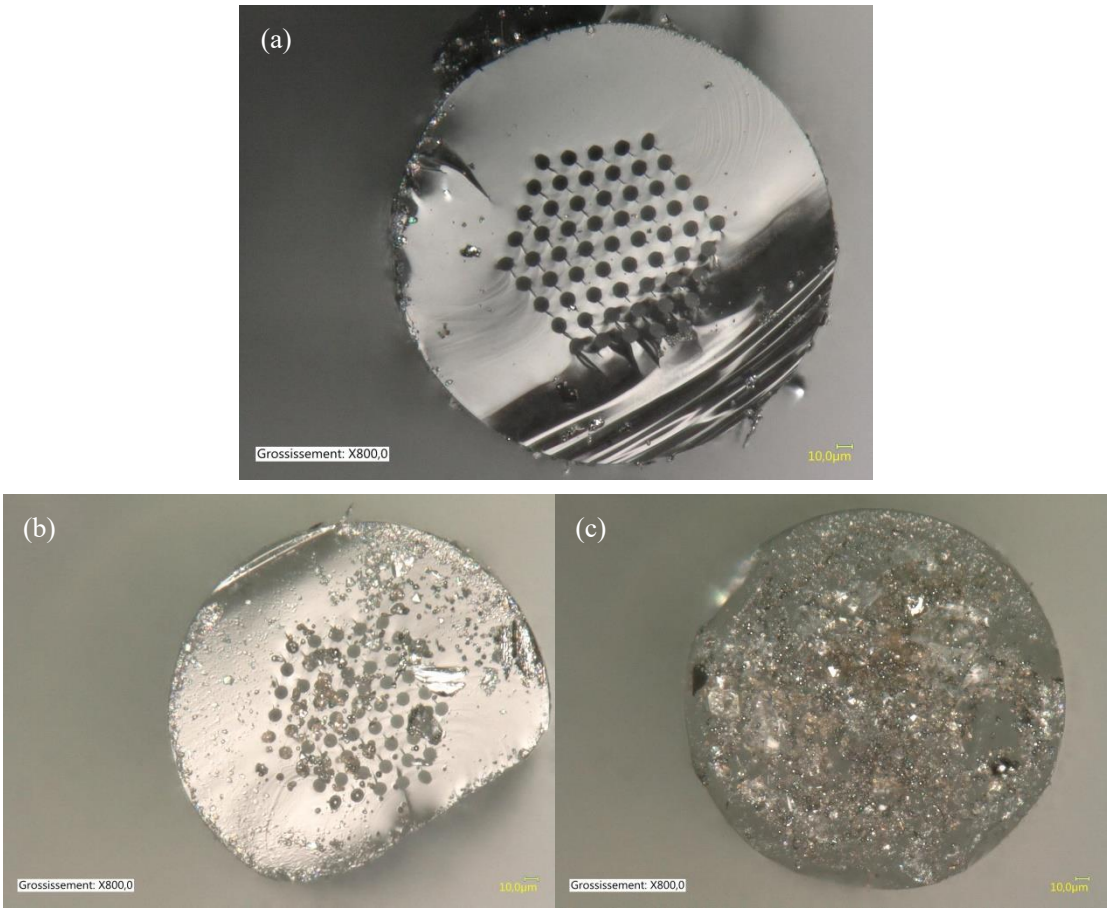

Figure 3.43 Images of cross section of PCF fiber (a) without scratching (b) slightly scratched (c) heavily scratched

It can be seen from the figure that, when the fiber end was slightly scratched, some of the air holes were already blocked by the TAS glass and almost all the air holes were covered with TAS glass when the fiber was heavily scratched. Obviously, the final result can be seriously affected by the cross section of the fiber dipped in the chalcogenide melt.

3.4.2.2 Modified filling

After a summary of all the possible causes of the results obtained previously, the experiment conditions and procedure were modified and a section of 8cm-long PCF filled with TAS glass was achieved which was the longest one that were ever obtained.

For a better consequence, the PCF fiber was well cleaved and carefully inserted into the silica ampoule. Then, the furnace was heated up to 500℃ in one hour instead of 450℃, and maintained for 2 hours instead of one hour. To keep the pressure inside the ampoule, the vacuum pump was switched on after the TAS glass fully melted and the PCF fiber was totally immersed in. Then the fiber was cleaved every 5mm from the bottom of the fiber and images were collected with the optical microscopic. The results are shown in Figure 3.44.

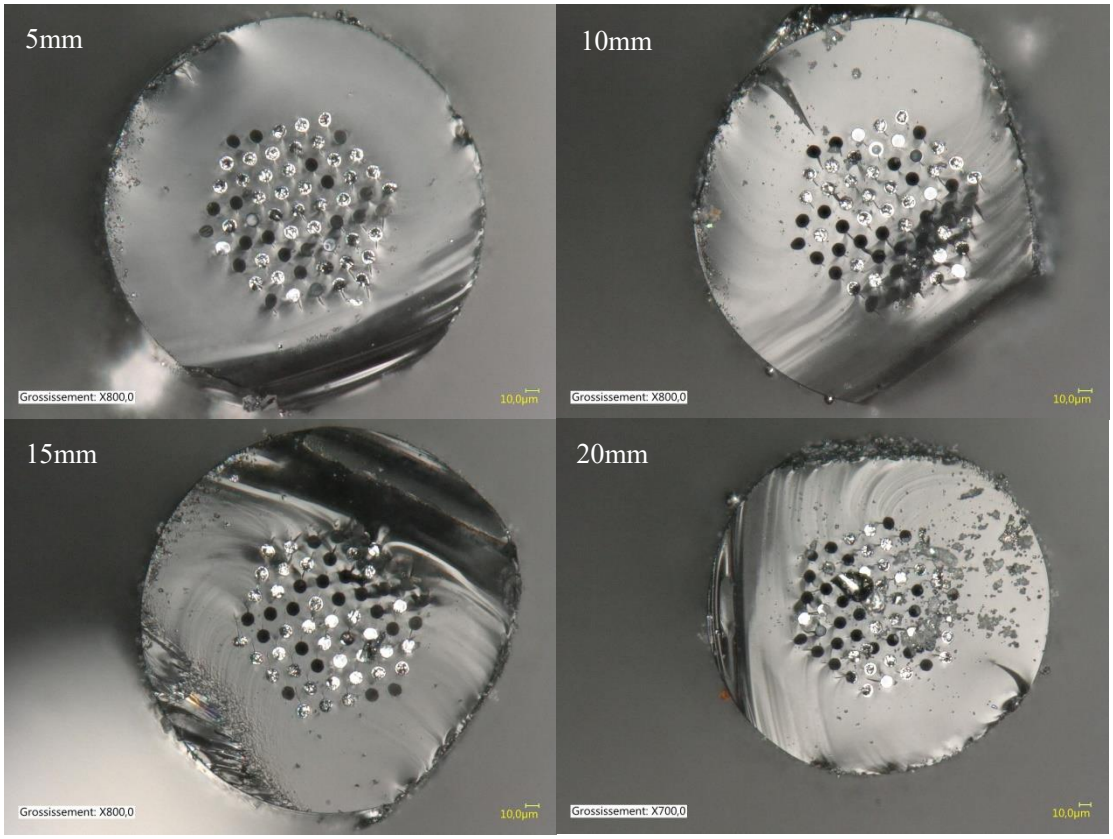

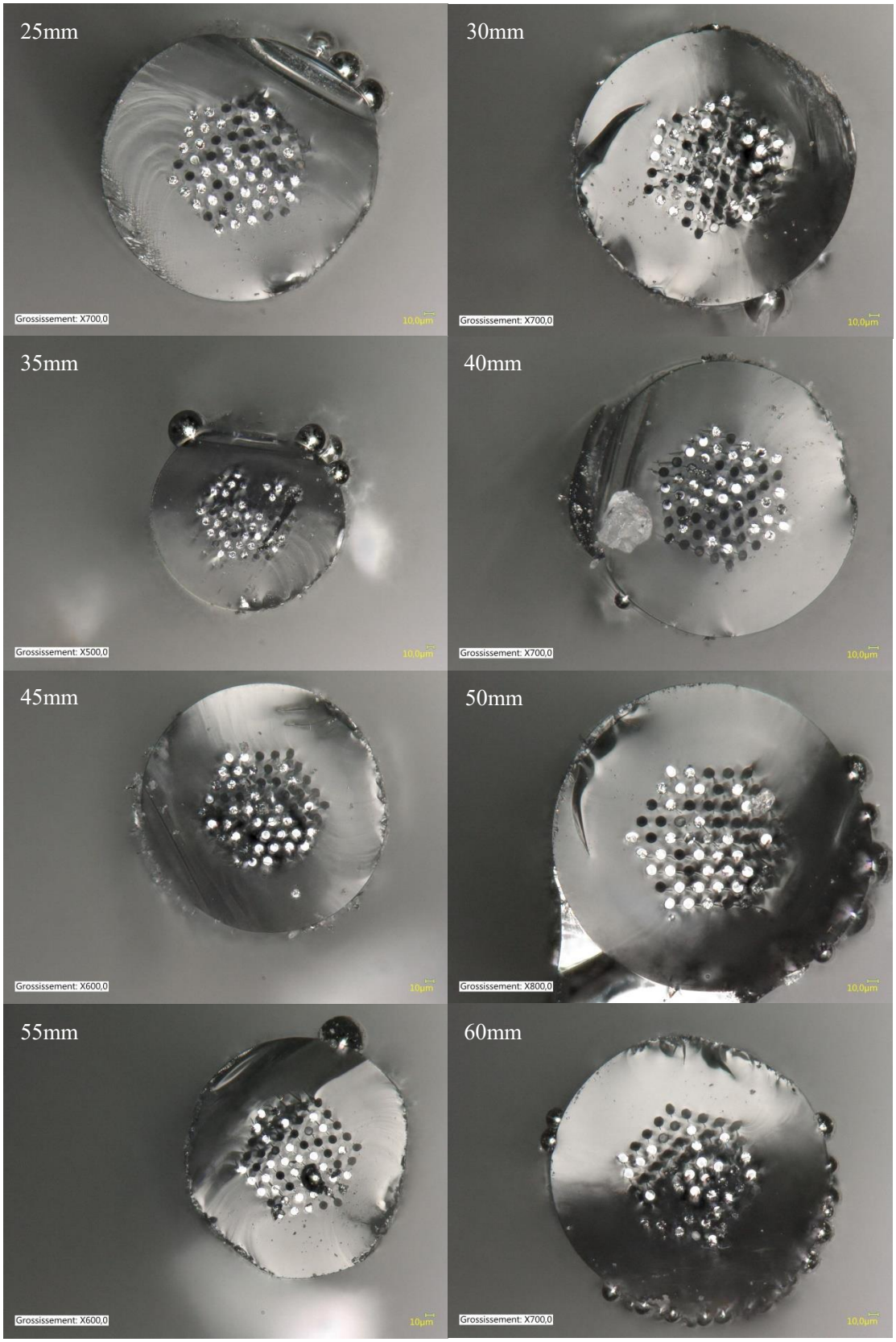
25mm
Grossissement: X700,0
30mm
Grossissement: X700,0
35mm
Grossissement: X500,0
40mm
Grossissement: X700,0
45mm
Grossissement: X600,0
50mm
Grossissement: X800,0
55mm
Grossissement: X600,0
60mm
Grossissement: X700,0

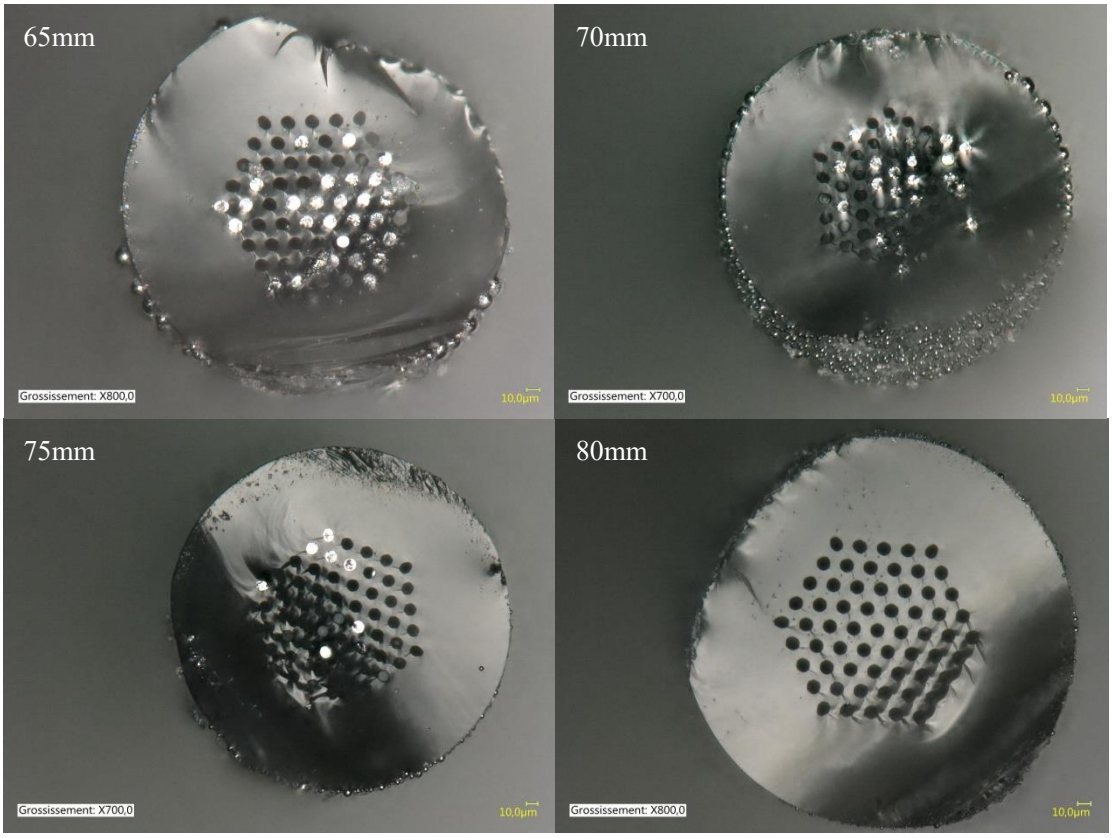

Figure 3.44 Images of the cross section of PCF fiber filled with TAS glass 5,15,20,25,30,35,40,45,50,55,60,60,70,75 and 80mm from the bottom of the fiber

As is shown in the Figure 3.44, the filled air holes in the silica PCF fiber could be seen until about 8cm away from the bottom of the PCF fiber, which verified the modification of the experimental conditions. However, the percentage of the filled air holes was still not ideal enough. Note that the distributions of the filled air holes on the cross section at different distance to the bottom of the fiber were in good match with each other. Therefore, it can be indicted that the imperfect filling of the air holes were mainly caused by plugging at the bottom of the PCF fiber. To achieve a better effect, the inevitable touch between the glass and fiber end has to be solved.

3.5 Conclusion

In this chapter, three different chalcogenide optical fibers with various structures were designed and fabricated

For the Te-Ge-AgI fibers, the glass with 10, 15 and 20% of AgI were chosen to be made into the fiber core or cladding according to the thermal properties obtained in previous research work. In order to acquire a fiber with low loss, the Tellurium used in the experiment was initially purified. In addition, a "two-step" purification procedure was utilized as it had been proved to have a positive impact on the glass synthesis. After the synthesis, the thermal property of the bulk glass was tested and no obvious crystallization peak was observed in the DSC curve and the glass transition temperature was in consistent with results obtained before. Also, the optical transmittance of the bulk glass showed a flat curve from 2μm to over 20μm and the only absorption peak around 4.3μm was attributed to the CO_2. Subsequently, the bulk glasses were drawn into single index fibers with the assistance of a home-made drawing tower. By using the cut-back technique, the attenuation curve of the obtained single index fibers was measured and a loss about 2dB/m at 10μm was achieved. Refractive index measurements showed that the glass composition of $(Te_4Ge)_{90}AgI_{10}$ was suited for the core of the fiber and the composition of $(Te_4Ge)_{85}AgI_{15}$ was more suitable for the cladding of the step-index fiber. Through altering the casting method which was originally used for PCF fabrication, a step-index structure preform was successfully assembled. Besides, the chemical durability of Te-Ge-AgI glass in hydrofluoric acid was put forward to verify the quality of the preform. Then, the preform was drawn into the final step-index fiber and a small section of the fiber was used to test the light guiding property. By injecting a CO_2 laser centered at 10.6μm into the step-index fiber, no light propagation was detected when covering the fiber with carbon, indicating that the light was mainly propagating in the cladding of the fiber. The consequences were considered to be related to the small refractive index difference between the core and the cladding. Additionally, influenced by the volatility of iodine, the fiber drawing process might induce a modification of the

composition of the fiber and further decreased the refractive index contrast between the core and the cladding.

In the case of graded-index fiber, the two glass compositions of $As_{38}Se_{62}$ and $Ge_{10}As_{22}Se_{68}$, with similar thermal properties and refractive index, were selected for the fabrication of the graded-index fiber. Refractive index measurement and attenuation curves verified the quality of the compositions. Then, the two compositions were synthesized and drawn into 10cm-long rods with a diameter of 450μm. Owing to that the bulk glasses were synthesized without purification, during the rods drawing process, obvious dots on the surface of the rods and breaking of the rods were observed in the cases of both compositions. For the composition of $Ge_{10}As_{22}Se_{68}$, purified bulk glass was synthesized again and the decrease of the possibility of dots and breaking phenomenon was obvious and sufficient numbers of rods were obtained. As for the composition of abundant numbers of rods fulfilling the demand of diameter had already been achieved, so no more synthesis of the purified $As_{38}Se_{62}$ glass was carried out. After the drawing process, the obtained rods were assembled following the designed distribution of the graded-index structure. For a more compact structure, the rod stack was pre-heated in the drawing tower to partially collapse the rods, so as to remove the interspace between different rods. Although the collapsing was not thoroughly, it can be further solved in the final fiber drawing process. Then, the stack was drawn into cane so as to be inserted in to the cladding tube to complete the graded-index fiber structure. A test of the propagating property of the cane was put forward in advance, and a light source operating at 10.6μm was injected into the cane through a $Ge_{10}As_{22}Se_{68}$ fiber with a diameter of 125μm. Both the near filed image and the collected intensity distribution have shown the light propagation in the cane. At the same time, a cladding tube with the composition of $Ge_{10}As_{22}Se_{68}$ was prepared using the rotational casting method and a cladding tube with an internal diameter of 12mm was achieved. For the final step of grade-index fiber drawing, a cane with a diameter of 5.5μm was inserted into the cladding tube prepared, and a 125μm grade-index fiber was drawn from the preform. However, the optical measurement showed no light propagation in the obtained graded-index fiber.

It could be attributed to the increase of the loss of the fiber during the drawing process which we believe was caused by crystallization of the unpurified $As_{38}Se_{62}$ glass and maybe different composition of glass should be considered in the next attempt.

As for the attempt of inclusion of silica PCF with chalcogenide glass, TAS glass was selected as the candidate by comparing the transmission and the refractive index of several mature chalcogenide glass system. In the first attempt of the filling, issues like the achieved filling length, the percentage of the air holes coverage and the conditions of the cross section at the bottom of the PCF fiber were noticed. Therefore, by modifying the experiment conditions such as heating temperature and time, cleaving the bottom of the fiber in advance, an 8cm-long silica PCF filled with TAS was finally obtained with a high percentage of air holes coverage. By cleaving and collect the cross section images of the obtained fiber every 5mm from the bottom, it was found out that the distribution of the filled air holes was basically the same, indicating the empty air holes should be plugged at the bottom of the fiber at the beginning. The assumption was then further verified by interaction between the TAS glass and the well-cleaved PCF fiber end, showing that the TAS glass could damage the PCF structure and block the air holes as well. Thus, this is going to be the priority problem to be solved in the future in order to get a fully inclusion of all the air holes in the PCF fiber.

References

[1]. P. Toupin, L. Brilland, C. Boussard-Plédel, B. Bureau, D. Mechin, J.-L. Adam, and J. Troles, "Comparison between chalcogenide glass single index and microstructured exposed-core fibers for chemical sensing," Journal of Non-Crystalline Solids **377**, 217-219 (2013).

[2]. K. Michel, B. Bureau, C. Boussard-Plédel, T. Jouan, J. Adam, K. Staubmann, and T. Baumann, "Monitoring of pollutant in waste water by infrared spectroscopy using chalcogenide glass optical fibers," Sensors and Actuators B: Chemical **101**, 252-259 (2004).

[3]. K. Michel, B. Bureau, C. Pouvreau, J.-C. Sangleboeuf, C. Boussard-Plédel, T. Jouan, T. Rouxel, J.-L. Adam, K. Staubmann, and H. Steinner, "Development of a chalcogenide glass fiber device for in situ pollutant detection," Journal of Non-Crystalline Solids **326**, 434-438 (2003).

[4]. P. Lucas, M. R. Riley, C. Boussard-Plédel, and B. Bureau, "Advances in chalcogenide fiber evanescent wave biochemical sensing," Analytical biochemistry **351**, 1-10 (2006).

[5].P. Lucas, D. Le Coq, C. Juncker, J. Collier, D. E. Boesewetter, C. Boussard-Plédel, B. Bureau, and M. R. Riley, "Evaluation of toxic agent effects on lung cells by fiber evanescent wave spectroscopy," Applied spectroscopy **59**, 1-9 (2005).

[6]. F. Charpentier, B. Bureau, J. Troles, C. Boussard-Plédel, K. Michel-Le Pierrès, F. Smektala, and J.-L. Adam, "Infrared monitoring of underground CO2 storage using chalcogenide glass fibers," Optical Materials **31**, 496-500 (2009).

[7]. F. Charpentier, J. Troles, Q. Coulombier, L. Brilland, P. Houizot, F. Smektala, C. Boussard-Plédel, V. Nazabal, N. Thibaud, and K. Le Pierres, "CO2 detection using microstructured chalcogenide fibers," Sensor letters **7**, 745-749 (2009).

[8].C. R. Petersen, N. Prtljaga, M. Farries, J. Ward, B. Napier, G. R. Lloyd, J. Nallala, N. Stone, and O. Bang, "Mid-infrared multispectral tissue imaging using a chalcogenide fiber supercontinuum source," Opt Lett **43**, 999-1002 (2018).

[9]. R. R. Alfano, S. G. Demos, M. Farries, J. Ward, I. Lindsay, J. Nallala, and P.

Moselund, "Fast hyper-spectral imaging of cytological samples in the mid-infrared wavelength region," presented at the Optical Biopsy XV: Toward Real-Time Spectroscopic Imaging and Diagnosis2017.

[10]. F. Borondics, M. Jossent, C. Sandt, L. Lavoute, D. Gaponov, A. Hideur, P. Dumas, and S. Février, "Supercontinuum-based Fourier transform infrared spectromicroscopy," Optica **5** (2018).

[11]. Y. Wang, S. Dai, X. Han, P. Zhang, Y. Liu, X. Wang, and S. Sun, "Broadband mid-infrared supercontinuum generation in novelAs2Se3-As2Se2Sstep-index fibers," Optics Communications **410**, 410-415 (2018).

[12]. M. Sinobad, C. Monat, B. Luther-davies, P. Ma, S. Madden, D. J. Moss, A. Mitchell, D. Allioux, R. Orobtchouk, S. Boutami, J.-M. Hartmann, J.-M. Fedeli, and C. Grillet, "Mid-infrared octave spanning supercontinuum generation to 85 μm in silicon-germanium waveguides," Optica **5** (2018).

[13]. R. A. Martinez, G. Plant, K. Guo, B. Janiszewski, M. J. Freeman, R. L. Maynard, M. N. Islam, F. L. Terry, O. Alvarez, F. Chenard, R. Bedford, R. Gibson, and A. I. Ifarraguerri, "Mid-infrared supercontinuum generation from 1.6 to >11 mum using concatenated step-index fluoride and chalcogenide fibers," Opt Lett **43**, 296-299 (2018).

[14]. Z. Zhao, B. Wu, X. Wang, Z. Pan, Z. Liu, P. Zhang, X. Shen, Q. Nie, S. Dai, and R. Wang, "Mid-infrared supercontinuum covering 2.0-16 μm in a low-loss telluride single-mode fiber," Laser & Photonics Reviews **11** (2017).

[15]. K. Yin, B. Zhang, J. Yao, Z. Cai, G. Liu, and J. Hou, "Toward High-Power All-Fiber 2–5 μm Supercontinuum Generation in Chalcogenide Step-Index Fiber," Journal of Lightwave Technology **35**, 4535-4539 (2017).

[16]. S. Xing, D. Grassani, S. Kharitonov, L. Brilland, C. Caillaud, J. Trolès, and C.-S. Brès, "Mid-infrared continuous-wave parametric amplification in chalcogenide microstructured fibers," Optica **4** (2017).

[17]. Y. Wang, S. Dai, G. Li, D. Xu, C. You, X. Han, P. Zhang, X. Wang, and P. Xu, "1.4-7.2 mum broadband supercontinuum generation in an As-S chalcogenide tapered fiber pumped in the normal dispersion regime," Opt Lett **42**, 3458-3461 (2017).

[18]. C. R. Petersen, R. D. Engelsholm, C. Markos, L. Brilland, C. Caillaud, J. Troles, and O. Bang, "Increased mid-infrared supercontinuum bandwidth and average power by tapering large-mode-area chalcogenide photonic crystal fibers," Opt Express **25**, 15336-15348 (2017).

[19]. D. Le Coq, S. Cui, C. Boussard-Plédel, P. Masselin, E. Bychkov, and B. Bureau, "Telluride glasses with far-infrared transmission up to 35 μm," Optical Materials **72**, 809-812 (2017).

[20]. D. D. Hudson, S. Antipov, L. Li, I. Alamgir, T. Hu, M. E. Amraoui, Y. Messaddeq, M. Rochette, S. D. Jackson, and A. Fuerbach, "Toward all-fiber supercontinuum spanning the mid-infrared," Optica **4** (2017).

[21]. S. Danto, P. Houizot, C. Boussard-Pledel, X. H. Zhang, F. Smektala, and J. Lucas, "A Family of Far-Infrared-Transmitting Glasses in the Ga–Ge–Te System for Space Applications," Advanced Functional Materials **16**, 1847-1852 (2006).

[22]. A. A. Wilhelm, C. Boussard-Pledel, Q. Coulombier, J. Lucas, B. Bureau, and P. Lucas, "Development of Far-Infrared-Transmitting Te Based Glasses Suitable for Carbon Dioxide Detection and Space Optics," Advanced Materials **19**, 3796-3800 (2007).

[23]. Z. Yang, and P. Lucas, "Tellurium-Based Far-Infrared Transmitting Glasses," Journal of the American Ceramic Society **92**, 2920-2923 (2009).

[24]. X. Zhang, H. Ma, C. Blanchetière, and J. Lucas, "Low loss optical fibres of the tellurium halide-based glasses, the TeX glasses," Journal of non-crystalline solids **161**, 327-330 (1993).

[25]. J.-C. B. Clément Conseil, Catherine Boussard-Plédel, Xiang-Hua Zhang, Pierre Lucas, Shixun Dai, Jacques Lucas, and Bruno Bureau, "Te-based chalcohalide glasses for far-infrared optical fiber," Optical Materials Express (2012).

[26]. X. Wang, Q. Nie, G. Wang, J. Sun, B. Song, S. Dai, X. Zhang, B. Bureau, C. Boussard, and C. Conseil, "Investigations of Ge–Te–AgI chalcogenide glass for far-infrared application," Spectrochimica Acta Part A: Molecular and Biomolecular Spectroscopy **86**, 586-589 (2012).

[27]. S. Maurugeon, B. Bureau, C. Boussard-Plédel, A. Faber, X. Zhang, W.

Geliesen, and J. Lucas, "Te-rich Ge–Te–Se glass for the CO2 infrared detection at 15 μm," Journal of Non-Crystalline Solids **355**, 2074-2078 (2009).

[28]. S. Maurugeon, C. Boussard-Plédel, J. Troles, A. Faber, P. Lucas, X. Zhang, J. Lucas, and B. Bureau, "Telluride glass step index fiber for the far infrared," Journal of Lightwave Technology **28**, 3358-3363 (2010).

[29]. S. Maurugeon, B. Bureau, C. Boussard-Plédel, A. Faber, P. Lucas, X. Zhang, and J. Lucas, "Selenium modified GeTe4 based glasses optical fibers for far-infrared sensing," Optical Materials **33**, 660-663 (2011).

[30]. A. M. Heidt, "Pulse preserving flat-top supercontinuum generation in all-normal dispersion photonic crystal fibers," JOSA B **27**, 550-559 (2010).

[31]. B. Siwicki, R. Kasztelanic, M. Klimczak, J. Cimek, D. Pysz, R. Stępień, and R. Buczyński, "Extending of flat normal dispersion profile in all-solid soft glass nonlinear photonic crystal fibres," Journal of Optics **18**, 065102 (2016).

[32]. B. Siwicki, A. Filipkowski, R. Kasztelanic, M. Klimczak, and R. Buczynski, "Nanostructured graded-index core chalcogenide fiber with all-normal dispersion-design and nonlinear simulations," Opt Express **25**, 12984-12998 (2017).

[33]. A. Méndez, and T. F. Morse, *Specialty optical fibers handbook* (Elsevier, 2011).

[34]. P. U. Nicolai Granzow, Markus A. Schmidt, Andrey S. Tverjanovich, Lothar Wondraczek, and Philip St. J. Russell, "Bandgap guidance in hybrid chalcogenide–silica photonic crystal fibers," (2011).

[35]. M. A. Schmidt, N. Granzow, N. Da, M. Peng, L. Wondraczek, and P. S. J. Russell, "All-solid bandgap guiding in tellurite-filled silica photonic crystal fibers," Optics Letters **34**, 1946-1948 (2009).

[36]. C. Markos, "Photo-induced changes in a hybrid amorphous chalcogenide/silica photonic crystal fiber," Applied Physics Letters **104**, 011114 (2014).

[37]. S. P. S. N. Granzow, M. A. Schmidt, A. S. Tverjanovich, L. Wondraczek, and P. St.J. Russell, "Supercontinuum generation in chalcogenide-silica step-index fibers," (2011).

[38]. M. A. S. N. Granzow, W. Chang,L. Wang,Q. Coulombier, J. Troles,P. Toupin,I. Hartl, K. F. Lee, M. E. Fermann, L. Wondraczek and P. St.J. Russell, "Mid infrared supercontinuum generation in As2S3 silica nano spike step index waveguide," (2013).

[39]. S. Xie, F. Tani, J. C. Travers, P. Uebel, C. Caillaud, J. Troles, M. A. Schmidt, and P. S. J. Russell, "As 2 S 3–silica double-nanospike waveguide for mid-infrared supercontinuum generation," Optics letters **39**, 5216-5219 (2014).

[40]. M. Karim, B. Rahman, and G. P. Agrawal, "Mid-infrared supercontinuum generation using dispersion-engineered Ge 11.5 As 24 Se 64.5 chalcogenide channel waveguide," Optics express **23**, 6903-6914 (2015).

[41]. S. Xie, N. Tolstik, J. C. Travers, E. Sorokin, C. Caillaud, J. Troles, P. S. J. Russell, and I. T. Sorokina, "Coherent octave-spanning mid-infrared supercontinuum generated in As 2 S 3-silica double-nanospike waveguide pumped by femtosecond Cr: ZnS laser," Optics Express **24**, 12406-12413 (2016).

[42]. T. Cheng, H. Kawashima, X. Xue, D. Deng, M. Matsumoto, T. Misumi, T. Suzuki, and Y. Ohishi, "Fabrication of a chalcogenide-tellurite hybrid microstructured optical fiber for flattened and broadband supercontinuum generation," Journal of Lightwave Technology **33**, 333-338 (2015).

[43]. S. Cui, "Synthesis and characterization of tellurium based glasses for far infrared sensing and thermoelectric applications," (Université Rennes 1, 2014).

[44]. V. Shiryaev, A. Velmuzhov, M. Churbanov, A. D. Plekhovich, C. Boussard-Plédel, J. Troles, C. Conseil, and V. Plotnichenko, "Preparation and investigation of high purity Ge–Te–AgI glasses for optical application," Journal of Non-Crystalline Solids **377**, 1-7 (2013).

[45]. R. F. Brebrick, "Tellurium vapor pressure and optical density at 370-615. degree," The Journal of Physical Chemistry **72**, 1032-1036 (1968).

[46]. R. E. Machol, and E. F. Westrum Jr, "Vapor pressure of liquid tellurium," Journal of the American Chemical Society **80**, 2950-2952 (1958).

[47]. H. G. Dantanarayana, N. Abdel-Moneim, Z. Tang, L. Sojka, S. Sujecki, D. Furniss, A. B. Seddon, I. Kubat, O. Bang, and T. M. Benson, "Refractive index

dispersion of chalcogenide glasses for ultra-high numerical-aperture fiber for mid-infrared supercontinuum generation," Optical Materials Express **4** (2014).

[48]. H. G. Dantanarayana, "Application of TLM for optical microresonators," (University of Nottingham, 2012).

[49]. H. Dantanarayana, A. Vukovic, P. Sewell, Z. Lian, D. Furniss, A. Seddon, E. Romanova, A. Konyukhov, B. Derkowska, and J. Orava, "The optical properties of chalcogenide glasses: From measurement to electromagnetic simulation tools," in *Transparent Optical Networks (ICTON), 2010 12th International Conference on*(IEEE2010), pp. 1-4.

[50]. J. Ballato, T. Hawkins, P. Foy, R. Stolen, B. Kokuoz, M. Ellison, C. McMillen, J. Reppert, A. Rao, and M. Daw, "Silicon optical fiber," Optics express **16**, 18675-18683 (2008).

[51]. P. J. Sazio, A. Amezcua-Correa, C. E. Finlayson, J. R. Hayes, T. J. Scheidemantel, N. F. Baril, B. R. Jackson, D.-J. Won, F. Zhang, and E. R. Margine, "Microstructured optical fibers as high-pressure microfluidic reactors," Science **311**, 1583-1586 (2006).

[52]. C. Sieutat, R. Peretti, J.-L. Leclercq, P. Viktorovitch, and X. Letartre, "Strong confinement of light in low index materials: the Photon Cage," Optics Express **21**, 20015-20022 (2013).

[53]. P. Houizot, C. Boussard-Plédel, A. Faber, L. Cheng, B. Bureau, P. Van Nijnatten, W. Gielesen, J. P. Do Carmo, and J. Lucas, "Infrared single mode chalcogenide glass fiber for space," Optics Express **15**, 12529-12538 (2007).

[54]. F. Désévédavy, G. Renversez, J. Troles, P. Houizot, L. Brilland, I. Vasilief, Q. Coulombier, N. Traynor, F. Smektala, and J.-L. Adam, "Chalcogenide glass hollow core photonic crystal fibers," Optical Materials **32**, 1532-1539 (2010).

General Conclusion

The optical and nonlinear properties of chalcogenide glasses and fibers are unique and prosperous which lead to enormous applications in the Mid-infrared range, especially supercontinuum generation. This work is mainly devoted to the innovative design of waveguides and fibers for Mid-infrared supercontinuum generations.

In chapter II, the influence of thermal annealing treatment on the enhancement of the refractive index contrast was investigated. Three different chalcogenide glasses (GLS, $Ge_{20}As_{20}S_{60}$, and $Ge_{15}As_{15}S_{70}$) were synthesized with conventional "melt and quench" method. The three compositions were tested in the static conditions first. However, the three glass samples reacted quite differently to the laser irradiation, where the refractive index contrast in GLS glass was decreasing with the annealing cycle number increase and the $Ge_{20}As_{20}S_{60}$ and $Ge_{15}As_{15}S_{70}$ glasses had enhancement after the first annealing and then decreased as the annealing cycle increase. By verifying the three samples in the dynamic conditions (waveguides photo-inscription with translating samples), similar results were obtained and the behavior in the static conditions were proved. Then the relationships between the laser doses received by the samples (i.e. exposure time of samples) and the index contrast were investigated and a threshold in terms of laser dose at which the photo-induced index contrast started to be measurable by PCM was discovered. Subsequently, it was confirmed that the first annealing cycle determined the enhancement of the interaction efficiency between the glass matrix and the laser pulses, but not the increase of the structural flexibility of the glass matrix (volume of the glass structure).

In chapter III, a step-index Te-Ge-AgI fiber was firstly presented. Based on the previous obtained thermal properties of Te-Ge-AgI glasses, the glass composition with 10, 15 and 20% of AgI were selected as the core or cladding of the fiber. Extra purification procedures such as purification of Tellurium and a two-step purification method were utilized. The thermal properties were measured and showed no obvious

crystallization and the optical transmittance was also in agreement with previous results. Subsequently, the bulk glasses were drawn into single index fibers with the attenuation measured around 2dB/m at 10μm. The compositions of $(Te_4Ge)_{90}AgI_{10}$ and $(Te_4Ge)_{85}AgI_{15}$ were chosen to be the core and the cladding respectively. With the assistance of a modified casting method, the fiber preform was achieved. As hydrofluorid acid was applied in removing the capillary, the chemical durability of Te-Ge-AgI glass in hydrofluoric acid was tested to verify the quality of the preform. Then, final step-index fiber was drawn and used to light propagation. However, no light propagation inside the fiber core was observed and it was attributed ti the small refractive index difference between the core and the cladding and modification of the composition of the fiber.

Then, we introduced a graded-index fiber, which was composed of two glass compositions of $As_{38}Se_{62}$ and $Ge_{10}As_{22}Se_{68}$ with similar thermal properties. The two glass compositions were first synthesized and drawn into 10cm-long rods with a diameter of 450μm. Later on, the obtained rods were assembled following the designed distribution of the graded-index structure. As the stack was drawn into cane, it was inserted in to the cladding tube to assemble the fiber preform. A cane with a diameter of 5.5μm was inserted into the cladding tube prepared, and a 125μm grade-index fiber was drawn from the preform. Due to the increase of the loss of the fiber during the drawing process and potential crystiallization, no light propagation was observed in the obtained grade-index fiber.

In the last part of chapter III, an innovative hybrid fiber structure was illustrated. The original plan was to insert melted TAS glass into the air holes of silica PCF. Experiments with various conditions as furnace temperature, vacuuming time and pre-treatment of the PCF endface were carried out to discover the optimal conditions. In the end, an 8-cm-long silica PCF filled with TAS glass was obtained.

Perspective:

Although different designs of waveguides and fibers were attempted in the aim of generating Mid-infrared supercontinuum generation, there are still improvements to be completed in the future:

a) A more considerable design of experiment for comparison of the impact of the thermal annealing treatment to disciver the inner mechanism of the results obtained in photo-inscription
b) Purification and polishing before drawing TeGe-AgI step-index fiber and considering of other glass composition for the core and cladding
c) Replacing AsSe glass in graded-index fiber fabrication inorder to avoid crystallization
d) Better treatment of the PCF endface and to avoid scratch when interacting with un-melted TAS glass

UNIVERSITE MATIERE BRETAGNE MOLECULES LOIRE ET MATERIAUX

UNIVERSITÉ DE RENNES 1

Titre : **Développement de verres au chalcogénide pour l'élaboration de guides d'ondes et de fibres innovants**

Mots clés : Verres en chalcogénure, Moyen infrarouge, Fibres optiques et guides d'ondes, Génération supercontinuum

Résumé: La thèse est divisée en trois chapitres distincts. Le premier chapitre, introductif, présente les propriétés générales des verres et fibres en verres de chalcogénures ainsi que leurs intérêts, notamment dans le développement de sources supercontinuum générant des longueurs d'onde de 2 à 12 µm (source large bande issue de phénomènes optiques non linéaires). Ce domaine de longueur d'onde est très apprécié dans le domaine de la spectroscopie, car c'est dans ce domaine que l'on retrouve la majorité des signatures infrarouges des toutes les substances chimiques et biologiques. Le deuxième chapitre exploite, la photosensibilité des verres de chalcogénures pour la réalisation de guides d'onde photo-inscrits. Dans ce chapitre, 3 différentes compositions ont été étudiées mais ont présenté un comportement différent voire contradictoire. Le dernier chapitre explore la réalisation de fibres optiques nouvelles à base de verre de chalcogénures. Les premières fibres étudiées sont les fibres réalisées avec des compositions à base de tellure, afin d'augmenter la fenêtre de transmission des fibres vers les grandes longueurs d'onde. La deuxième partie du chapitre présente une méthode originale qui pourrait permettre de réaliser des fibres en verres de chalcogénures à gradient d'indice. Puis la dernière partie est consacrée au développement de fibres hybrides en verres de silice et verres de chalcogénures.

Title : **Chalcogenide glasses development for the elaboration of innovative waveguides and fibers**

Keywords : Chalcogenide glasses, Mid-infrared optics, optical fibers，waveguides, supercontinuum generation

Abstract: This thesis is divided into three separate chapters. The introductory chapter introduces the general properties of chalcogenide glasses and fibers, as well as their interest, particularly in the development of supercontinuum sources generating wavelengths of 2 to 12 µm (broadband source from nonlinear optical phenomena). This wavelength range is very popular in the field of spectroscopy, because it is in this area that we find the majority of infrared signatures of all chemical and biological substances. The second chapter exploits the photosensitivity of chalcogenide glasses for the production of photo-inscribed waveguides. In this chapter, 3 different compositions were studied but presented a different behavior even contradictory. The last chapter explores the realization of new optical fibers based on chalcogenide glass. The first fibers studied are fibers made with tellurium-based compositions in order to increase the transmission window of the fibers towards the long wavelengths. The second part of the chapter presents an original method that could be used to produce index gradient chalcogenide glass fibers. Then the last part is dedicated to the development of hybrid fibers in silica glasses and chalcogenide glasses.